MODULATION OF STEM CELL DELIVERY STRATEGY BY PLATELET LYSATE UTILIZATION AND CELL AGGREGATION FOR ENHANCED BONE REGENERATION

A Dissertation

Presented to

The Academic Faculty

by

Ashley Beth Allen

In Partial Fulfillment

of the Requirements for the Degree

Doctor of Philosophy in Bioengineering in the

School of Biomedical Engineering

Georgia Institute of Technology

August 2015

MODULATION OF STEM CELL DELIVERY STRATEGY BY PLATELET LYSATE UTILIZATION AND CELL AGGREGATION FOR ENHANCED BONE REGENERATION

Approved by:

Dr. Robert E. Guldberg, Advisor
School of Mechanical Engineering
Georgia Institute of Technology

Dr. Zulma Gazit
Regenerative Medicine Institute
Cedars-Sinai Medical Center

Dr. Andrés J. García
School of Mechanical Engineering
Georgia Institute of Technology

Dr. Todd C. McDevitt
Center for Cardiovascular Disease
Gladstone Institutes

Dr. Ian B. Copland
School of Medicine
Emory University

Date Approved: June 24, 2015

To my mom and dad

ACKNOWLEDGEMENTS

The last six years have been an invaluable growing experience, impossible to summarize fully within the framework of this dissertation. A community of individuals helped to define this journey and I owe them all the gratitude in the world. I came to Georgia Tech to learn a thing or two about biomedical research, but am leaving with a scientific awareness and level of emotional fulfillment that far exceed initial expectations.

I'd first like to thank my thesis advisor, Dr. Robert E. Guldberg. Bob has been instrumental in defining my research experience. He's provided the hands off and big picture guidance that's allowed me to creatively explore within the laboratory setting. Under his tutelage, I've learned to conduct hypothesis-driven research, evaluate when it's appropriate to go full steam ahead pursuing a research tangent (and when it's time to switch gears), and how to place benchtop findings in the context of big picture objectives. The freedom he's afforded me to make independent design and troubleshooting decisions throughout the course of my research project has defined this experience for me.

My thesis committee has been instrumental in guiding my research as well. In fact, I'm fortunate to have gained significant encouragement and advice from every single committee member. Dr. Andrés J. García has consistently made himself available to provide insightful and unfiltered counsel on an informal basis. I also had the opportunity to work closely with him as president of the Bioengineering Graduate Association (BGA; formerly known as BGSAC) and greatly admire everything he's done to shape and grow our interdisciplinary program. Dr. Ian B. Copland provided the product, troubleshooting guidance, and clinical perspective fundamental to completion of

the human platelet lysate (hPL) studies. He's continually been enthusiastic and accessible to discuss results and clinical applicability over the last six years. Dr. Todd C. McDevitt enabled me to pursue all of the MSC aggregate studies through collaboration with his laboratory. He challenged me to carefully design and convey the results of my experiments, in order to present my findings in the most thoughtful and accurate way possible. Finally, Dr. Zulma Gazit was instrumental to implementing the bioluminescent imaging (BLI) technique used throughout the course of my project. Although she's often had to advise me remotely, I've also had the invaluable experience of visiting her laboratories at Cedars-Sinai Medical Center (Los Angeles, CA) and Hebrew University (Jerusalem, Israel). In addition to gaining honest and practical advice from our conversations, I've also admired her as a role model.

I'd like to thank my past and present labmates in the Guldberg Lab, without whom this work would not have been possible. I thank Dr. Ken Dupont, Dr. Joel Boerckel, Dr. Jessica O'Neal, Dr. Christopher Dosier, and Dr. Brent Uhrig for their willingness and enthusiasm to provide guidance from the moment I entered the lab. I further thank Dr. Nick Willett, Dr. Laxmi Krishnan, Dr. Tanushree Thote, Dr. Alice Li, Dr. Lauren Priddy, Jason Wang, David Reece, Marian Hettiaratchi, Brennan Torstrick, Albert Cheng, Giuli Salazar-Noratto, Andrew Miller, Brett Klosterhoff, and Marissa Ruehle for their help and support with experiments as well as being a fine bunch of individuals to work side-by-side with. I'd also like to acknowledge Emily Butts, a fantastic undergraduate researcher who dedicated a remarkable amount of effort and focus to the platelet lysate research. I look forward to her continuing to do great work in medical school and beyond. A special thanks to Olivia Burnsed and Josh Zimmermann

for making the MSC aggregate work possible, especially when that meant arriving in lab before 6AM the day of an *in vivo* study!

Thanks to Angela Lin and Hazel Stevens for contributing their expertise and attention to make the Guldberg Lab such a fantastic environment to conduct research in. In particular, I appreciate Hazel as a resource for all things cells as well as being my British mom (at least, until she turned American) here in Atlanta. Her willingness and proficiency to discuss experimental results, next steps, and troubleshooting measures enabled me to continue down the PhD road even when experimental data were less than favorable. Furthermore, the words "pants" and "awesome" will forever remind me of my horrible American accent thanks to her gentle mockery.

I have to acknowledge the IBB and PRL staff for making this work possible as well. None of this research would be feasible without the outstanding IBB core and animal facilities. Additionally, thank you to Vivian Johnson, Laura Paige, Christopher Ruffin, Colly Mitchell, and Meg McDevitt for all they've done administratively to keep the Guldberg Lab, Bioengineering program, and student groups (namely, BGA and BBUGS) flourishing. IBB is a high functioning, multi-faceted, and positive work environment due to the efforts of so many talented and dedicated individuals.

I'd like to thank my colleagues and friends in the Garcia Lab for being an additional source of scientific expertise as well as a welcome distraction through athletic competition (Lair Olympics!) and plentiful baked goods. I also have to thank the greater Bioengineering and BME communities for fostering such a rich selection of extracurricular activities. I hope events such as BGA frisbee golf and Buzz of Biotech continue to be epic and successful endeavors. Operating as an Education and Outreach

chair for BBUGS was a highlight of my time at Georgia Tech and I'd like to thank Patricia Pacheco and Jessilyn Dunn for being my partners in crime. Viscoelasticity will forever be synonymous with Elmer's glue and Borax!

Thanks to all my friends in Atlanta who made these six years so meaningful. From our adventurous undertakings (e.g. Alabama bike rides, camping trips, and Hooch shooting) to those less extreme (e.g. Beltline walks, festivals, brewery tours, and potlucks), you've been responsible for memories I'll never forget. I'd also like to acknowledge support from childhood and college friends, several of whom took the time to visit Atlanta and were inevitably wooed by the "tall buildings" and festival-centric culture of our city in the South. I owe a special thanks to Brian Cafferty for being my heart and support system over the past two years. I've found so much joy and inspiration in his positivity, thoughtfulness, and scientific smarts (or rather, "smaahhts" now that he's in Boston). I can't wait to continue our next chapter in New England!

Finally, I owe the completion of this PhD work to my family. To Dawn Block and Spencer Allen, thanks for shaping me into the person I am. You taught me to work hard, think creativity, and be an honest person. You never failed to raise my spirits and provide encouragement when this thesis felt like an insurmountable task. Furthermore, I'm doubly fortunate to have a wonderful set of "bonus parents" in Mikey Harris and Lynn Clifford. I also have to thank Lindsay Allen, who's always been there for me and understood me when no one else could. Despite being my younger seester, she's always been a huge inspiration and source of wisdom. I dedicate this work to my family. You continuously reminded me that, while the course of scientific endeavors may be

unpredictable, family provides an unwavering and consistent source of strength, optimism, and love.

TABLE OF CONTENTS

ACKNOWLEDGEMENTS IV

LIST OF FIGURES XIII

LIST OF ABBREVIATIONS XV

SUMMARY XVIII

CHAPTER 1 SPECIFIC AIMS 1

Aim I 2

Aim II 2

Aim III 3

CHAPTER 2 LITERATURE REVIEW 4

2.1 Introduction to Bone Tissue and Repair 4

2.1.1 Bone Function and Composition 4

2.1.2 Bone Remodeling 5

2.1.3 Bone Fracture and Repair 7

2.1.4 Non-Healing Bone Defects 8

2.1.5 Stem Cell Delivery for Bone Repair 10

2.2 Mesenchymal Stem Cell (MSC) Delivery for Large Bone Defect Repair 11

2.2.1 MSC Isolation and Properties 11

2.2.2 MSC Delivery for Bone Regeneration 13

2.2.3 *In Vivo* MSC Tracking Strategies 14

2.3 Human Platelet Lysate 16

2.3.1 Platelet-Rich Plasma 16

2.3.2 Production and Characteristics of Human Platelet Lysate 17

2.3.3 hPL for hMSC Culture 18

2.3.4 hPL for Bone Tissue Engineering 19

2.4 MSC Aggregation 20

2.4.1 Introduction to Cell Aggregates 20

2.4.2 Characterization of MSC Aggregates 20

2.5 Motivations for Research 22

CHAPTER 3 DEVELOPMENT OF AN *IN VIVO* BIOLUMINESCENT MESENCHYMAL STEM CELL TRACKING PROTOCOL 24
3.1 Introduction 24
3.2 Materials and Methods 26
3.2.1 hMSC Culture 26
3.2.2 hMSC Labeling 26
3.2.3 Alginate/Mesh and Agarose/Mesh Construct Preparation 27
3.2.4 Subcutaneous Implantation in Nude Rats 30
3.2.5 *In Vivo* BLI 30
3.2.6 Construct Vasculature Quantification 31
3.2.7 Histological Analysis 32
3.2.8 Digest of Alginate/Mesh Explants and Flow Cytometry 32
3.2.9 Data Analysis 33
3.3 Results 34
3.3.1 Validation of hMSC Labeling and Construct Embedding 34
3.3.2 Development and Implementation of BLI Tracking Protocol 38
3.3.3 Longitudinal Assessment of BLI Protocol 40
3.3.4 Construct Vasculature 44
3.4 Discussion 47
CHAPTER 4 EVALUATION OF HUMAN PLATELET LYSATE FOR MESENCHYMAL STEM CELL DELIVERY 52
4.1 Introduction 52
4.2 Materials and Methods 55
4.2.1 MSC Culture 55
4.2.2 Platelet Lysate Preparation 55
4.2.3 2D *In Vitro* Analysis 56
4.2.4 Alginate Construct Preparation 57
4.2.5 3D *In Vitro* Analysis 58
4.2.6 Surgical Procedures 59
4.2.7 *In Vivo* and Explant Analyses 61
4.2.8 Statistical Analysis 62
4.3 Results 62

4.3.1 Implantation of hMSCs Receiving hPL Pre-Treatment 62
4.3.2 Addition of hPL to Hydrogels *In Vitro* 67
4.3.3 Implantation of hPL Containing Constructs 69
4.3.4 Limitations of an Immunocompromised Rodent Animal Model 73
4.3.5 Limitations of a Syngeneic Rodent Animal Model 75
4.4 Discussion 77
CHAPTER 5 MESENCHYMAL STEM CELL AGGREGATION FOR LARGE BONE DEFECT REPAIR 83
5.1 Introduction 83
5.2 Materials and Methods 85
5.2.1 MSC Culture and Aggregate Formation 85
5.2.2 Alginate Embedding of hMSCs 86
5.2.3 Alginate Embedding of rMSCs 87
5.2.4 Subcutaneous Implantation 88
5.2.5 Subcutaneous BLI, Vascular, and Histological Analyses 88
5.2.6 Segmental Defect Implantation 89
5.2.7 Segmental Defect Radiography and μCT Analyses 90
5.2.8 Segmental Defect Biomechanical and Histological Analyses 91
5.2.9 Statistical Analysis 91
5.3 Results 91
5.3.1 Subcutaneous Implantation of hMSC Aggregates in Nude Rats 91
5.3.2 hMSC Aggregation for Large Bone Defect Repair in Nude Rats 97
5.3.3 *In Vitro* Characterization of rMSC Aggregates 101
5.3.4 Subcutaneous Implantation of rMSC Aggregates in Lewis Rats 104
5.3.5 Release of BMP-2 from rMSC-Seeded Constructs *In Vitro* 111
5.3.6 rMSC Aggregate Delivery for Bone Defect Repair in Lewis Rats 113
5.4 Discussion 123
CHAPTER 6 CONCLUSIONS AND FUTURE DIRECTIONS 128
6.1 Summary 128
6.2 Future Directions for hPL Utilization 131
6.3 Future Directions for MSC Aggregate Delivery 132
6.4 Discussion of Cell Delivery for Volumetric Tissue Regeneration 133

6.5 Final Conclusions and Significance 138

REFERENCES 140

LIST OF FIGURES

Figure 1: Hydrogel/Mesh Construct Preparation 29
Figure 2: Characterization of GFP/Luc-Labeled hMSCs 35
Figure 3: Evaluation of Dual-Syringe Hydrogel/Cell Delivery 36
Figure 4: hMSC Spatial Distribution Following Dual-Syringe Technique 37
Figure 5: Development of BLI Protocol and Determination of hMSC Survival 39
Figure 6: Shift in BLI Profile after 1 Week *In Vivo* 41
Figure 7: Construct Encapsulation and Tissue Ingrowth at 1 Week *In Vivo* 43
Figure 8: Construct Vascularization at 1 Week Post Implantation *In Vivo* 45
Figure 9: Construct Vascularization and BLI Signal Profile with Hydrogel Type 46
Figure 10: hPL Pre-Treatment and Co-Delivery Experimental Designs 60
Figure 11: Effects of hPL Culture on hMSC Expansion 63
Figure 12: hMSC Viability within hPL Pre-Treatment Groups on Day 0 65
Figure 13: hMSC Survival and Construct Vasculature through Day 7 *In Vivo* 66
Figure 14: Addition of hPL to Hydrogels *In Vitro* 68
Figure 15: *In Vivo* Bioluminescent Imaging (BLI) and Construct Vasculature 70
Figure 16: Tissue Development and Morphology on Day 14 Post Implantation 72
Figure 17: Limitations of an Immunocompromised Rodent Model 74
Figure 18: Limitations of a Syngeneic Rodent Model 76
Figure 19: Embedding of hMSC Aggregates in Alginate Hydrogel 93
Figure 20: Effect of hMSC Aggregation on Viability through 14 Days *In Vivo* 95
Figure 21: Effect of hMSC Aggregation on Construct Composition at 14 Days 96
Figure 22: Effect of hMSC Delivery for Large Bone Defect Repair in Nude Rats 98
Figure 23: Biological Variability within the Nude Rat Model 100
Figure 24: Formation and In Vitro Characterization of rMSC 102
Figure 25: Hypoxic Culture of rMSCs within Alginate Hydrogels 103

Figure 26: BLI Heatmaps of rMSCs Implanted Subcutaneously through 14 Days 105
Figure 27: Longitudinal BLI of Subcutaneously Implanted rMSCs 106
Figure 28: Longitudinal BLI of Acellular Constructs through 14 Days *In Vivo* 107
Figure 29: Effect of rMSC Aggregation on Construct Vasculature at 14 Days 109
Figure 30: Effect of rMSC Aggregation on Construct Composition at 14 Days 110
Figure 31: Effect of rMSC and PFTBA Delivery on *In Vitro* BMP-2 Release 112
Figure 32: Viability of Alginate-Embedded rMSCs following Syringe Incubation 114
Figure 33: Embedded rMSC Viability Across Segmental Defect Treatments 115
Figure 34: Radiographs of Large Bone Defect Repair in Lewis Rats 117
Figure 35: μCT Reconstruction of Bone Defect Repair in Lewis Rats at 12 Weeks 118
Figure 36: Properties of Regenerated Bone Tissue within Lewis Rat Defects 119
Figure 37: Biomechanical Testing of Lewis Rat Defects at 12 Weeks 120
Figure 38: Histological Examination of Lewis Rat Defects at 12 Weeks 122
Figure 39: Construct Vascular Volume by Animal Model 137

LIST OF ABBREVIATIONS

2D	two-dimensional space
3D	three-dimensional space
ALP	alkaline phosphatase
ANOVA	analysis of variance
ATP	adenosine triphosphate
FGF	fibroblast growth factor
BLI	bioluminescent imaging
BMP-2	bone morphogenetic protein 2
BrdU	bromo-2'-deoxy-uridine
BSA	bovine serum albumin
μCT	microcomputed tomography
CXCR4	chemokine receptor 4
DAPI	4’,6-diamidino-2-phenylindole
Dkk-1	dickkopf 1
DNA	deoxyribonucleic acid
DT	doubling time
EGF	epidermal growth factor
ELISA	enzyme-linked immunosorbent assay
FBS	fetal bovine serum
FSC	forward side scatter
GFP	green fluorescent protein

HAGG	heat-aggregated immunoglobulin
HBSS	Hank's Balanced Salt Solution
H&E	hematoxylin and eosin
hMSC	human mesenchymal stem cell
hPL	human platelet lysate
hPL-HI	heat-inactivated human platelet lysate
IACUC	Institutional Animal Care and Use Committee
IDO	indoleamine 2,3-dioxygenase
IFN-γ	interferon gamma
IGF	insulin-like growth factor
IL-1	interleukin 1
IL-6	interleukin 6
IL-24	interleukin 24
IVIS	*in vivo* imaging system
MAC	membrane attack complex
αMEM	Minimum Essential Medium alpha
MSC	mesenchymal stem cell
NBF	neutral buffered formalin
OPG	osteoprotegrin
PBS	phosphate-buffered saline
PCL	polycaprolactone
PDGF	platelet-derived growth factor
PFTBA	perfluorotributylamine

PGE2	prostaglandin E_2
PL	platelet lysate
p-NPP	phosphate substrate
PRP	platelet-rich plasma
PSL	penicillin streptomycin L-glutamine
RANK(L)	receptor activator of nuclear factor kappa-B (ligand)
RGD	arginylglycylaspartic acid
rMSC	rat mesenchymal stem cell
rnu	Rowett nude rat
ROI	region of interest
rPL	rat platelet lysate
SafO	safranin O
SEM	standard error of mean
TGF-β	transforming growth factor beta
TNF-α	tumor necrosis factor alpha
TSG-6	tumor necrosis factor-inducible gene 6 protein
VEGF	vascular endothelial growth factor
VOI	volume of interest
vWF	von Willebrand factor

SUMMARY

Large bone defects, such as those resulting from trauma or tumor resection, are currently repaired using autografts as the gold standard. However, major limitations of this therapeutic strategy, including restricted tissue availability and donor site morbidity, have necessitated the development of cell- and protein-based approaches. Cell-based bone tissue engineering strategies can enable localization of both an osteoprogenitor cell source and differentiation stimulus directly to the defect space. This reduced dependency on endogenous cell migration as well as the prospective benefit of delivered cell paracrine signaling position cell-based approaches as a promising alternative to the delivery of osteoinductive protein alone. However, challenges to control delivered cell behavior, including viability and differentiation, remain a significant barrier to clinical translation.

Our research objectives were to evaluate a bioluminescent imaging (BLI) technique for the longitudinal monitoring of delivered mesenchymal stem cell (MSC) number and subsequently evaluate the effect of two MSC delivery strategies on cell survival and facilitated bone regeneration. Despite the widespread employment of BLI for tracking delivered cells *in vivo*, this technique had not yet been validated for large volume, multicomponent vehicles. To accomplish this goal, we developed and evaluated a BLI protocol using our alginate/mesh delivery platform implanted subcutaneously within an immunocompromised rat model. Correlation between BLI signal and viable MSC number was observed to persist through 1 week *in vivo*. While this work culminated in a powerful tool for subsequent studies, it also highlighted the potential role of confounding factors, including fibrotic and vascular tissue development, on BLI signal

correlation strength. Next we evaluated the utility of human platelet lysate (hPL), an enriched cytokine mixture, for the maintenance of delivered MSC viability and promotion of construct vasculature. Although hPL when implemented as either a pre-treatment or co-delivery strategy had no influence on either outcome measure, limitations in the applicability of hPL pre-clinical testing via rodent testbeds, both immunocompromised and syngeneic, were identified through complementary *in vitro* analysis.

Finally, we determined the effect of MSC aggregation, a strategy shown to enhance cell immunomodulatory properties, on delivered MSC survival and cell-based bone regeneration. Delivery of MSC spheroids was initially investigated within an immunocompromised rodent model (Nude rats) and found to have no effect on cell survival, construct vascularization, nor critically-sized bone defect repair. Interestingly, animal-to-animal variability within this model was found to be a significant predictor of cell-based bone regeneration, prompting the decision to conduct further studies within a syngeneic model. When examined within a syngeneic rodent model (Lewis rats), rMSC aggregates elicited a surviving cell fraction and construct vasculature comparable to that of single cell delivery. Despite *in vitro* observation that the osteoinductive potential of alginate/mesh constructs was increased with rMSC seeding, delivery of rMSC-containing treatments to the femoral defect space attenuated bone repair. In comparison to acellular treatment, regenerated bone volume and biomechanics were reduced with either single cell or aggregate delivery.

The studies presented here explore two stem cell delivery strategies for large volume tissue regeneration. This research implemented a novel imaging platform to relate

key cell-based tissue regeneration metrics, namely delivered cell survival, construct vasculature, and functional outcomes, in an effort to elucidate fundamental principles for development of an effective MSC-based large bone defect therapeutic strategy. Importantly, this body of work also drew attention to several aspects of rodent model selection including xenogenicity, cross-reactivity, and biological variability.

CHAPTER 1 SPECIFIC AIMS

Large bone defects, such as those resulting from trauma or tumor resection, are repaired using graft tissue as the current gold standard. However, limitations of this treatment approach, including limited tissue availability and poor revascularization post-grafting, have motivated the development of cell- and protein-based strategies. Recombinant human bone morphogenetic protein-2 (BMP-2) is an FDA-approved osteoinductive protein clinically utilized to promote bone repair in incidences of non-union. However, supra-physiologic dosing of BMP-2, as is often required for the repair of critically-sized defects, can result in adverse effects including heterotopic bone formation and systemic inflammation.

Cell-based bone tissue engineering strategies offer several potential advantages over the use of osteoinductive protein alone. The co-delivery of stem cells and BMP-2 localizes both an osteoprogenitor cell source and differentiation stimulus directly to the defect space, thereby lessening the reliance on an individual's endogenous repair capacity compared to equivalent acellular approaches. Furthermore, implanted stem cells may promote bone repair indirectly via paracrine signaling to host cell populations.

Despite the promise of cell-based therapeutics for volumetric tissue regeneration, their present efficacy is challenged by poor integration and early death of delivered cells upon implantation. Irrespective of therapeutic mechanism, delivery strategies capable of maintaining stem cell viability following implantation are likely to improve regenerative outcome. Therefore, delivery strategies serving to enhance cell-based bone repair could act through, but are not limited to, an increase in implanted cell viability.

The *overall objectives* of this thesis were to (1) develop and validate a bioluminescent cell tracking protocol and (2) investigate stem cell delivery strategies to enhance viability and bone regeneration. The *central hypotheses* were that platelet lysate (PL) utilization and cell aggregation would better maintain delivered cell viability and improve cell-based bone regeneration. To this end, we proposed the following Specific Aims:

Aim I: Develop a bioluminescence imaging (BLI) protocol for tracking mesenchymal stem cells (MSCs) within large hydrogel constructs *in vivo*.[1] BLI enables the non-invasive and longitudinal monitoring of viable cells labeled for constitutive luciferase reporter protein expression. However, a host of exterior variables, including sample positioning, method of luciferin delivery, and tissue development, impact BLI measurement of a 3D system. *We hypothesized that BLI could be used to quantify viable MSC number through 1 week in vivo.* Within this aim, we sought to develop and validate a BLI protocol capable of monitoring MSCs delivered within large, multicomponent delivery constructs and investigate the influence of potentially confounding factors.

Aim II: Evaluate the effects of platelet lysate (PL) pre-treatment and incorporation on hydrogel-embedded MSCs *in vitro* and *in vivo*. Human PL is an enriched cytokine mixture shown to enhance the expansion of MSCs in 2D by promoting increased

---

[1] Allen, AB; Gazit, Z, Su, S; Stevens, HY; Guldberg, RE; *In Vivo Bioluminescent Tracking of Mesenchymal Stem Cells within Large Hydrogel Constructs*. Tissue Engineering Part C Methods (2014)

proliferation and preserving stem cell phenotype. *We hypothesized that the utilization of hPL would better maintain hMSC viability and enhance vascular ingrowth in vivo.* This work examined the impact of hPL expansion, construct pre-culture, and co-delivery on viable hMSC retention following implantation within large, multicomponent constructs. In pursuing these studies, *we further hypothesized that rodent models for hPL pre-clinical testing would be limited by issues of xenogenicity and species variability.*

Aim III: Quantify the effects of MSC aggregation on cell survival and large bone defect repair. MSC aggregation has been shown to inhibit cell apoptosis as well as enhance cell angiogenic and anti-inflammatory properties. *We hypothesized that MSC aggregation would improve cell survival in vivo*. The impact of aggregation on viable MSC retention was evaluated within a subcutaneous implantation model and subsequently challenged for bone repair within a critically-sized femoral defect. As bone regeneration is a process finely tuned to its local inflammatory environment, *we further hypothesized that the delivery of MSC aggregates would enhance large bone defect repair in comparison to single cell or acellular approaches*.

CHAPTER 2 LITERATURE REVIEW

2.1 Introduction to Bone Tissue and Repair

2.1.1 Bone Function and Composition

Our skeleton provides the structural framework for other organs in the body. Bone tissue behaves viscoelastically, achieving tensile strength and mechanical stability due to a mix of organic and inorganic components (Boskey and Posner 1984, Buckwalter and Cooper 1987). Bone is anisotropic with the greatest elastic modulus being in the longitudinal direction and able to withstand the highest magnitude of stress in compression (Novitskaya, Chen et al. 2011). In addition to this structural purpose, bones serve the critical function of maintaining calcium and phosphate homeostasis in the body through regulated resorption and regeneration of the bone matrix (Yates, Gutierrez et al. 1988). Furthermore, bone marrow, as the environment in which hematopoiesis occurs, represents a key component of the immune system (Morrison and Scadden 2014).

Bone is a matrix comprised of organic and inorganic constituents. The primary organic component is a glycoprotein called type I collagen and the dominant inorganic component is calcium hydroxyapatite (Buckwalter and Cooper 1987). These entities make up two types of tissue within the bone: cortical and trabecular (Buckwalter and Cooper 1987). Cortical tissue is the hard and dense outer layer of bone while trabecular tissue is the porous structure within the interior. Trabecular bone consists of strut-like bone elements surrounded by blood and marrow. Trabeculae quantity and orientation are influenced by several factors, including qualities of the individual (e.g. gender, age,

activity levels, and diet) and function of a particular bone segment, and impact the mechanical properties of bone (Wolfram, Wilke et al. 2010).

The bone matrix is formed and remodeled by predominantly three bone cell types: osteoblasts, osteocytes and osteoclasts (Buckwalter and Cooper 1987). Osteoblasts are bone forming cells that differentiate into osteocytes upon entrapment within the bone matrix (Aarden, Burger et al. 1994). These cells secrete type I collagen in addition to other proteins (e.g. fibronectin, osteopontin, and osteocalcin) that make up the organic matrix as well as mediate bone mineralization (Marotti 1996). Mineralization acts via increased alkaline phosphatase (ALP) activity that furthers organic phosphate levels in the cell vicinity, culminating in the growth and deposition of hydroxyapatite onto collagen fibers within the bone matrix (Boskey and Posner 1984). Osteocytes are located within osteon structures consisting of concentric lacunae rings surrounding a single Haversian canal (Metz, Martin et al. 2003). Canaliculi extend from each osteocyte for the purpose of nutrient and waste exchange. This exchange occurs ultimately by way of the Haversian canals as these run parallel to the long axis of the bone and surround the nerves and blood vessels which are necessary to provide sensory and biochemical input to the bone tissue (Metz, Martin et al. 2003). Finally, osteoclasts are bone resorbing cells which allow for release of calcium and phosphate in response to growth factor or cytokine stimuli (Suda, Nakamura et al. 1997).

2.1.2 Bone Remodeling

Bone remodeling is governed by both mechanical and biochemical cues. Mechanically induced stimuli include the responsiveness of osteocytes and bone lining cells to strain, piezoelectric effects, and fluid flow (Vaananen, Zhao et al. 2000, You,

Temiyasathit et al. 2008). Biochemical signaling, either the consequence of mechanotransduction or arising independently, acts through a range of mechanisms as well. Nitric oxide and prostaglandins serve as signaling molecules to stimulate or inhibit activity of the osteoblast and osteoclast effector cells (Wimalawansa 2010). The soluble factors osteoprotegrin (OPG) and receptor activator of nuclear factor kappa-B ligand (RANKL) play a role in bone remodeling through regulation of osteoclastogenesis (Blair, Zhou et al. 2006). OPG acts as a decoy receptor for RANKL and thereby decreases the quantity available to activate osteoclast precursor cells through binding of their RANK receptor. In the event of activation, precursor cells enlarge and fuse in order to form mature osteoclasts, which subsequently dissolve hydroxyapatite matrix through formation of resorption pits on the bone surface (Blair, Zhou et al. 2006).

A myriad of soluble factors and signaling cascades play a role in bone homeostasis. The canonical Wnt pathway acts through increased accumulation of β–catenin to up-regulate Rux2 expression (Lodewyckx and Lories 2009). Runx2 induces ALP activity and expression of bone matrix proteins, resulting in osteoblastogenesis and down-regulated osteoclast differentiation through inhibition of RANKL. Other major contributors to bone mass increase are members of the transforming growth factor beta (TGF-β) superfamily known as bone morphogenetic proteins (BMPs) (Moustakas and Heldin 2005). These act through BMP receptors on the cell surface, activating the smad signaling cascade and promoting osteoblastic differentiation (Nishimura, Hata et al. 2003). Numerous negative feedback mechanisms are present in bone tissue such that resorption and repair are coupled (Jones, Gray et al. 1994). In the late stage of development, osteocytes secrete the protein sclerostin which acts through the inhibition

of BMP activity to prevent downstream gene expression and subsequent increase in bone mass (Poole, van Bezooijen et al. 2005). Reciprocally, resorption of bone matrix releases insulin-like growth factor (IGF) and TGF-β growth factors that promote bone formation by increasing osteoblast number and activity (Crane and Cao 2014). The endocrine system plays a role in bone mass control and remodeling as well including signaling via estrogen, androgens, and growth hormone (Parfitt 1976, Dobnig, Kainer et al. 1995).

2.1.3 Bone Fracture and Repair

In the event of injury to long bones, normal fracture healing is accomplished via progression through phases of hematoma, inflammation, callus formation, and eventual remodeling (McKibbin 1978, Gaston and Simpson 2007, Bahney, Hu et al. 2015). Initiation of tissue regeneration occurs concomitantly with the infiltration of inflammatory cells, beginning with neutrophils and macrophages sequentially (Bastian, Pillay et al. 2011). In circumstances progressing to tissue repair, resolution of this acute inflammatory stage affords an environment permissive to ossification via intramembranous or endochondral pathways (Colnot 2009). In the case of endochondral ossification, progenitor cells undergo chondrogenesis and hypertrophic maturation, serving to establish a calcified cartilage matrix that is ultimately replaced by bone (Roach 1992, Kronenberg 2003).

Many factors influence the inflammatory environment of regenerating bone tissue and thereby play a role in repair efficacy (Mountziaris, Spicer et al. 2011, Thomas and Puleo 2011). These include arachidonic acid metabolites (e.g. prostaglandin E_2 (PGE2)), cytokines (e.g. tumor necrosis factor alpha (TNF-α) and interleukins), and growth factors (e.g. BMP-2, vascular endothelial growth factor (VEGF), and platelet-derived growth

factor (PDGF)) (Caplan and Correa 2011, Thomas and Puleo 2011, Bahney, Hu et al. 2015). Interestingly, several of these inflammatory mediators promote both regenerative and resorptive events (Mountziaris, Spicer et al. 2011, Thomas and Puleo 2011). Although interleukin 6 (IL-6) promotes osteoclastogenesis, this chemoattractant also furthers bone healing acting as a mediator of macrophage recruitment and has been identified as a requisite for fracture callus maturation (Gorny, Shaw et al. 2004, Yang, Ricciardi et al. 2007, Bastian, Pillay et al. 2011). Adding to an already multifaceted progression of inflammatory processes, resident bone cells (e.g. osetoblasts and chondrocytes), rather than those of the immune system, are shown to be the chief source of inflammatory cytokines following acute regenerative events (Kon, Cho et al. 2001, Mountziaris, Spicer et al. 2011). Ultimately, a great body of work has exposed the temporal and complex nature of bone tissue repair via orchestrated inflammatory processes (Gerstenfeld, Cho et al. 2003, Schmidt-Bleek, Schell et al. 2012, Kovach, Dighe et al. 2015).

2.1.4 Non-Healing Bone Defects

Despite the notable ability of bone tissue to regenerate and remodel, cases of non-union present a significant clinical challenge and occur in instances of large bone defects or approximately 5-10% of fractures (Johnson, Urist et al. 1992, Calori, Albisetti et al. 2007, Tzioupis and Giannoudis 2007, Hollinger, Hart et al. 2008, Calori, Mazza et al. 2011). Large bone defects exceeding a length of 3 cm in the forearm or 6 cm in the femur represent a significant clinical challenge, as ingrowth of soft tissue at the defect site can lead to eventual non-union (Calori, Mazza et al. 2011, Zhang, Teoh et al. 2012). These critically-sized injuries can arise from incidences of trauma or bone resection (for

example, in the case of tumor or infection) and will lead to non-union without therapeutic intervention (Johnson, Urist et al. 1992). The current gold standard to treat or prevent non-union is grafting of autologous bone tissue to the defect site and it is estimated that 1.5 million of such operations take place in the United States annually (Einhorn 2003, Jones, Bucholz et al. 2006, Calori, Mazza et al. 2011). However, use of autografts has several disadvantages that preclude its utility for large bone defect treatment, including limited tissue availability, donor-site morbidity, and prolonged surgical time (Younger and Chapman 1989, Banwart, Asher et al. 1995, Goulet, Senunas et al. 1997, St John, Vaccaro et al. 2003). Allografts are a plausible alternative, but have shown difficulty re-vascularizing upon implantation and can experience subsequent fracture (Berrey, Lord et al. 1990, Finkemeier 2002, Kim, Kang et al. 2010).

Limitations of grafting techniques have motivated the development of cell- and protein-based approaches. Bone morphogenetic proteins were first identified as osteoinductive factors in the 1980s and today human recombinant bone morphogenetic proteins 2 (rhBMP-2) and 7 (rhBMP-7) are both clinically-approved for delivery using an absorbable collagen sponge (Wang, Rosen et al. 1988, Wozney, Rosen et al. 1988, Gautschi, Frey et al. 2007, Bessa, Casal et al. 2008). While patient treatment has been successful in many instances, overall efficacy of BMP delivery is lower than that seen in pre-clinical animal studies (Einhorn 2003). Recent research has focused on tailoring BMP release kinetics through the implementation of novel deliver systems (Seeherman, Wozney et al. 2002, Termaat, Den Boer et al. 2005, Ripamonti, Heliotis et al. 2007, Bessa, Casal et al. 2008, Boerckel, Kolambkar et al. 2011, Priddy, Chaudhuri et al. 2014, Shekaran, Garcia et al. 2014).

2.1.5 Stem Cell Delivery for Bone Repair

Cell-based bone regeneration approaches have many potential advantages over the presentation of osteoinductive cue alone. Acellular approaches rely on the infiltration and subsequent osteogenic differentiation of host cells in the defect space (Perry 1999, Hutmacher 2000, Hutmacher, Schantz et al. 2007, Calori, Mazza et al. 2011). However, in instances where patients are aged, have undergone radiation therapy, or have an adjacent soft tissue injury, availability of these endogenous cell populations is compromised (Bruder and Fox 1999, Service 2000, Fehrer and Lepperdinger 2005, Sethe, Scutt et al. 2006, Caplan 2007, Cao, Luo et al. 2011). Additionally, the co-delivery of cells with an osteoinductive factor, such as rhBMP-2 or rhBMP-7, may enable use of a lower protein dose in order to produce similar efficacy. Several adverse effects, including ectopic mineralization, inflammation, and bone resorption, have been observed when delivering rhBMP-2 at high doses (Hollinger, Brekke et al. 1996, Marsh and Li 1999, Poynton and Lane 2002, Shields, Raque et al. 2006, Smucker, Rhee et al. 2006, Giannoudis, Einhorn et al. 2007, Perri, Cooper et al. 2007, Benglis, Wang et al. 2008, Lee, Taghavi et al. 2012).

Delivered stem cells have the capacity to contribute both directly and indirectly to bone formation (Waese, Kandel et al. 2008, Maraldi, Riccio et al. 2011). Implanted cells can indirectly enhance bone repair either via an inherent or engineered secretome. Embryonic, adult, and fetal stem cell sources have each demonstrated the ability to modulate the angiogenic response *in vivo* (Mirabella, Cilli et al. 2011, Rustad, Wong et al. 2012). Furthermore, cell delivery can enable the presentation of osteoinductive factor via genetic engineering, a strategy that has shown efficacy by several research groups

(Lieberman, Daluiski et al. 1999, Lou, Xu et al. 1999, Parikh 2002, Jin, Anusaksathien et al. 2003, Wang, Kanim et al. 2003, Gafni, Pelled et al. 2004, Termaat, Den Boer et al. 2005, Kim, Kang et al. 2010, Mumaw, Jordan et al. 2012).

2.2 Mesenchymal Stem Cell (MSC) Delivery for Large Bone Defect Repair

2.2.1 MSC Isolation and Properties

Human mesenchymal stem cells (hMSCs) were first isolated from bone marrow tissue in the 1960s and have since been identified within a variety of additional tissues including periosteum, skeletal muscle, fat, and other postnatal tissues (Friedenstein, Piatetzky et al. 1966, Barry and Murphy 2004, da Silva Meirelles, Chagastelles et al. 2006). MSCs have also been isolated from a variety of fetal tissues and animal species (Campagnoli, Roberts et al. 2001, In 't Anker, Scherjon et al. 2003, Meirelles Lda and Nardi 2003, Bieback, Kern et al. 2004, Sarugaser, Lickorish et al. 2005, Carrade and Borjesson 2013). Traditionally, MSCs have been characterized by their multipotency: an ability to differentiate into bone, cartilage, and fat (Owen and Friedenstein 1988, Caplan 1991, Prockop 1997, De Bari, Dell'Accio et al. 2003, De Ugarte, Morizono et al. 2003, Kim, Kang et al. 2010). Subsequent work has found they may be capable of differentiating into muscle, ligament, neuronal, and cardiac cells as well (Wakitani, Saito et al. 1995, Kopen, Prockop et al. 1999, Banfi, Muraglia et al. 2000, Woodbury, Schwarz et al. 2000, Toma, Pittenger et al. 2002, Kawada, Fujita et al. 2004, Kostura, Kraitchman et al. 2004, Monaco, Bionaz et al. 2012). The multipotent capacity and phenotype of MSCs is similar and potentially identical to pericyte cells; however, assertion of their equivalence has been difficult to prove (da Silva Meirelles, Caplan et al. 2008, Caplan

2009, Caplan and Correa 2011, Zhang, Teoh et al. 2012). *In vitro* hMSCs have also been characterized according to immunophenotype, showing positive expression of CD105, CD73 and CD90 and absence of CD34, CD45, and HLA-II (Barry and Murphy 2004, Dominici, Le Blanc et al. 2006, Mamidi, Nathan et al. 2012, Qian, Le Blanc et al. 2012, Zhang, Teoh et al. 2012). Although MSCs constitute a small proportion of the nucleated cells in bone marrow (0.001-0.01%), their ease of isolation and culture expansion have made them a promising candidate for tissue engineering applications (Simmons and Torok-Storb 1991, Pittenger, Mackay et al. 1999, Banfi, Muraglia et al. 2000, Lodie, Blickarz et al. 2002, Sawada, Ito et al. 2006, Aguilar, Nye et al. 2007, Bernardo, Zaffaroni et al. 2007, Meza-Zepeda, Noer et al. 2008). However, MSCs exhibit reduced expansion efficiency and the ability to differentiate along multiple lineages over time in fetal bovine serum (FBS)-supplemented culture, implying that obtainable cell yield and applications for autologous therapies are limited (Banfi, Muraglia et al. 2000, Wagner, Horn et al. 2008, Ben Azouna, Jenhani et al. 2012).

MSCs have been investigated for therapeutic potential using both local and systemic delivery methods (Banfi, Muraglia et al. 2000, Mauney, Volloch et al. 2005). They have been examined for a range of applications, including orthopedic, cardiovascular, graft-versus-host disease, and spinal cord injury treatment, and have been featured in hundreds of clinical trials (Barry and Murphy 2004, Haack-Sorensen, Hansen et al. 2012, Zhang, Teoh et al. 2012). Several studies have illustrated the ability of MSCs to promote angiogenesis through paracrine signaling (Bhang, Lee et al. 2012, Osugi, Katagiri et al. 2012, Rustad, Wong et al. 2012, Schlosser, Dennler et al. 2012). MSCs have a degree of immune privilege due to lack of HLA Class II expression and their

ability to modulate T cell proliferation and phenotype (Moretta, Bottino et al. 2001, Bartholomew, Sturgeon et al. 2002, Aggarwal and Pittenger 2005, Ren, Su et al. 2009, De Miguel, Fuentes-Julian et al. 2012). When delivered systemically, MSCs have proven capable of homing to sites of injury (Mackenzie and Flake 2001, Bittira, Shum-Tim et al. 2003).

2.2.2 MSC Delivery for Bone Regeneration

The utility of MSC delivery for bone repair has been investigated in a range of studies (Aggarwal and Pittenger 2005, Kim, Kang et al. 2010, Ciapetti, Granchi et al. 2012). hMSCs can facilitate surface (2D) and scaffold (3D) mineralization when osteogenically differentiated *in vitro* (Kolambkar, Peister et al. 2010, Jones and Yang 2011, Peister, Woodruff et al. 2011). Furthermore, MSC delivery *in vivo* can augment both fracture and large bone defect repair (Kadiyala, Young et al. 1997, Quarto, Mastrogiacomo et al. 2001, Dallari, Fini et al. 2006, Nather, David et al. 2010, Jones and Yang 2011, Cao, Liu et al. 2012, Dupont, Boerckel et al. 2012, Zhang, Teoh et al. 2012, Dosier, Uhrig et al. 2015). However, despite some promising experimental results, development of a reliable MSC-based bone repair strategy is plagued by considerable difficulties and slow clinical translation (Bruder, Jaiswal et al. 1998, Janicki and Schmidmaier 2011, Osugi, Katagiri et al. 2012). Delivered MSCs exhibit poor long-term engraftment rates and optimal design criteria, such as MSC tissue source, cell dose, delivery timeline, and scaffold selection, are still not established (Freyman, Polin et al. 2006, Newcomb, Ajmo et al. 2006, Olivo, Alblas et al. 2008, Waese, Kandel et al. 2008, Ide, Nakai et al. 2010, Grieshaber, Nie et al. 2011, Burdick 2012, Kim, Shin et al. 2012, Monaco, Bionaz et al. 2012, Rustad, Wong et al. 2012, Dosier, Uhrig et al. 2015). Donor-

to-donor variability, lack of information regarding cell fate, and dissimilarity of pre-treatment and delivery strategies employed across the field, challenge the establishment of a potent and predictable MSC-based therapeutic (Barry and Murphy 2004, Pelled and Gazit 2004, de Boer, van Blitterswijk et al. 2006, Janicki and Schmidmaier 2011, Yew, Huang et al. 2012, Zhang, Teoh et al. 2012).

Discussing volumetric tissue regeneration more broadly, efforts to develop cell-based therapeutics have been challenged by poor integration and early death of delivered cells upon implantation (Tasso, Augello et al. 2009, Giannoni, Scaglione et al. 2010). Endogenous cells are typically situated within 200 μm of a vascular network and rely on diffusion for their nutrient and oxygen supplies (Lovett, Lee et al. 2009). Cells implanted within tissue engineering constructs, however, in the absence of pre-vascularized networks, may initially experience physiologically abnormal oxygen tension and reduced transport of nutrients and waste to and from the implantation site (Muschler, Nakamoto et al. 2004, Becquart, Cambon-Binder et al. 2012).

2.2.3 *In Vivo* MSC Tracking Strategies

Given the challenge of and focus on better maintaining MSC viability post-implantation, several tools have emerged to enable the monitoring of delivered cells. Non-invasive cell tracking strategies include bioluminescence, fluorescence, and magnetic resonance imaging (MRI) (Bulte, Douglas et al. 2002, Arbab, Bashaw et al. 2003, Jager, Michalet et al. 2005, Mook, Jonker et al. 2008). However, techniques that rely on the monitoring of cell-contained particles are limited in their utility for longer durations *in vivo*. For example, particles may be phagocytized upon cell death, leading to the tracking of host macrophages (Terrovitis, Stuber et al. 2008, Dupont, Sharma et al.

2010, Vreys, Soenen et al. 2011). Furthermore, although particle-based labels are conferred to daughter cells upon proliferation, per cell signal magnitude is altered (Alivisatos, Gu et al. 2005, Walczak, Kedziorek et al. 2007, Taylor, Wilson et al. 2012). This limitation disrupts the ability to detect cell number increase, of particular importance when tracking rapidly dividing stem cells. In contrast, bioluminescent imaging (BLI) is contingent on expression of a reporter gene that has been inserted into the delivered cell genome, thereby monitoring specifically the viable cell population of interest as signal is tied exclusively to labeled cell viability and passed through genetic code upon cell division (Zhang and Wu 2007).

BLI measures photons released from the luciferase-catalyzed oxidation of D-luciferin substrate and uses this metric as an indicator of luciferase gene expression from genetically-modified cells (Herschman 2004, de Boer, van Blitterswijk et al. 2006, Ottobrini, Martelli et al. 2011). Although BLI is largely used to monitor cell number, placement of luciferase expression under control of a non-constitutive promoter facilitates detection of delivered cell function, such as the differentiation of an implanted stem cell (Sheyn, Kallai et al. 2011, Oh, Hwang et al. 2013). Due to its collective advantages over alternate tracking strategies, BLI has become an invaluable optical imaging technique for the development of cancer therapies and regenerative medicine strategies within experimental models (O'Neill, Lyons et al. 2010, de Almeida, van Rappard et al. 2011). Several groups have used BLI to track the spatial and temporal behavior of implanted cells for development of cell-based therapeutics (Hara, Murakami et al. 2008, Sacco, Doyonnas et al. 2008, Wang, Cao et al. 2009, Sheyn, Kallai et al. 2011). The ability to monitor luciferase-labeled cell viability *in vivo* through 6-7 weeks

has been demonstrated in several studies (Olivo, Alblas et al. 2008, Geuze, Prins et al. 2010). For these experiments, cells have typically been delivered using a relatively small vehicle volume (less than $75mm^3$) with administration of luciferin substrate via intraperitoneal (IP) injection (Olivo, Alblas et al. 2008, Wang, Cao et al. 2009, Geuze, Prins et al. 2010). However, in the case of larger constructs with increased transport limitations, development of an appropriate BLI protocol presents a more substantial challenge (Miki, Hirose et al. 2009). BLI signal is dependent on variables including construct composition, luciferin delivery method, animal model, sample positioning, and progression of tissue development *in vivo* (de Boer, van Blitterswijk et al. 2006, Inoue, Kiryu et al. 2010, O'Neill, Lyons et al. 2010, Liu, Hilderink et al. 2013). Thus, validation of imaging technique within each experimental system is necessary to ensure an accurate live cell representation.

2.3 Human Platelet Lysate

2.3.1 Platelet-Rich Plasma

Platelet-rich plasma (PRP) is a blood-derived product that is clinically approved for autologous therapy and has been used in a variety of wound-healing and tissue repair applications, including in sports medicine, plastic surgery, and bone regeneration (Dohan Ehrenfest, Rasmusson et al. 2009, Redler, Thompson et al. 2011). PRP is produced through separation of apheresis product to obtain plasma of a high platelet concentration and its delivery serves to localize supra-physiological levels of growth factors contained within the platelet α-granules (Feltsan, Mracna et al. 2011, Redler, Thompson et al. 2011). Delivered proteins, including PDGF, VEGF, TGF-β, and IGF, are capable of

stimulating cell proliferation, extracellular matrix production, and angiogenesis at the site of injury (Filvaroff 2003, Anitua, Andia et al. 2004, El-Sharkawy, Kantarci et al. 2007, Keramaris, Calori et al. 2008, Beamer, Hettrich et al. 2010, Feltsan, Mracna et al. 2011, Anitua and Orive 2012). These factors have also been shown to impact bone regeneration and remodeling, thus several studies have investigated the utility of PRP for bone defect treatment (Ross, Raines et al. 1986, Canalis 1993, Roberts 1995, Marx, Carlson et al. 1998, Keramaris, Calori et al. 2008). Investigators have found PRP to contribute positively to bone regeneration in instances where it has been co-delivered with stem cells or an osteogenic stimulus (Berner, Boerckel et al. 2012, Monteiro, Del Carlo et al. 2012, Zhong, Sumita et al. 2012). However, efficacy of PRP treatment has been variable, likely due to differences in product composition arising from variations between apheresis donor, preparation protocol, and platelet activation strategy (Dohan Ehrenfest, Rasmusson et al. 2009, Macher, Sipurzynski-Budrass et al. 2010, Redler, Thompson et al. 2011).

2.3.2 Production and Characteristics of Human Platelet Lysate

Although PRP has a shelf-life of only five days, platelets have been shown to retain their growth factor activity through several weeks (Chan, Liu et al. 2005, Rauch, Feifel et al. 2011). Expired PRP can be taken through a series of freeze-thaw cycles, filtered, and combined with that of additional donors to generate pooled human platelet lysate (hPL), a solution retaining growth factor stability over several months of storage (Doucet, Ernou et al. 2005, Schallmoser, Bartmann et al. 2007, Rauch, Feifel et al. 2011, Lohmann, Walenda et al. 2012). hPL is an enriched growth factor mixture, containing PDGF, VEGF, latent TGF-β, IGF, basic fibroblast growth factor (bFGF), and epidermal

growth factor (EGF) (Reed, Fitzgerald et al. 2000, Rendu and Brohard-Bohn 2001, King and Reed 2002, Maguire and Fitzgerald 2003, Lohmann, Walenda et al. 2012). hPL has several advantages over PRP, including greater consistency in its composition and the ability to be administered as an allogeneic therapeutic. Donor-to-donor and cell content variability are lessened for hPL due to the fact that several donors are pooled and residual cell membrane and platelet body components are filtered (Rauch, Feifel et al. 2011, Lohmann, Walenda et al. 2012). This removal of antigen-containing components along with the capacity to conduct multiple rounds of donor testing prior to utilization, made possible by the extended shelf-life, allow hPL to be used allogeneically with reduced safety concern (Schallmoser, Bartmann et al. 2007).

2.3.3 hPL for hMSC Culture

The fibrinogen content of hPL allows it to be present either in a coagulated gel form or, through methods of fibrinogen depletion or anticoagulant addition, as a liquid (Harrison and Cramer 1993, Walenda, Hemeda et al. 2012). However, hPL has predominantly been explored in its liquid form as a substitute to fetal bovine serum (FBS) for cell culture expansion (Doucet, Ernou et al. 2005, Schallmoser, Bartmann et al. 2007, Bernardo, Cometa et al. 2011). In addition to eliminating the risks of xenogenic immune response and bovine virus transmission associated with FBS culture, hPL-supplemented media has been shown to enhance cell proliferation and colony-forming unit (CFU) size (Muller, Kordowich et al. 2006, Bernardo, Avanzini et al. 2007, Reinisch, Bartmann et al. 2007, Carrancio, Lopez-Holgado et al. 2008). Furthermore, the immunophenotype, differentiation capacity, and immunomodulatory properties of hMSCs cultured in hPL-

supplemented media remain unaltered (Doucet, Ernou et al. 2005, Schallmoser, Bartmann et al. 2007, Azouna, Berraeis et al. 2011, Flemming, Schallmoser et al. 2011).

2.3.4 hPL for Bone Tissue Engineering

While hPL does not directly stimulate bone formation, several studies have identified its role as an "osteopromoter" (De Long, Einhorn et al. 2007). PDGF, a major component of hPL, has been shown to be a potent mitogen in all three dimer forms (Hart, Bailey et al. 1990, Anitua and Orive 2012). Additionally, PDGF-BB is a chemoattractive agent and has the capacity to modulate both bone and vascular remodeling *in vivo* through its promotion of pericyte release (Caplan and Correa 2011). Heightened pericyte release activity leads to an increase in MSC and osteoprogenitor cell availability that can enhance local bone formation (Caplan 2005, Caplan 2009, Caplan and Correa 2011). Recombinant human PDGF-BB (rhPDGF-BB) is clinically approved and has consistently demonstrated an ability to enhance bone regeneration when co-delivered with β-tricalcium phosphate matrix for treatment of orthopaedic injuries (Hollinger, Hart et al. 2008). Although the impact of hPL-supplemented media on *in vitro* osteogenic differentiation has been well explored, the utility of hPL as a matrix component for bone regeneration has been minimally studied (Schallmoser, Bartmann et al. 2007, Santo, Duarte et al. 2012). Results from Dozza et al. found that co-delivery of platelet lysate and MSCs promoted femoral prosthesis integration in comparison to the treatment of prosthesis alone; however, from this study, one cannot conclude whether this enhancement was due to the lysate or cellular component (Dozza, Chiari et al. 2011).

2.4 MSC Aggregation

2.4.1 Introduction to Cell Aggregates

Mammalian cell aggregation has been performed on a variety of cell types, including pluripotent, multipotent, and differentiated, for a wide range of objectives such as hepatic culture, tumor and microgravity models, drug development, facilitated 3D printing, and cell differentiation (Wartenberg, Donmez et al. 2001, Boland, Mironov et al. 2003, Kunz-Schughart, Freyer et al. 2004, Fukuda, Sakai et al. 2006, Ulbrich, Wehland et al. 2014, Toyoda, Mae et al. 2015). Aggregates can be formed through a variety of methods including micro-wells, hanging drops, and microfluidic culture systems (Torisawa, Takagi et al. 2007, Bartosh, Ylostalo et al. 2010). Such approaches have been used to form aggregates ranging in size (50–1200 μm diameter) and cell number (200–250,000 cells/spheroid) (Torisawa, Takagi et al. 2007, Bartosh, Ylostalo et al. 2010, Ulbrich, Wehland et al. 2014, Zimmermann and McDevitt 2014).

2.4.2 Characterization of MSC Aggregates

To a certain extent, the properties of aggregated MSCs vary as a function of culture conditions. Metabolic activity and apoptosis are found to be dependent on spheroid size in an inverse and proportional manner, respectively (Murphy, Fang et al. 2014). Change in aggregated cell number over time in culture is a function of variables including spheroid size as well as media composition (Murphy, Fang et al. 2014, Zimmermann and McDevitt 2014). However, despite heterogeneity in the response of MSCs to spheroid culture, several therapeutic benefits of this approach have been identified and corroborated in the field. Multiple studies have identified an improvement in angiogenic properties with aggregation. Up-regulated VEGF secretion has been

observed for MSC spheroids in suspension or encapsulated within hydrogels cultured *in vitro* (Lee, Park et al. 2012, Murphy, Fang et al. 2014). Delivery of aggregates to ischemic tissue has improved cell grafting, vasculature, and regenerative outcome (Wang, Chen et al. 2009, Bhang, Cho et al. 2011, Lee, Park et al. 2012). Aggregation may also have therapeutic potential for cancer treatment, as spheroid MSCs increased production of chemokine receptor 4 (CXCR4) and interleukin 24 (IL-24), factors involved in MSC homing and tumor suppression (Potapova, Brink et al. 2008, Bartosh, Ylostalo et al. 2010, Frith, Thomson et al. 2010).

Of particular interest to cell-based bone regeneration strategies are the effects of aggregation on MSC immunomodulatory secretome and osteogenic differentiation capacity. Aggregation improves the efficiency of MSC differentiation down adipogenic or osteogenic lineage through a combination of up-regulated differentiation genes and down-regulated genes governing self-renewal phenotype (Wang, Itaka et al. 2009, Frith, Thomson et al. 2010, Murphy, Fang et al. 2014, Yamaguchi, Ohno et al. 2014). Furthermore, expression of dickkopf 1 (Dkk-1), an inhibitor of Wnt signaling, has been observed to decrease with aggregate culture in the absence of a differentiation stimulus (Bartosh, Ylostalo et al. 2010, Frith, Thomson et al. 2010). When challenged *in vivo*, delivery of MSC spheroids to an orthotopic bone defect promoted healing over that of single cells or vehicle alone (Yamaguchi, Ohno et al. 2014). This bone repair efficacy could be due to the superior differentiation or paracrine signaling capacity of MSC spheroids, as cell immunomodulatory properties are altered with aggregation as well. Spheroid culture increased production of immunomodulatory factors, including tumor necrosis factor-inducible gene 6 protein (TSG-6), indoleamine 2,3-dioxygenase (IDO),

IL-6, and PGE2, in comparison to MSCs cultured in monolayer (Bartosh, Ylostalo et al. 2010, Zimmermann and McDevitt 2014). Additionally, exposure of MSC spheroids to pro-inflammatory cytokines, as found within injured tissue, further enhanced this factor secretion (Zimmermann and McDevitt 2014). MSC aggregate co-culture with stimulated macrophages decreased their expression of pro-inflammatory cytokines (Bartosh, Ylostalo et al. 2010). Upon delivery to a zymosan-induced peritonitis mouse model, intraperitoneal implantation of either aggregated or aggregate-derived MSCs decreased inflammation, with intact aggregates proving the more efficacious strategy (Bartosh, Ylostalo et al. 2010).

2.5 Motivations for Research

Despite the promise of cell-based therapeutics for large bone defect repair, their potential as a clinically viable solution has not been realized. A major barrier to translational efficacy is the challenge to control delivered cell behavior, including viability, differentiation, and factor secretion. Efforts to engineer these properties inevitably fall short due to a fundamental lack of understanding about the relative influence of these parameters on each other as well as regenerative outcome. To add critical dialogue to this conversation, this thesis work explores two stem cell delivery strategies. hPL utilization and cell aggregation have each demonstrated the ability to impact a range of MSC outcomes, including cell number, phenotype, and secretome. However, neither strategy has been explored for developing an MSC-based solution to critically-sized bone defect repair. In addition to engineering an efficacious MSC-based

bone regeneration strategy, this research aimed to relate key principles influencing cell-based tissue regeneration more globally.

CHAPTER 3 DEVELOPMENT OF AN *IN VIVO* BIOLUMINESCENT MESENCHYMAL STEM CELL TRACKING PROTOCOL

3.1 Introduction

Bioluminescent imaging (BLI) has emerged as a valuable tool for tracking cell populations *in vivo* (de Boer, van Blitterswijk et al. 2006, de Almeida, van Rappard et al. 2011). By measuring photon release from the luciferase-catalyzed oxidation of luciferin substrate, BLI can non-invasively and longitudinally monitor the presence of viable cells labeled by means of constitutive luciferase reporter protein expression. Alternatively, by placing luciferase expression under the control of a non-constitutive promoter, BLI can follow delivered cell function, such as the differentiation of an implanted stem cell (Sheyn, Kallai et al. 2011, Oh, Hwang et al. 2013).

In addition to luciferase quantity, several variables influence BLI measurement and can potentially impact its utility as an indicator of viable cell number. These variables include sample positioning, machine sensitivity, luciferin delivery technique, and measurement acquisition time (O'Neill, Lyons et al. 2010). The impact of confounding factors in 2D *in vitro* systems is relatively limited. BLI signal shows a linear relationship with viable cell number with little influence from variations in cell seeding density or time in culture (Sun, Lee et al. 2009, Giannoni, Scaglione et al. 2010). In 3D cell culture systems, BLI signal is affected by a range of additional variables such as luciferin transport kinetics and light scattering properties of the construct (O'Neill, Lyons et al. 2010, Liu, Hilderink et al. 2013). BLI measured from cells seeded within constructs

of significantly different material properties has been found to differ in magnitude, but to be linearly correlated to luciferase content when evaluated *in vitro* (Logeart-Avramoglou, Oudina et al. 2010).

Given the complexity of the 3D system *in vitro*, this evaluation becomes even more complicated when the 3D construct is implanted. The validity of BLI technique has not been rigorously evaluated for these 3D systems *in vivo*. While many confounding factors can be mitigated through implementation of consistent experimental practice, the development of tissue ingrowth within and around scaffolds over time is unavoidable and fundamental to tissue engineering procedures. Several studies that have demonstrated the feasibility of using BLI to track delivered cells for several weeks following implantation, have also observed the development of various tissue types (including vascular, fibrotic, and mineralized) within constructs over the associated time-course (Olivo, Alblas et al. 2008, Geuze, Prins et al. 2010, Giannoni, Scaglione et al. 2010, Logeart-Avramoglou, Oudina et al. 2010, Rustad, Wong et al. 2012, Bago, Aguilar et al. 2013). Thus, the impact of this tissue invasion on the accuracy of BLI measurement remains unclear.

The work in this aim constitutes an initial examination of longitudinal BLI technique applicability for use with a cell-seeded construct of large volume (>200 mm^3), approaching the scale necessary to evaluate clinical applicability (Muschler, Nakamoto et al. 2004). Luciferase-labeled human mesenchymal stem cells (hMSCs) were delivered subcutaneously within two hydrogel systems to investigate firstly, the effects of cell dose and construct material on cell survival and secondly, the development of contiguous tissues, including vascular and fibrotic. Our objectives were to develop a technique

capable of tracking hMSCs implanted within large volume constructs and assess the potential influence of construct material and tissue ingrowth on *in vivo* BLI measurement.

3.2 Materials and Methods

3.2.1 hMSC Culture

Bone marrow-derived human mesenchymal stem cells (hMSCs) harvested from male donors 20-25 years old, with established multipotency, were purchased from the Texas A&M University Health Science Center, College of Medicine. Two individual donor cell lines were expanded at a starting density of 50 cells/cm^2 on petri dishes in Minimum Essential Medium alpha (αMEM) containing 16.7% fetal bovine serum (FBS; Atlanta Biologicals; Lawrenceville, GA) and 100 units/mL penicillin/100 μg/mL streptomycin/2 mM L-glutamine (PSL; Invitrogen; Carlsbad, CA) at 37ºC and 5% CO_2. For all cell culture conducted in this study, medium was changed twice weekly unless otherwise stated. At passage 2, cells from each donor were detached using 0.25% trypsin-EDTA (Invitrogen), combined in a 1:1 ratio to produce a pooled hMSC population, and then plated for lentiviral labeling at a density of 3,500 cells/cm^2.

3.2.2 hMSC Labeling

Cells were co-transduced using a lentiviral vector containing green fluorescent protein (GFP) and firefly luciferase (Luc) downstream of the ubiquitin promoter as previously described (Sun, Lee et al. 2009, Sheyn, Kallai et al. 2011). Briefly, hMSCs were suspended in polybrene (Sigma; St. Louis, MO) and viral vector at a MOI of 20 and incubated in flasks at a density of 10,000 cells/cm^2 overnight. Culture medium was replaced daily for 3-5 days, during which time the labeling efficiency of GFP/Luc hMSCs

was determined using fluorescence microscopy (Axio Observer; Carl Zeiss; Thornwood, NY) and flow cytometry (Accuri C6; BD Biosciences; San Jose, CA). Labeled hMSCs were replated at 500-700 cells/cm^2 and cultured for 5-7 days prior to analysis of proliferation, luciferin exposure, or *in vivo* construct preparation. *In situ* proliferation of labeled and unlabeled hMSCs (n=5) was measured using uptake of bromo-2'-deoxy-uridine (BrdU) (Roche Applied Science; Indianapolis, IN). Cells, plated at a density of 8,000 cells/cm^2, were incubated with BrdU for 90 minutes following 48 hours of culture. Subsequent steps were carried out according to manufacturer's instructions, using a DAPI nuclear counterstain (Invitrogen) prior to image acquisition. ImageJ (U.S. National Institutes of Health; Bethesda, MD) was used to quantify BrdU+ and DAPI+ events in triplicate for each sample. To investigate potential luciferin toxicity on cell viability, hMSCs (n=6) were plated at 2,000 cells/cm^2 and exposed to either continual (31.5 μg/mL) or pulsed (31.5 μg/mL for two 20-minute sessions) beetle luciferin (Fisher Scientific; Hampton, NH) or vehicle only. After 48 hours, samples were harvested for DNA content using the Quant-iT PicoGreen dsDNA Kit (Molecular Probes; Eugene, OR).

3.2.3 Alginate/Mesh and Agarose/Mesh Construct Preparation

A dual-syringe protocol, similar to that previously described by Kolambkar et al. (Kolambkar, Dupont et al. 2011) for production of acellular constructs, was adapted to embed the GFP/Luc hMSCs within hydrogels (final weight percentage 2% w/v). Cells were embedded in low molecular weight irradiated RGD-functionalized alginate (FMC BioPolymer; Ewing, NJ) (Alsberg, Kong et al. 2003, Silva and Mooney 2007) or SeaPlaque Agarose (Lonza; Basel, Switzerland) at densities of 0, 0.25, 0.5, 1.0, and 2.0

$x10^6$ cells/150 μL of gelled volume (Figure 1A). Following incorporation of hMSCs, alginate hydrogels were cross-linked by adding calcium sulfate (Sigma) to a final concentration of 8.4 mg/mL. Constructs, prepared by injecting 150 μL of cell-seeded hydrogel into an electrospun, polycaprolactone (PCL) nanofiber mesh tube (Kolambkar, Dupont et al. 2011), were then incubated in culture medium on custom made vertical supports within a 24-well low-attachment plate (Corning, Lowell, MA) for 2-6 hours prior to implantation (Figure 1B). To evaluate hMSC viability and distribution following inclusion in hydrogels, constructs (n=3) were stained with ethidium homodimer using a LIVE/DEAD Kit (Invitrogen) and imaged using an inverted microscope. To confirm seeding density, alginate and agarose hydrogels (n=3) ranging 0-1.0 $x10^6$ hMSCs/150 μL were evaluated for cell viability using the CellTiter-Blue assay (Promega; Fitchburg, WI). The viability assay was conducted according to manufacturer's instructions using a 3 hour reagent incubation period.

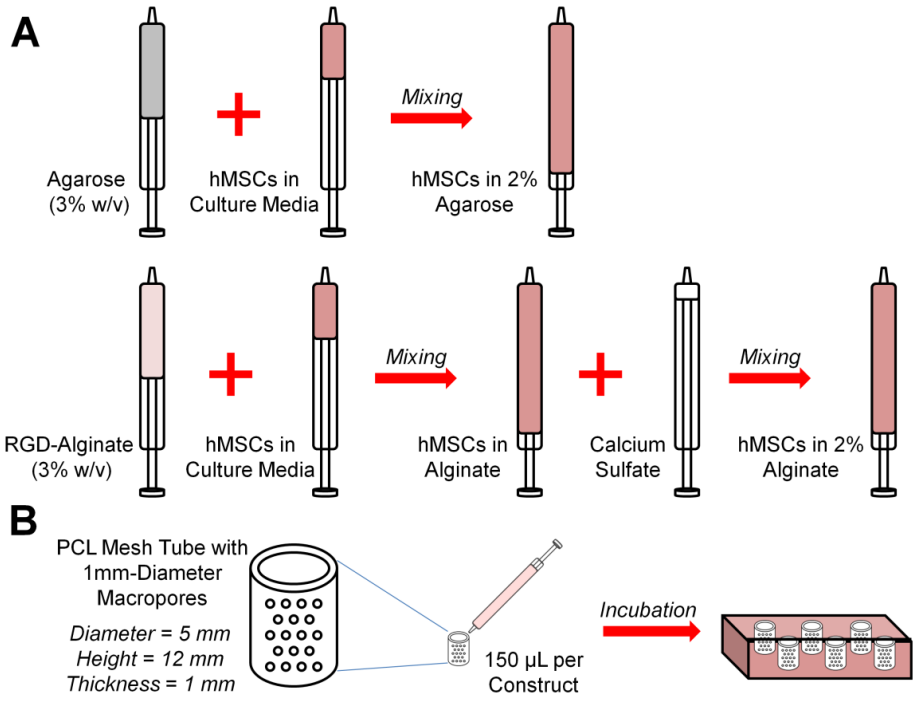

Figure 1: Hydrogel/Mesh Construct Preparation A) To produce hMSC-seeded hydrogels, components were added to 1-mL Luer-Lok syringes, attached via syringe connector, and mixed for 15 seconds. B) Resulting hydrogels were injected through a 20-gauge into PCL nanofiber mesh tubes (150 µL per construct) and incubated in control media prior to implantation.

3.2.4 Subcutaneous Implantation in Nude Rats

All animal procedures were conducted in accordance with the Georgia Institute of Technology Institutional Animal Care and Use Committee (IACUC) protocol #A10021. Eighteen 11-week-old female, athymic nude rats (Charles River Labs; Wilmington, MA) were anesthetized using isoflurane. Two incisions were made slightly lateral to the spine of each animal and a custom made tunneling device was used to create four subcutaneous pockets. One construct was placed in each pocket. Alginate or agarose constructs containing 0, 0.25, 0.5, 1.0, or 2.0 $x10^6$ hMSCs (n=4) were implanted in a balanced manner, such that every group contained an implant placed at each of the subcutaneous pocket locations and samples were randomly distributed across the operated animals. Following construct implantation, incisions were closed using suture and wound clips and rats were maintained under anesthesia to perform Day 0 BLI. After imaging, a 0.03 mg/kg subcutaneous dose of buprenorphine was administered to each animal. On Day 7, these samples were assessed for cell survival, construct vasculature, and histology.

3.2.5 *In Vivo* BLI

BLI was performed on each animal at Days 0 and 7. Rats were anesthetized using isoflurane and 300 μL luciferin (21 mg/mL in saline) was injected subcutaneously at a distance of 2-4 mm from the construct site. Using an *in vivo* imaging system (IVIS) Lumina machine (Caliper Life Sciences; Hopkinton, MA), animals were positioned with lateral side facing up and scanned at 10, 20, and 30 minutes post luciferin injection (10 second exposure; 12.5 cm field of view). The animals were then scanned on their other side and maintained in the dorsal position when not actively being scanned. BLI images were evaluated by demarcation of a 4 cm^2 elliptical region of interest (ROI) centered on

each construct using Living Image software version 3.2 (Caliper Life Sciences). BLI counts were normalized first by exposure time and ROI area and then to the corresponding Day 0 value for each sample. BLI signal profile values were calculated by normalizing the difference between two same-day BLI measures by the BLI value obtained at 30 minutes.

3.2.6 Construct Vasculature Quantification

Following Day 7 BLI acquisition, ten rats underwent a vascular perfusion protocol modified from Duvall *et al*. (Duvall, Taylor et al. 2004, Boerckel, Uhrig et al. 2011). Briefly, after induction of anesthesia, rats were maintained at 4% isoflurane and the thoracic cavity opened to insert an 18 gauge catheter (SURFLO Teflon IV catheter; Terumuo Medical; Somerset, NJ) through the left ventricle of the heart into the ascending aorta. The inferior vena cava was cut and 0.9% saline was perfused through the vasculature using a peristaltic pump (Masterflex; Cole Parmer; Vernon Hills, IL) until complete clearance was achieved. A solution of 0.9% saline containing 0.4% (w/v) papaverin hydrochloride was then perfused followed by 10% neutral buffered formalin (NBF) for 5 min. Animals received a final perfusion of 20-25 mL of the radiopaque contrast agent Microfil (Flow Tech; Carver, MA) and were left to cure at 4ºC overnight. In this way, animals were euthanized by the combined effects of isoflurane overdose and exsanguination. Explants were then excised, incubated in NBF for 24 hours, and imaged via microcomputed tomography (μCT) scans on a MicroCT42 (Scanco Medical; Brüttisellen, Switzerland) at 55kVp, 145μA, and a 12μm voxel size. Acquired slices were contoured to define a volume of interest (VOI) of tissue within the construct interior alone. To segment perfused vasculature from the surrounding soft tissue within each

construct, a range of global thresholds were applied and evaluated by visual inspection to determine a minimum threshold value which best reflected the 2D grayscale tomograms. This threshold and a low-pass Gaussian filter (sigma=1.2, support=2) were then applied to all explants evaluated.

3.2.7 Histological Analysis

Perfused samples were prepared for histological analysis following μCT scans. Constructs were paraffin embedded and 5μm-thick sections were cut using a microtome (Microm; Walldorf, Germany). Masson's trichrome and immunostaining for von Willebrand factor (vWF) were performed and images were collected using an Axio Observer fluorescent microscope (Zeiss). vWF staining was conducted using overnight incubation with rabbit anti-rat vWF primary (Abcam; Cambridge, MA) at 1:200 dilution, followed by an incubation of Alexa Fluor 568 donkey anti-rabbit secondary antibody (Invitrogen) and DAPI counterstain. Incubation in serum-free protein block (Dako; Carpinteria, CA) preceded application of each antibody.

3.2.8 Digest of Alginate/Mesh Explants and Flow Cytometry

In a parallel study to evaluate the applicability of Day 7 BLI measurement, alginate constructs containing a range of cell densities up to 1.0 $x10^6$ hMSCs were implanted using the previously described technique. Following Day 7 BLI, these constructs were analyzed using *ex vivo* flow cytometry. Rats were euthanized by CO_2 asphyxiation and constructs removed by careful dissection. Each explant was cut into ten pieces, placed in a digest solution of 1 mg/mL collagenase 1A (≥125 U/mg; Sigma) in Hank's Balanced Salt Solution (HBSS; Invitrogen), and incubated on a rocker plate at 37ºC for 30-40 minutes. After this time, digest solutions were analyzed by flow

cytometry until 20,000 live cell events had been collected or 2 minutes had expired. The remaining solution was then diluted in 10 mL of isotonic solution and analyzed using a Multisizer 3 Coulter Counter (Beckman Coulter; Brea, CA) which measures cell size and number distribution. A Flow Cytometry Size Calibration Kit (Invitrogen) was used to equate forward scatter (FSC) values from flow cytometry with diameter data from the Multisizer to obtain estimates of the live cell events per construct.

3.2.9 Data Analysis

For flow cytometry analysis of labeling efficiency on cell cultures, a GFP+ threshold was set using an unlabeled hMSC population with the assumption that 95% of the events were sub-threshold. Data were analyzed using one-way and two-way analyses of variance (ANOVA) with Tukey post hoc analyses and Minitab software (State College, PA,) unless otherwise stated. Linear regressions were conducted using GraphPad Prism 5 software (GraphPad Software; La Jolla, CA). For flow cytometry analysis of digested explants, the GFP+ event threshold was set at 20-fold higher than the mean GFP emission value for each sample to negate interference from surrounding tissue debris. A linear regression was performed on the Day 7 BLI vs. GFP+ events data for all samples. Correlations between BLI and vascular data were assessed using GraphPad software (two-tailed analysis; assumed Gaussian distribution) and data from cell-seeded constructs only. After performing a Grubbs' test on the acquired vascular data for each hydrogel type, one sample in the alginate construct data set was found to be a mathematical outlier and excluded from the analysis. Data are displayed as mean +/- standard error of mean (SEM) with corresponding values of n and statistical significance defined by $p<0.05$, if not otherwise specified.

3.3 Results

3.3.1 Validation of hMSC Labeling and Construct Embedding

GFP/Luc-labeled hMSCs retained a fusiform morphology and expressed GFP as early 24 hours following lentiviral co-transduction, as indicated by fluorescent microscopy (Figure 2A). Flow cytometry determined that the labeling efficiency was sufficient for *in vivo* tracking, with approximately 92% of hMSCs expressing GFP (Figure 2B). To investigate any impact of labeling on cell phenotype, proliferation and viability assays were conducted *in vitro*. Labeling did not impact hMSC proliferation and frequency of luciferin exposure had no effect on hMSC viability in culture (Figure 2C, D).

In preparation for *in vivo* delivery, the dual-syringe protocol used to embed hMSCs within hydrogel constructs was evaluated for resulting cell viability and seeding accuracy. It was determined that sufficient hMSC viability, GFP expression, and spatial distribution were achieved for both hydrogel types (Figure 3A). hMSC seeding density was validated for both agarose and alginate hydrogels (Figure 3B). Embedded cell dose was linearly related to metabolic activity for agarose (r^2=0.992) and alginate (r^2=0.977) gels. Spatial distribution of the embedded hMSCs was also confirmed using confocal microscopy (Figure 4).

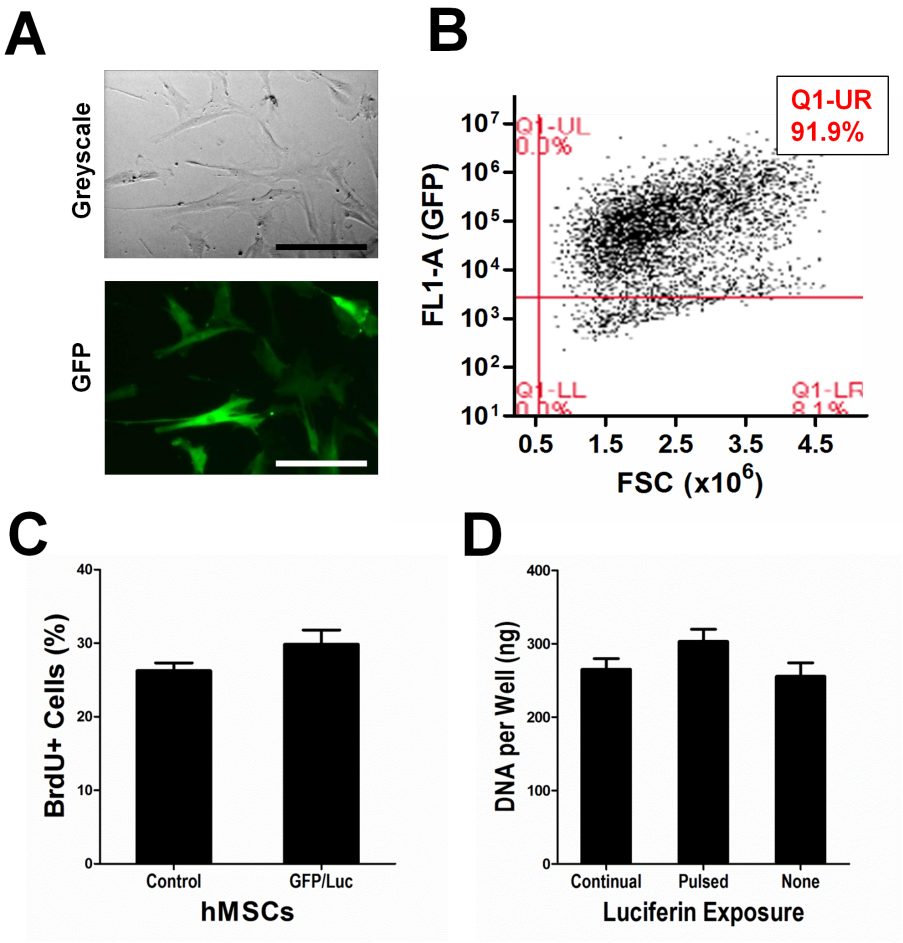

Figure 2: Characterization of GFP/Luc-Labeled hMSCs A) Labeled hMSCs retained a fusiform morphology and expressed GFP (green) as early as 24 hours following lentiviral co-transduction (scale bar = 100 µm). B) Flow cytometry analysis of GFP expression showed 91.9% cells to be labeled. C) hMSC proliferation was not affected by GFP/Luc labeling. D) Frequency of luciferin exposure had no impact on hMSC viability over 48 hours in culture.

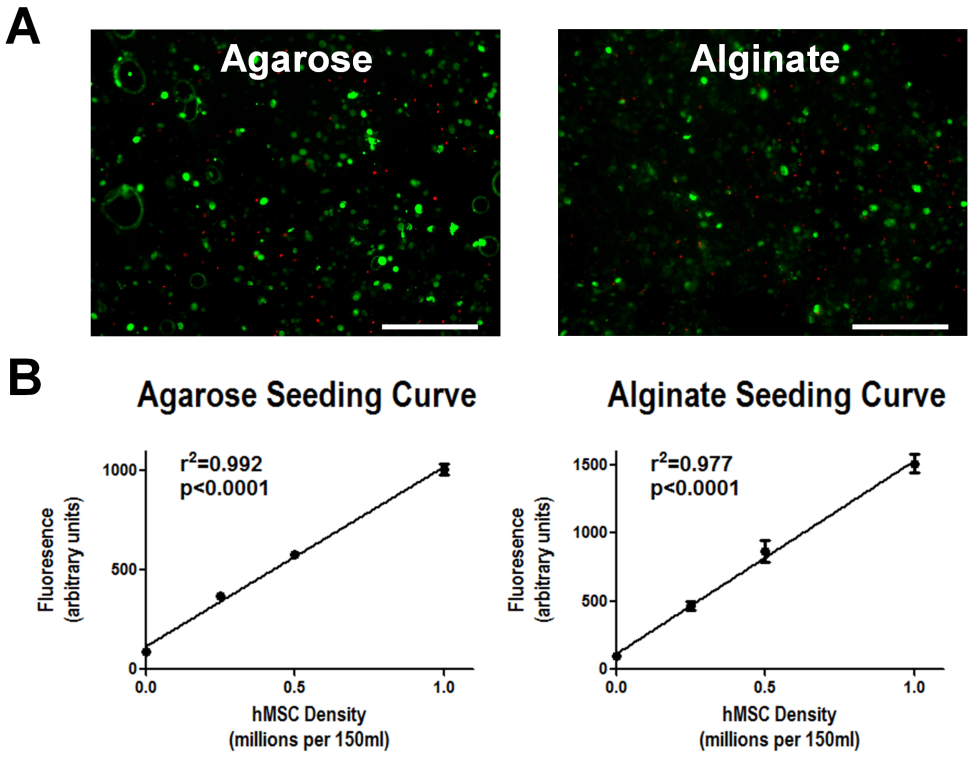

Figure 3: Evaluation of Dual-Syringe Hydrogel/Cell Delivery Labeled-hMSCs were incorporated into 2% w/v hydrogels using a dual-syringe technique. A) Seeded hMSCs remained largely viable (live = GFP (green); dead = ethidium homodimer (red)), retained GFP expression, and were well distributed following embedding (scale bar = 500 μm). B) Metabolic assays showed strong positive correlation to the seeding density of hMSC-seeded agarose and alginate hydrogels.

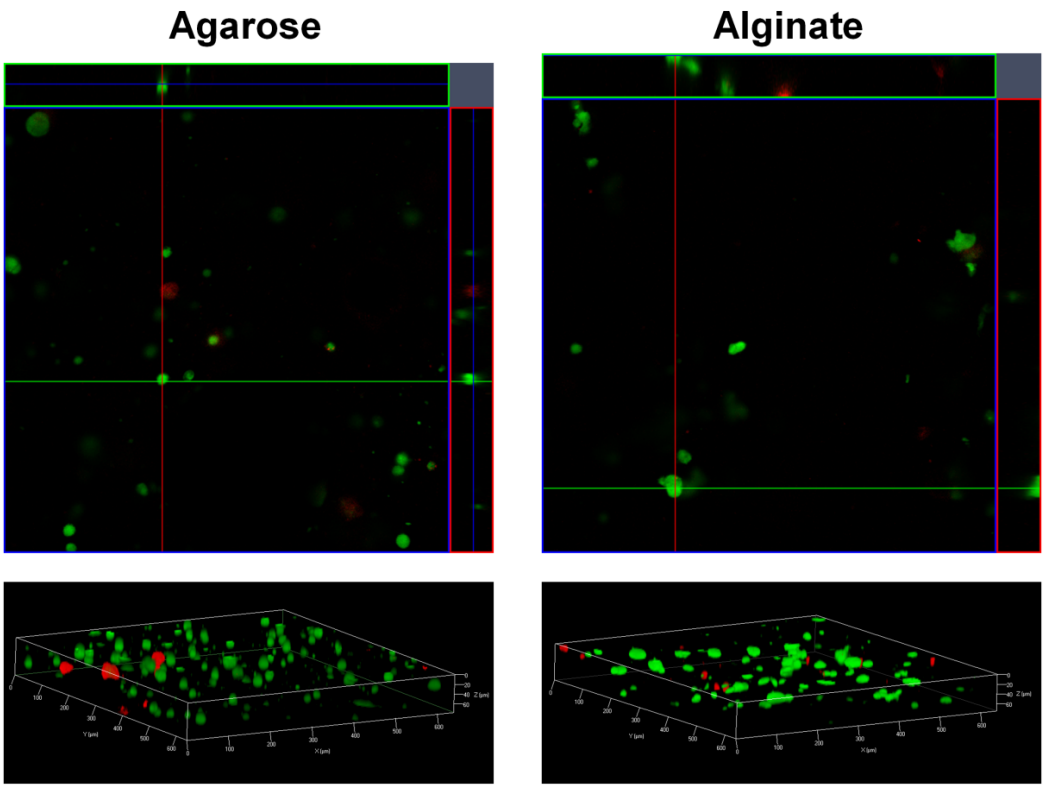

Figure 4: hMSC Spatial Distribution Following Dual-Syringe Technique Unlabeled hMSCs were incorporated into 2% agarose or RGD-alginate (0.25 million cells per 150 µL hydrogel), stained with calcein and ethidium homodimer, and imaged using confocal microscopy. Z-stack images illustrated the viability and spatial distribution of live (green) and dead (red) cells following hydrogel embedding.

3.3.2 Development and Implementation of BLI Tracking Protocol

hMSC-seeded constructs ranging in cell dose up to 2.0 x10^6 were subcutaneously implanted and Day 0 BLI was conducted at 10, 20, and 30 minute timepoints following injection of luciferin substrate (Figure 5A). Linear regression analysis demonstrated a strong relationship between BLI signal and cell number for each hydrogel type irrespective of BLI measurement time. The highest correlation coefficients for agarose (r^2=0.71) and alginate (r^2=0.91) constructs were observed using the 30 minute acquisition time (Figure 5B, C). Although a similar BLI protocol was effective for both hydrogel types, the magnitude of BLI signal differed with hydrogel type such that alginate constructs exhibited approximately 2-fold greater counts than agarose constructs at comparable hMSC doses.

To evaluate the effects of hydrogel type and cell dose on hMSC survival, BLI data obtained using the 30 minute acquisition protocol on Days 0 and 7 *in vivo* were compared. Although all agarose groups showed a decrease in live cell number over one week, the 0.25 x10^6 cell dose displayed a significantly higher cell survival ratio (67%) compared to all other doses (Figure 5D). For the alginate delivery vehicles, only the highest two cell doses exhibited a significant decrease in cell number (Figure 5E). By Day 7, a larger percentage of hMSCs remained viable for the 0.25 x10^6 cell dose group (61% survival) compared to the 2.0 x10^6 dose (3.8% survival).

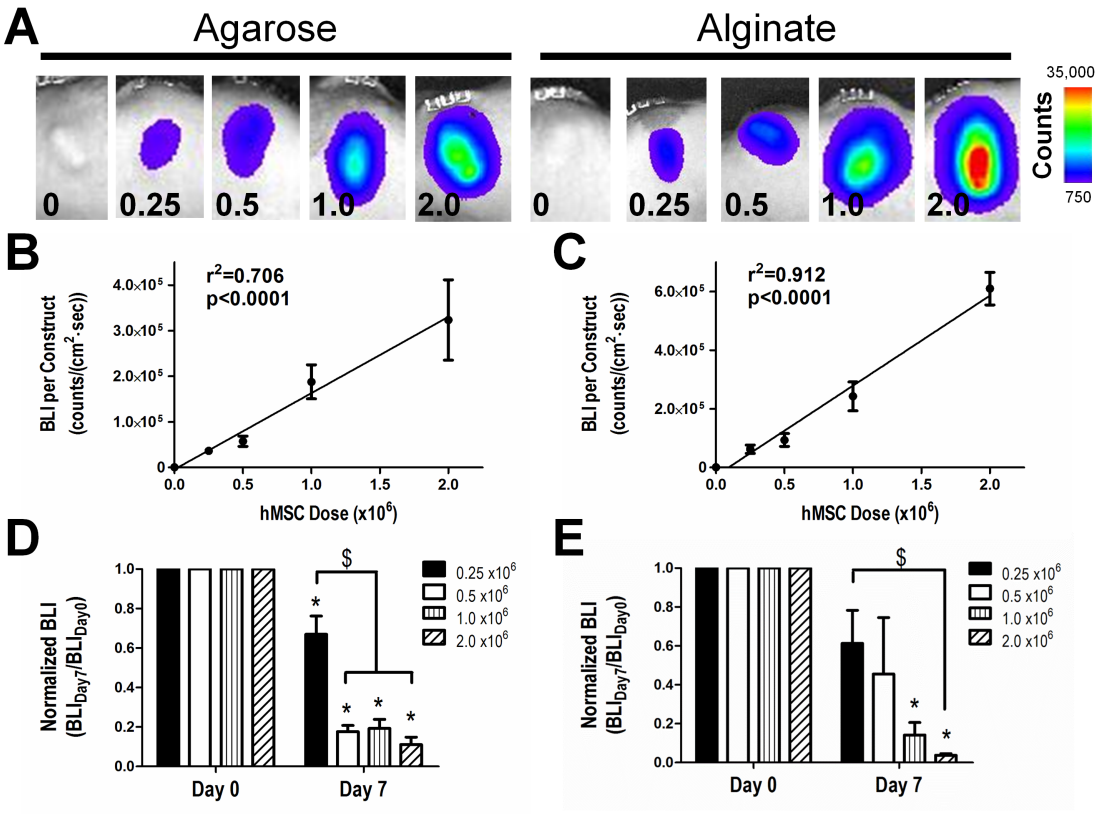

Figure 5: Development of BLI Protocol and Determination of hMSC Survival Agarose and RGD-alginate constructs were used to deliver a range of hMSC cell doses: 0 - 2.0 x106. Positive correlation between BLI signal and implanted cell number was observed at all imaging acquisition time points (10, 20, and 30 minutes) following luciferin delivery. A) Representative BLI heat-maps for agarose and alginate constructs using the 30-minute BLI protocol are shown. B) For agarose hydrogels, the highest correlation coefficient (r2 = 0.706) was observed using the 30-minute BLI protocol. C) The best fit (r2 = 0.912) for alginate hydrogels was also achieved using the 30-minute BLI protocol. D) By Day 7 post implantation, the number of live cells had decreased in all agarose cell groups, with the 0.25 x106 dose exhibiting proportionately the greatest cell survival. E) Within the alginate delivery system, the higher cell groups showed proportionately smaller live cell numbers after one week. The 0.25 x106 cell dose group had improved hMSC survival in comparison to the 2.0 x106 dose. ($ = $p < 0.05$ as indicated; * = $p < 0.05$ compared to Day 0)

3.3.3 Longitudinal Assessment of BLI Protocol

To investigate the applicability of BLI measurement following implantation *in vivo*, hMSC-seeded alginate constructs were explanted at one week and subjected to *ex vivo* analysis using flow cytometry. While Day 7 BLI counts were significantly correlated to GFP+ events under flow (Figure 6A), goodness of fit (r^2=0.422) was less than that observed on Day 0 (Figure 5C). In addition to examining the BLI signal for each construct on Day 7, BLI signal profile (defined as the change in BLI signal over the 30 minutes following luciferin delivery) was evaluated. The BLI signal profiles for alginate constructs on Day 7 suggested a delay in signal rise over the 30 minute imaging span compared to Day 0 (Figure 6B). This observation was supported quantitatively by evaluating the BLI signal at 10 minutes (BLI_{10min}/BLI_{30min}) for each construct group. This value was significantly decreased at Day 7 compared to Day 0 for both agarose and alginate constructs (Figure 6C, D). There was no apparent effect of cell dose on BLI signal kinetics.

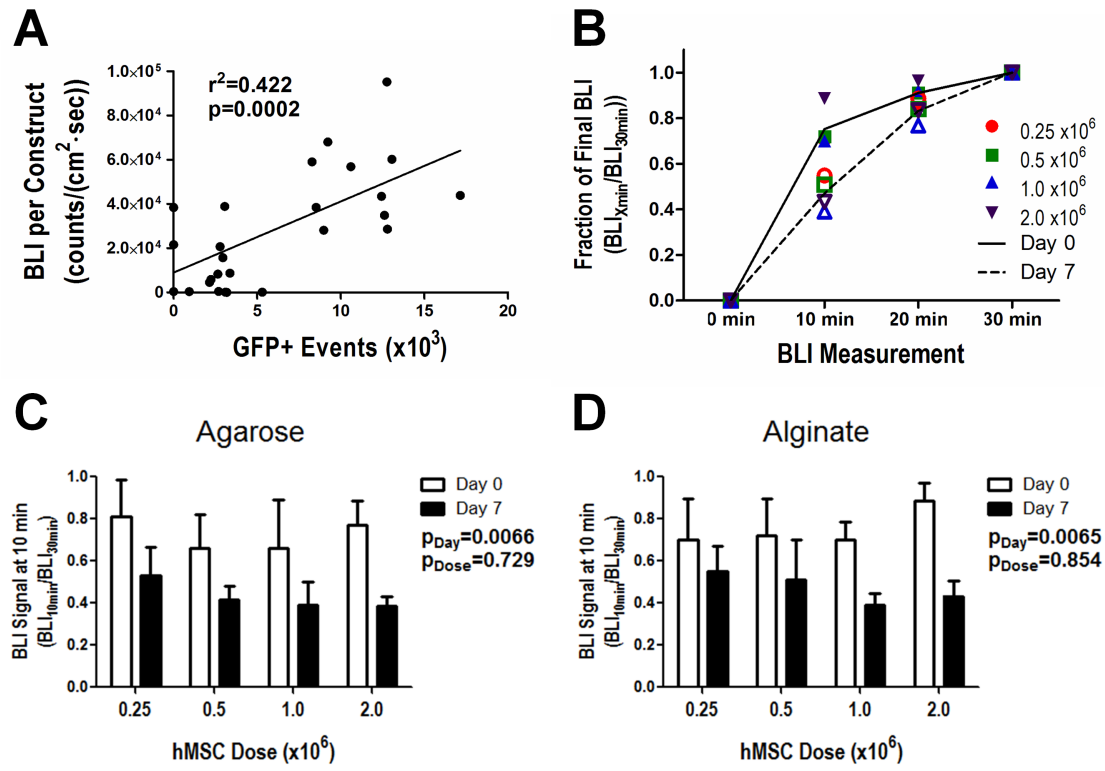

Figure 6: Shift in BLI Profile after 1 Week *In Vivo* A) At Day 7, construct BLI was positively correlated to GFP+ events (r2 = 0.422). B) BLI signal exhibited a delayed increase to 30-minute value after one week in vivo (solid line = Day 0 average; dashed line = Day 7 average). Day 0 and Day 7 cell dose averages represented by solid and outlined symbols, respectively. C) For agarose constructs, the increase in BLI signal following luciferin injection was attenuated on Day 7 compared to Day 0. D) Alginate constructs also showed a slower rate of progression to the 30-minute BLI signal on Day 7.

Tissue development within and exterior to the constructs on Day 7 was assessed using Masson's trichrome staining for fibrotic tissue. Tissue growth was localized predominantly to the construct exterior (Figure 7A). Irrespective of hydrogel type and cell dose, the construct mesh was lined with a layer of cells and fibrotic tissue. Construct interiors were composed of hydrogel islands containing vacant and cell-occupied pockets (Figure 7B). Qualitatively, pocket density appeared to be dependent on the initial cell dose, but independent of hydrogel type. The extent of tissue infiltration through macroscopic mesh pores and tube ends of each construct was variable and unrelated to hydrogel type, cell dose, or Day 7 BLI signal attenuation (Figure 7C, D). Although all samples contained a fibrous capsule, capsule thickness and vascularization were inconsistent and did not appear related to experimental group, interior construct vasculature, or Day 7 BLI profile behavior.

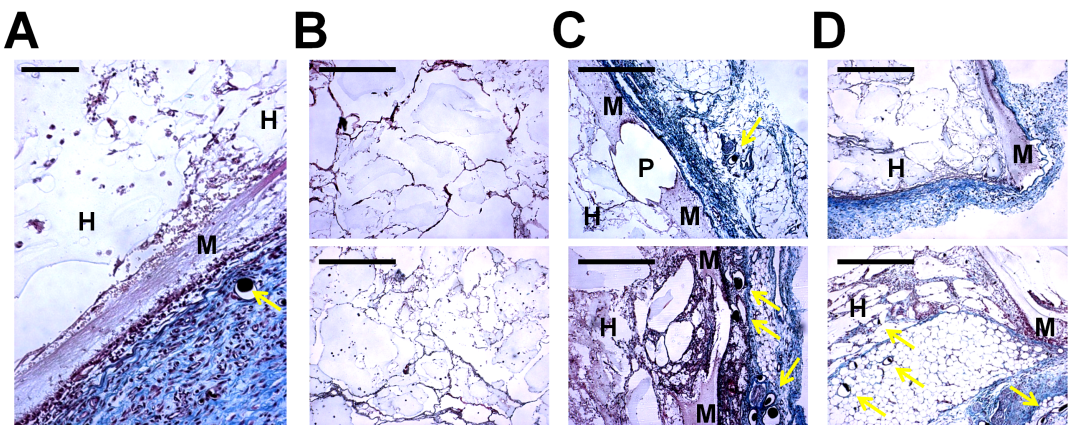

Figure 7: Construct Encapsulation and Tissue Ingrowth at 1 Week *In Vivo* A) Construct interiors were predominantly comprised of hydrogel islands (H) and the nanofiber mesh (M) exterior was lined with cells (red), fibrous capsule (blue), and regions of vascularized tissue (perfusion agent = black, indicated by yellow arrows; scale bar = 100 µm). B) Hydrogel islands within the construct interior contained vacant and cell-occupied pockets. Alginate constructs of acellular (above) and 2 x10^6 cell dose (below) are shown (scale bar = 500 µm). C) Tissue ingrowth through macroscopic pores (P; labeled in upper image only) in the construct mesh was variable (scale bar = 500 µm). D) Fibrous capsule extended along the mesh exterior and across the tube end. Construct ends contained mixed degrees of cellular infiltration and vascularization (scale bar = 500 µm).

3.3.4 Construct Vasculature

μCT reconstruction of the explant vasculature illustrated the presence of blood vessels surrounding the nanofiber mesh exterior as well as infiltrating the construct through 1mm-diameter macropores in the tube (Figure 8A). Quantification of vessel volume within the construct interior determined that all groups contained vasculature and there was no difference between cell dose groups for either hydrogel type (Figure 8B, C). Histological analysis was used to corroborate vascular perfusion data (Figure 8D). Both agarose and alginate groups showed pockets of perfusion contrast agent contained within immature vasculature localized near the construct periphery. Specificity of the perfusion technique was supported by co-localization of the contrast agent and vWF immunostaining.

The association between development of vasculature and live cell number (BLI signal) on Day 7 was examined. For agarose constructs, there was no correlation between vascular volume and either BLI signal (30-minute measurement) or BLI signal profile (Figure 9A, B). Alginate constructs showed no correlation between live cell number (BLI signal) and vascular volume on Day 7 (Figure 9C). However, alginate construct vasculature was significantly correlated to BLI signal profile (Figure 9D). Higher vascular volumes were associated with a smaller rise in BLI signal during the first 10 minutes following luciferin delivery, but accelerated BLI signal increase thereafter.

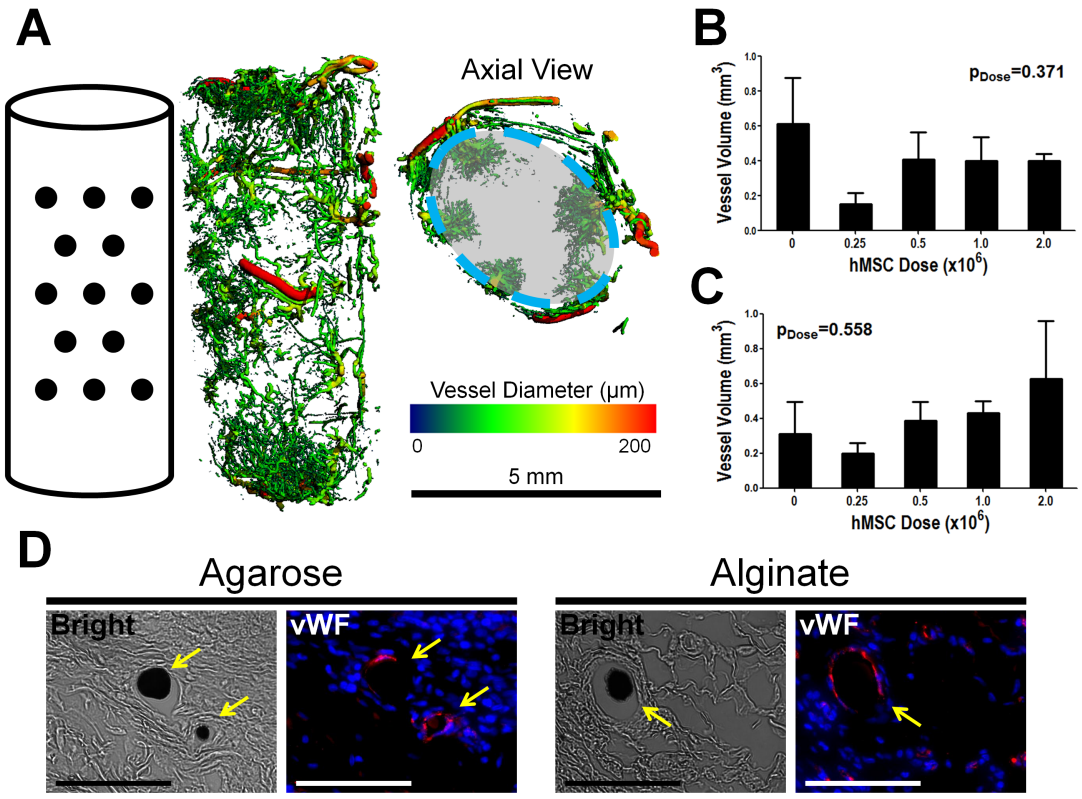

Figure 8: Construct Vascularization at 1 Week Post Implantation *In Vivo* A) Blood vessels were present along the construct exterior (orientation as indicated by illustration) as well as infiltrating macropores of the nanofiber mesh tube (axial view; dashed line signifies location of vascular contouring). B) Agarose construct vascular volume was independent of delivered hMSC dose. C) hMSC dose did not impact vasculature formed within alginate constructs. D) Vasculature (indicated by yellow arrows) within agarose and alginate constructs was confirmed histologically by brightfield microscopy (perfusion agent = black) and vWF immunostaining (endothelium = red, cell nuclei = blue; scale bar = 100 μm).

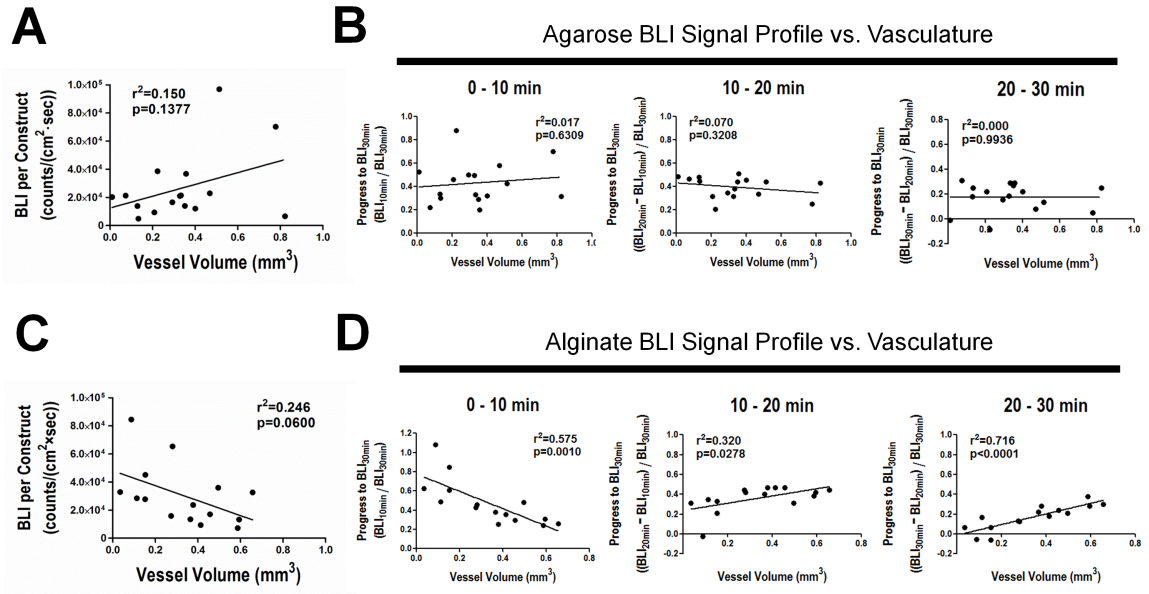

Figure 9: Construct Vascularization and BLI Signal Profile with Hydrogel Type A) 30-minute BLI signal and vasculature for hMSC-seeded agarose constructs were not correlated. B) Construct vasculature did not impact the BLI signal profile for agarose delivery vehicles on Day 7. C) 30-minute BLI signal and vasculature for alginate constructs were not correlated. D) Vascular volume perturbed the BLI signal profile for alginate constructs on Day 7. Increased vasculature was negatively correlated with an increase in BLI signal over the initial 10 minutes following luciferin injection and positively correlated with the rise in BLI signal thereafter.

3.4 Discussion

BLI has emerged an invaluable optical imaging technique for the development of cancer therapies and cell-based regenerative medicine strategies within experimental models (O'Neill, Lyons et al. 2010, de Almeida, van Rappard et al. 2011). In preparation to implement this monitoring tool in subsequent dissertation aims, we first developed and characterized a BLI protocol compatible with our large, multi-component delivery platform. Additionally, this effort investigated the effect of hydrogel type on BLI measurement and delivered hMSC viability.

Following subcutaneous implantation of agarose/mesh and alginate/mesh constructs, we found a strong correlation between BLI signal and viable cell number within each hydrogel type at Day 0. The implementation of a 30-minute window between luciferin injection and BLI acquisition provided a good representation of live cell number contained within these systems while operating within the constraints of an *in vivo* model. Although both hydrogel types showed a linear correlation between BLI signal and live cell number using the 30-minute imaging protocol, there was a difference in the magnitude of BLI signal measured between the agarose and alginate constructs. Previous work has noted a difference in BLI signal magnitude for materials of significantly distinct opacity and physiochemical properties (Logeart-Avramoglou, Oudina et al. 2010). However, the agarose and alginate constructs examined in this study each consist of translucent hydrogels reconstituted at similar density. Within these materials, diffusive transport is shown to be limited for molecules greater than 6.5-70 kDa, a size roughly 200-fold larger than that of luciferin (Tanaka, Matsumura et al. 1984, Pluen, Netti et al. 1999, Drury and Mooney 2003). Therefore, differences in luciferin transport kinetics are unlikely to account for the material-dependent magnitude of BLI signal. The observed

phenomenon could be due to a difference in construct light scattering properties resulting from dissimilar hydrogel rearrangement behavior. Following syringe-injected construct preparation, the ionically cross-linked alginate is capable of reforming under physiological conditions whereas agarose hydrogel would require a temperature increase in order to reassemble (Pluen, Netti et al. 1999, Lee and Mooney 2012).

Irrespective of hydrogel type, the lower cell doses were found to survive one week *in vivo* proportionally better than the high cell doses. Although the presence of a necrotic core is not seen *in vitro*, it is possible that cells compete for nutrients and only a fraction of the implanted cells could be supported *in vivo*. This is suggested by the fact that, in contrast to the proportional viability just discussed, there were no differences in absolute live cell number between groups on Day 7. This might indicate the attainment of an equilibrium live cell number that can be initially supported or sustained in the absence of an integrated vasculature. The alginate constructs supported improved hMSC viability in comparison to the agarose vehicles. This may be due to functionalization of the alginate hydrogel with the RGD peptide in order to facilitate cell attachment and manipulation (Lee and Mooney 2012). In the absence of RGD modification, agarose and alginate hydrogels lack adhesive sequences, resulting in abnormal morphology and reduced viability of encapsulated cells (Awad, Wickham et al. 2004).

Despite its employment for tracking viability and location of injected cells *in vivo*, BLI has yet to be validated for large 3D cellular constructs. Variations in tissue ingrowth over time following implantation lead to development of an inherently noisy system for optical imaging analysis (Muschler, Nakamoto et al. 2004). Even *in vitro*, transport properties of cell-seeded agarose and alginate hydrogels change over time in culture,

presumably due to cell-mediated matrix synthesis (Leddy, Awad et al. 2004). Previous work has corroborated *in vivo* BLI measurement to *ex vivo* construct analysis of luciferase content or histological staining (Jenkins, Oei et al. 2003, Olivo, Alblas et al. 2008, Logeart-Avramoglou, Oudina et al. 2010, Becquart, Cambon-Binder et al. 2012). In this report, we evaluated BLI measurement of large constructs subsequent to tissue ingrowth *in vivo* by directly quantifying labeled cell number on a whole construct basis. BLI signal correlated linearly to GFP+ flow cytometry events with a coefficient lower than that observed on Day 0. This reduction in correlation is suggestive of confounding variables present within the system on Day 7.

An examination of the factors which could affect the BLI signal on Day 7 reveals the dependency of BLI signal on oxygen and ATP levels within the tissue engineered constructs (O'Neill, Lyons et al. 2010). This is generally viewed as a positive feature, as it constrains measurement to the presence of live cells. However, in exceptionally hypoxic environments, such as those simulating a tumor necrotic core, oxygen can become rate limiting within the bioluminescent system (Moriyama, Niedre et al. 2008). Aside from the luciferase enzyme, photon release is highly dependent on the availability of luciferin substrate. Luciferin is a small molecule that readily diffuses through tissue (Honigman, Zeira et al. 2001). However, endogenous cell populations may deplete luciferin en route to the labeled cells of interest through uptake of substrate across the cell membrane (Berger, Paulmurugan et al. 2008). Adding to the complexity of luciferin availability, vascular networks have the potential to impact substrate delivery by providing a means of convective transport.

For both agarose and alginate constructs, increase of BLI signal over the 30-minute imaging window was attenuated on Day 7 in comparison to Day 0. To investigate whether the modified BLI profile might be attributed to hindered luciferin transport kinetics, tissue within and proximal to the explant on Day 7 was examined by histology. Neither fibrous capsule thickness nor degree of the peripheral vascular network exhibited a relationship to hydrogel type, initial cell dose, or Day 7 BLI profile. However, the presence of a fibrous capsule across all experimental groups may be responsible for the attenuated BLI profile observed on Day 7, as a logical consequence of such tissue development would be restricted luciferin availability.

Although MSC delivery has been shown to promote angiogenic and vasculogenic processes, this effect was not significant in the current study, perhaps due to particulars of the vehicle or timescale examined (Au, Tam et al. 2008, Egana, Danner et al. 2009, Jackson, Nesti et al. 2012). Vasculature did weakly correlate to BLI signal behavior in the alginate constructs over the 30-minute imaging window, suggesting an impact of vascular volume on luciferin availability within the construct. Interestingly, greater vasculature correlated to a delayed rise in BLI signal following luciferin delivery initially, but then accelerated BLI signal increase between 10 and 30 minutes. No correlations were observed in the agarose constructs. These results provide further insight on the temporal and matrix dependent effects of vasculature on BLI measurements (Levenberg, Rouwkema et al. 2005).

In support of our Aim I hypothesis, these results validate that BLI can be implemented to longitudinally track hMSC number within our large, multi-component delivery system. However, this work draws attention to the impact of hydrogel carrier

type as well as tissue and vascular ingrowth on longitudinal BLI measurement. Such observations motivate that validation of BLI protocol and investigation of potentially confounding variables be conducted on a system-by-system basis in order to draw representative conclusions. Subsequent application of BLI tracking within this dissertation considered the limitations of this analytical technique in evaluating the potential impact of platelet lysate utilization and cell aggregation on implanted MSC survival. Furthermore, results from this study encouraged continued testing of the alginate carrier platform on the basis of its improved support of hMSC viability compared to agarose hydrogel.

CHAPTER 4 EVALUATION OF HUMAN PLATELET LYSATE FOR MESENCHYMAL STEM CELL DELIVERY

4.1 Introduction

Human platelet lysate (hPL), a solution produced from platelet-rich plasma (PRP), is enriched in growth factors including platelet-derived growth factor (PDGF), vascular endothelial growth factor (VEGF), latent transforming growth factor beta (TGF-β), insulin-like growth factor (IGF), basic fibroblast growth factor (bFGF), and epidermal growth factor (EGF) (Reed, Fitzgerald et al. 2000, Rendu and Brohard-Bohn 2001, King and Reed 2002, Maguire and Fitzgerald 2003, Lohmann, Walenda et al. 2012). hPL has been explored as a substitute to fetal bovine serum (FBS) for cell culture and found to have advantages exceeding that of eliminating xenogeneic concerns. Exposure of human mesenchymal stem cells (hMSCs) to hPL *in vitro* has positive effects including increased proliferation, decreased doubling time (DT), maintained immunophenotype, and delayed senescence (Doucet, Ernou et al. 2005, Muller, Kordowich et al. 2006, Reinisch, Bartmann et al. 2007, Schallmoser, Bartmann et al. 2007, Carrancio, Lopez-Holgado et al. 2008, Avanzini, Bernardo et al. 2009, Azouna, Berraeis et al. 2011, Flemming, Schallmoser et al. 2011, Griffiths, Baraniak et al. 2013, Rubio-Azpeitia and Andia 2014).

Although hPL has predominantly been explored in liquid form, its fibrinogen content enables it to produce a hydrogel as well (Harrison and Cramer 1993, Walenda, Hemeda et al. 2012). The initial objectives of this thesis aim were to examine whether hPL could be implemented as either a pre-treatment or co-delivery strategy to augment the (i) survival and (ii) facilitated bone regeneration of hMSCs delivered within alginate

matrices. However, in pursuing these studies, concerns arose as to whether the utility of hPL could be accurately informed using rodent pre-clinical testing models. Thus, immunocompromised (Nude rat) and syngeneic (Lewis rat) animal models were studied for issues of xenogenicity and species variability.

Immunocompromised animal models, such as the athymic Rowett nude (rnu) rat, enable pre-clinical testing of human components (e.g. proteins, cells, and tissues) due to deficient T-cell-mediated immune response (Festing, May et al. 1978, Berridge, O'Kech et al. 1979, Rolstad 2001). However, while Nude rats are without T cell function, the activities of other lymphocyte subtypes, including B cells and natural killer cells, remain conserved (de Jong, Steerenberg et al. 1980, Vos, Kreeftenberg et al. 1980). Furthermore, in addition to immune defenses imparted by the host, mechanisms retained in the delivered human therapeutic must be considered as well. A range of anti-animal antibodies is naturally occurring in human circulation and thereby present in collected PRP (Kricka 1999, Cramer 2000, Dhurat and Sukesh 2014). Existence of xenoantibodies in combination with complement proteins, the concentrations of which are amplified upon lysis of platelet α-granules during hPL production, allow for the possibility of classical or alternative complement system activation resulting in membrane attack complex (MAC)-mediated host cell death (Romanella, Aminian et al. 1997, Blair and Flaumenhaft 2009, Rubio-Azpeitia and Andia 2014, Morgan 2015). Apart from immunity related challenges, species mismatch between the delivered components (hMSCs and hPL) and endogenous cell populations present within an immunocompromised model system could potentially limit observed therapeutic efficacy (Zara, Siu et al. 2011).

Limitations of an autologous or syngeneic rodent model, such as the inbred Lewis

rat, include species-dependent properties of the therapeutic components being scrutinized. Interspecies variability of bone tissue characteristics includes biochemical composition, osteoblast phenotype, and osteoinduction behavior (Aerssens, Dequeker et al. 1994, Aspenberg and Turek 1996, Yang, Yuan et al. 1996, Torricelli, Fini et al. 2003). Of particular interest for cell-based bone regeneration strategies is the divergent behavior of human vs. rat MSCs, comprised of distinct immunosuppressive, cell signaling, and osteogenic differentiation characteristics (Chaudhary and Avioli 1997, Ren, Su et al. 2009, Huang, Cai et al. 2013). Variation in platelet properties as a function of animal species has been previously explored, uncovering both significant similarities and differences in platelet proteome depending on the study and species examined (van den Dolder, Mooren et al. 2006, Yu, Leng et al. 2010). While delivery of platelet-derived plasma (PRP) has promoted bone repair within several species-matched models, including rat and rabbit, the effect of platelet-derived factors on cell-based bone regeneration is left minimally interrogated (Rai, Oest et al. 2007, Zhang, Huang et al. 2013). Even in culture, the impact of exposing rMSCs to rPL-supplemented media is largely unproven in comparison to the well-established hMSC/hPL relationship. Some studies have found the exposure of rMSCs to rat platelet-derived factors to further proliferative or osteogenic capacity, yet these findings remain preliminary due to a scarcity of corroborating investigations (van den Dolder, Mooren et al. 2006, Huang and Wang 2012).

The following research examined the utility of hPL as a pre-treatment or co-delivery strategy to augment hMSC survival and construct vasculature upon implantation within an immunocompromised rodent model. Subsequently, the potential limitations of

using rodent pre-clinical testbeds for the evaluation of hPL were investigated via *in vitro* experimentation.

4.2 Materials and Methods

4.2.1 MSC Culture

Bone marrow-derived hMSCs were purchased from the Texas A&M University Health Science Center and cultured as previously described (Allen, Gazit et al. 2014). Briefly, two donor cell lines were expanded in Minimum Essential Medium alpha (αMEM) containing 16% v/v fetal bovine serum (FBS; Atlanta Biologicals; Lawrenceville, GA) and 100 units/mL penicillin/100 µg/mL streptomycin/2 mM L-glutamine (PSL; Invitrogen; Carlsbad, CA) at 37ºC and 5% CO_2. At passage 2, cells were detached using 0.25% trypsin-EDTA (Invitrogen) and combined 1:1 to form a pooled hMSC population. Lewis rMSCs, characterized for multipotency, were purchased (Sciencell Research Laboratories; Carlsbad, CA) and expanded until passage 2 in similar culture conditions.

4.2.2 Platelet Lysate Preparation

Recently expired human platelet-rich plasma (PRP) from seven donors was acquired from the American Red Cross, pooled, and stored at -20°C (Griffiths, Baraniak et al. 2013). Rat PRP was prepared from the whole blood of twelve Lewis rats and pooled. In a terminal procedure approved by the Georgia Institute of Technology Institutional Animal Care and Use Committee (IACUC) protocol #A10021, blood was drawn from anesthetized rats via cardiac stick and transferred to vacutainers containing

acid citrate dextrose (BD Worldwide; Franklin Lakes, NJ). Collected blood underwent sequential rounds of centrifugation (10 min @ 1,200 RPM, 5 min @ 1,500 RPM, and 5 min @ 1,500 RPM) using an IEC Centra CL2 (Thermo Scientific; Waltham, MA) with the non-erythrocyte volume collected subsequent to each step. Collected product was centrifuged (10 min @ 3,500 RPM), concentrated through partial supernatant removal to achieve a platelet concentration matching that of the human PRP (1-1.5 $x10^6$ platelets/μL), and stored at -20°C. To generate human and rat platelet lysate (PL), PRP was thawed, re-frozen, and thawed a second time. PDGF-AB content (n=3) for each PL product was measured via species-specific ELISA assay (R&D Systems; Minneapolis, MN). To produce hPL supplemented media, hPL was filtered through a 0.8/0.2 μm membrane (Pall Corporation; Port Washington, NY) and added to αMEM containing PSL and 2 units/mL heparin (Sagent Pharmaceuticals; Schaumburg, IL). To prepare heat-inactivated hPL (hPL-HI) media, hPL was heated to 56°C for 30 minutes prior to filtration and use. When processed identically to hPL, rPL media was observed to form a hydrogel in culture. Thus, rPL supplemented media was prepared using an increased heparin concentration (5 units/mL), but otherwise comparably.

4.2.3 2D *In Vitro* Analysis

To investigate the effect of hPL culture on hMSC expansion, passage 3 cells (n=9) were expanded over 8 days in FBS (16%) or hPL (5%) supplemented media and cell DT was calculated. To determine whether hPL culture had prolonged impact, expanded hMSCs were transitioned to serum starvation media containing 1% w/v bovine serum albumin (BSA) and cultured under normoxic (17% O_2) or hypoxic (5% O_2) conditions (n=11-12). Change in DNA content through 1 and 3 days was quantified via

the Quant-iT PicoGreen dsDNA Kit (Molecular Probes; Eugene, OR). To explore the impact of PL culture on MSC expansion over multiple passages, hMSCs (n=3-6) plated at 250 cells/cm^2 were cultured in FBS (16%) or hPL (5% or 10%) supplemented media over 4 days, at which point cells were enumerated. This was repeated twice more, such that cell DT was calculated for passages 2-4. rMSCs (n=5-6) cultured in FBS (16%) or rPL (5% or 10%) supplemented media were similarly analyzed. To evaluate acute response to hPL culture, hMSCs or rMSCs at passage 3 were plated at 5,000 cells/cm^2 in FBS (16%) media. Following a 48-hr adhesion period, media was switched to FBS (16%), no serum (NS), hPL (10%), or hPL-HI (10%) supplemented. Cells were stained with calcein and ethidium homodimer at 24 hrs using a LIVE/DEAD Kit (Invitrogen) and imaged by inverted microscope (Axio Observer; Carl Zeiss; Thornwood, NY). At 24 hrs, C5b-9 supernatant concentration (n=4) and DNA content (n=11-12) were quantified. C5b-9 was measured via a MicroVue SC5b-9 Plus assay (Quidel; San Diego, CA) and compared alongside negative (acellular) and positive (containing 10% v/v heat-aggregated immunoglobulin G (HAGG; Quidel) controls. Samples harvested at 0 hrs were used to calculate percent change in DNA.

4.2.4 Alginate Construct Preparation

Prior to alginate embedding, hMSCs were lentivirally co-transduced with a vector containing ubiquitin promoter-driven expression of green fluorescent protein (GFP) and firefly luciferase (Luc) as previously described (Sun, Lee et al. 2009, Sheyn, Kallai et al. 2011). Using a dual-syringe mixing technique, GFP/Luc hMSCs were incorporated into RGD-functionalized alginate (FMC BioPolymer; Ewing, NJ) at a density of 0.5 x10^6 cells/150 µL with 0 or 20% v/v hPL. hMSC-seeded hydrogels (2% w/v) were then cross-

linked via calcium sulfate (8.4 mg/mL; Sigma-Aldrich; St. Louis, MO) and constructs were prepared by injecting 150 μL of resultant hydrogel into an electrospun, polycaprolactone (PCL) mesh tube.

4.2.5 3D *In Vitro* Analysis

For the investigation of hPL pre-treatment, hMSC-seeded constructs were prepared using GFP/Luc hMSCs expanded in either FBS (16%) or hPL (5%) media. In the pre-cultured group, alginate/mesh constructs were assembled 3 days prior to implantation and cultured on vertical supports in media matching that of the expansion conditions. In the case of direct syringe injection, hydrogels were prepared the morning of surgery and constructs were assembled in the surgical suite immediately prior to implantation. hMSC viability (n=3) and DNA content (n=4-6) within these treatment groups at the time of implantation was evaluated using the LIVE/DEAD (Invitrogen) and PicoGreen (Molecular Probes) kits.

For investigation of hPL co-delivery, hMSC-seeded constructs with 0 or 20% hPL (n=8) were cultured on custom made vertical supports within 24-well low-attachment plates over 1 week. Longitudinal bioluminescent imaging (BLI) was performed on Days 0, 1, 3, and 7. At each timepoint, beetle luciferin (Fisher Scientific; Hampton, NH) was added to the culture media (0.21 mg/mL) and incubated 20 minutes prior to image acquisition (5 second exposure; 12.5 cm field of view) using an IVIS Lumina machine (Caliper Life Sciences; Hopkinton, MA). BLI images were evaluated within the Living Image software version 3.2 (Caliper Life Sciences) using a circular region of interest (ROI) centered over each well. Total BLI counts were divided by exposure time and ROI area (Absolute BLI), then normalized to the corresponding Day 0 value for each sample

(Normalized BLI). Culture media (2 mL/well) was replaced following each timepoint. In a parallel study, constructs (n=2) were stained at 48 hrs using a LIVE/DEAD kit and imaged (Zeiss) to observe cell morphology. Evaluation of hPL release was performed on hMSC-seeded and acellular constructs with 0 or 20% hPL (n=4) cultured over 1 week with media collected at 4, 12, 24, 72, and 168 hrs and analyzed via hPDGF-AB ELISA assay.

4.2.6 Surgical Procedures

Surgical implantation was conducted in accordance with the Georgia Institute of Technology IACUC protocol #A10021 as described previously (Allen, Gazit et al. 2014). Ten 11-week-old female, athymic nude rats (Charles River Labs; Wilmington, MA) were anesthetized using isoflurane. Two dorsal incisions were made to prepare four subcutaneous pockets per animal. In the pre-treatment study, hMSCs expanded in FBS (16%) or hPL (5%) media were alginate-embedded and either assembled as constructs 3 days prior to surgery (to allow pre-culture in media matching that of the expansion conditions) or assembled as constructs within the surgical suite following syringe crosslinking 4-7 hrs prior (n=6; Figure 10A). In the co-delivery study, all hMSC-seeded or acellular constructs with 0 or 20% hPL were assembled within the surgical suite (n=10; Figure 10B). In all studies, an alginate/mech constructs was delivered to each pocket and incisions were closed using suture and wound clips. A 0.03 mg/kg subcutaneous dose of buprenorphine was administered to each animal following Day 0 BLI.

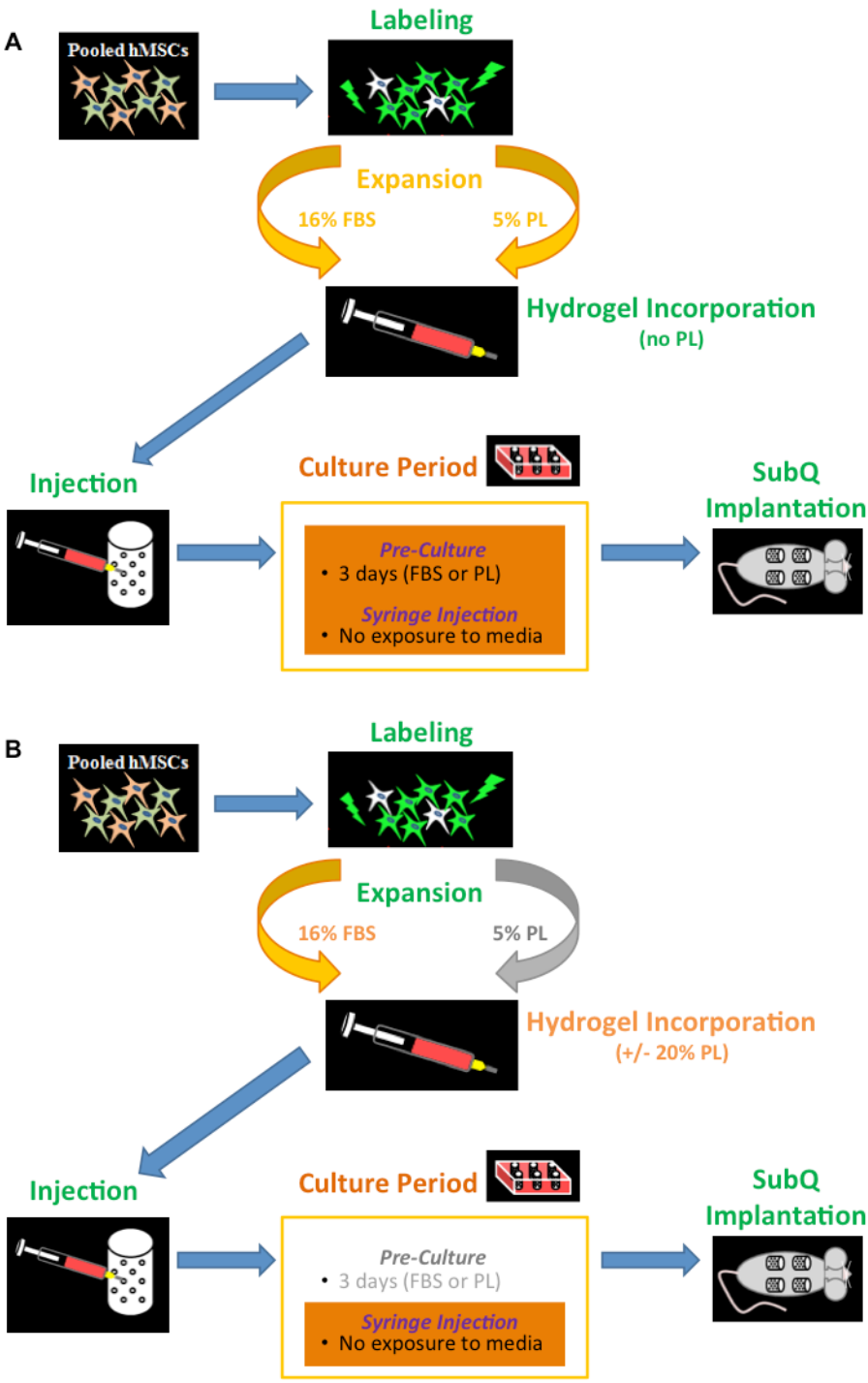

Figure 10: hPL Pre-Treatment and Co-Delivery Experimental Designs A) To examine hPL as a pre-treatment strategy, labeled hMSCs were expanded in FBS or hPL media, assembled into alginate/mesh constructs and either pre-cultured over 3 days or immediately implanted. B) To investigate the effect of co-delivered hPL, all hMSCs were expanded in FBS media, assembled into alginate/mesh constructs with or without 20% v/v/ hPL, and immediately delivered *in vivo*.

4.2.7 *In Vivo* and Explant Analyses

Longitudinal BLI was performed on Days 0 and 7 (pre-treatment study) or Days 0, 1, 7, and 14 (co-delivery study) using a previously established protocol (Allen, Gazit et al. 2014). Rats were anesthetized and 300 µL luciferin (21 mg/mL in saline) was injected subcutaneously at a distance of 2-4 mm from each construct site. The animals were scanned on either side 30 minutes post luciferin injection (10 second exposure; 12.5 cm field of view). BLI images were evaluated by demarcation of a 4 cm^2 elliptical ROI and calculations were carried out as described in sub-section 4.2.5. Following Day 14 BLI acquisition, rats underwent vascular perfusion using an 18 gauge catheter (SURFLO Teflon IV catheter; Terumuo Medical; Somerset, NJ) inserted into the ascending aorta and peristaltic pump (Masterflex; Cole Parmer; Vernon Hills, IL). Saline (0.9% w/v), papaverin hydrochloride (0.4% w/v in saline), neutral buffered formalin (10% v/v), and the radiopaque contrast agent Microfil (Flow Tech; Carver, MA) were perfused in order. Explants were excised and imaged via microcomputed tomography (µCT) scans on a MicroCT42 (Scanco Medical; Brüttisellen, Switzerland) at 55kVp, 145µA, and a 12µm voxel size. Acquired slices were contoured and segmented using a low-pass Gaussian filter (sigma=1.2, support=2) to evaluate vascular volume within the construct interior alone. To reduce variability associated with the perfusion procedure, construct vascular volume was normalized by that of the intra-animal "acellular + 0% hPL" group (n=8). Following µCT scans, explants were paraffin embedded and histologically sectioned via microtome (Microm; Walldorf, Germany). 5µm-thick sections were stained with hematoxylin and eosin (H&E) or Masson's trichrome and imaged (Zeiss).

4.2.8 Statistical Analysis

Values are displayed as mean +/- standard error of mean (SEM) with corresponding values of n and statistical significance defined by $p<0.05$. Data were analyzed using two-way analyses of variance (ANOVA) with Tukey post hoc comparisons within the Minitab software (State College, PA). For C5b-9 evaluation, statistical analysis excluded acellular control groups.

4.3 Results

4.3.1 Implantation of hMSCs Receiving hPL Pre-Treatment

In preparation for *in vivo* delivery, the effect of hPL (5%) culture on hMSC expansion was compared to traditional FBS (16%) supplemented media. hPL culture was found to decrease cell doubling time (Figure 11A). Furthermore, upon removal of hMSCs from hPL media, the benefits of initial culture showed long-lasting effects. Culture conditions produced comparable hMSC expansion through Day 1, as measured via DNA content (Figure 11B). However, beneficial effects of preceding hPL culture ($p=0.001$) and subsequent hypoxic conditions ($p<0.001$) were observed by Day 3 (Figure 11C).

A

Media	Doubling Time (Days)
FBS	1.95 ± 0.03
PL	1.64 ± 0.09

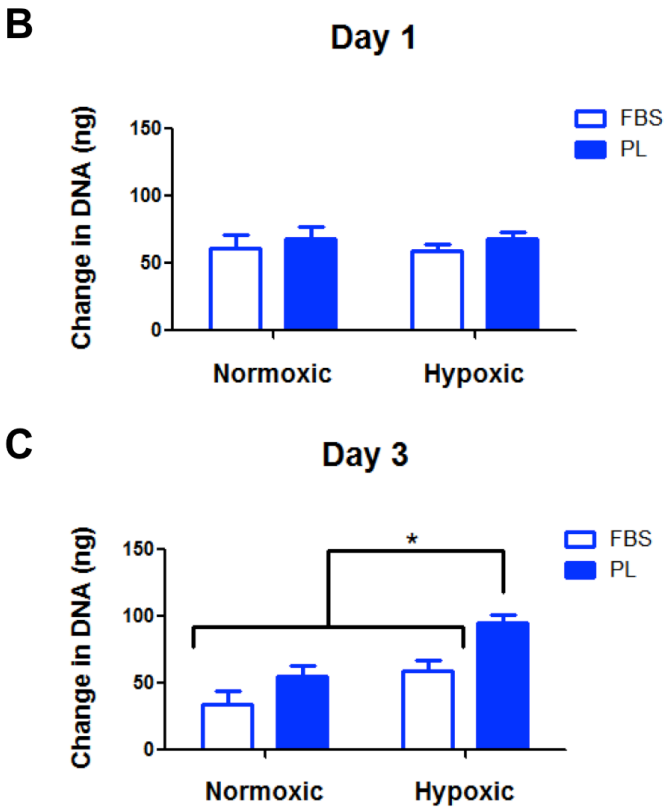

Figure 11: Effects of hPL Culture on hMSC Expansion A) Expansion in hPL (5%) media led to a decrease in cell DT compared to FBS (16%) culture. B) Following removal of hMSCs from expansion media stimulus and culture under normoxic or hypoxic conditions, no differences in continued expansion were observed through Day 1. C) However, by Day 3, improved hMSC expansion resulting from previous hPL culture ($p=0.001$) or subsequent hypoxic conditions ($p<0.001$) were demonstrated.

Given the promising consequence of hPL pre-treatment on hMSCs *in vitro*, this strategy was further challenged using a subcutaneous implant model. GFP/Luc hMSCs were expanded in either FBS or hPL media and then either delivered via immediate syringe injection (SI) or construct pre-culture (PC) strategy. Hydrogels delivered in the syringe injectable treatment were prepared the morning of surgery and assembled into alginate/mesh constructs within the surgical suite immediately prior to implantation. Pre-cultured alginate/mesh constructs were assembled 3 days before surgery and cultured within media matching that of the hMSC expansion conditions. Analysis of hMSC-seeded treatments at the time of implantation revealed a qualitatively reduced fraction of live cells (Figure 12A) and decreased DNA content (Figure 12B) contained within each PC group (PC, FBS; PC, PL).

In vivo BLI performed immediately following implantation determined that significantly fewer hMSCs were delivered within the hPL-expanded, pre-cultured (PC, PL) treatment group (Figure 13A). By Day 7, viable cell number within the hPL-expanded, syringe injected (SI, FBS) and FBS-expanded, pre-cultured (PC, FBS) groups decreased from their corresponding Day 0 values. Examining the surviving fraction of delivered hMSCs through Day 7, only the FBS-expanded, syringe injected (SI, FBS) treatment exhibited no reduction in viable cell number, maintaining hMSC viability better than all other delivery strategies (Figure 13B). Despite these differences observed in delivered hMSC survival, all treatments achieved comparable construct vascular volume (Figure 13C).

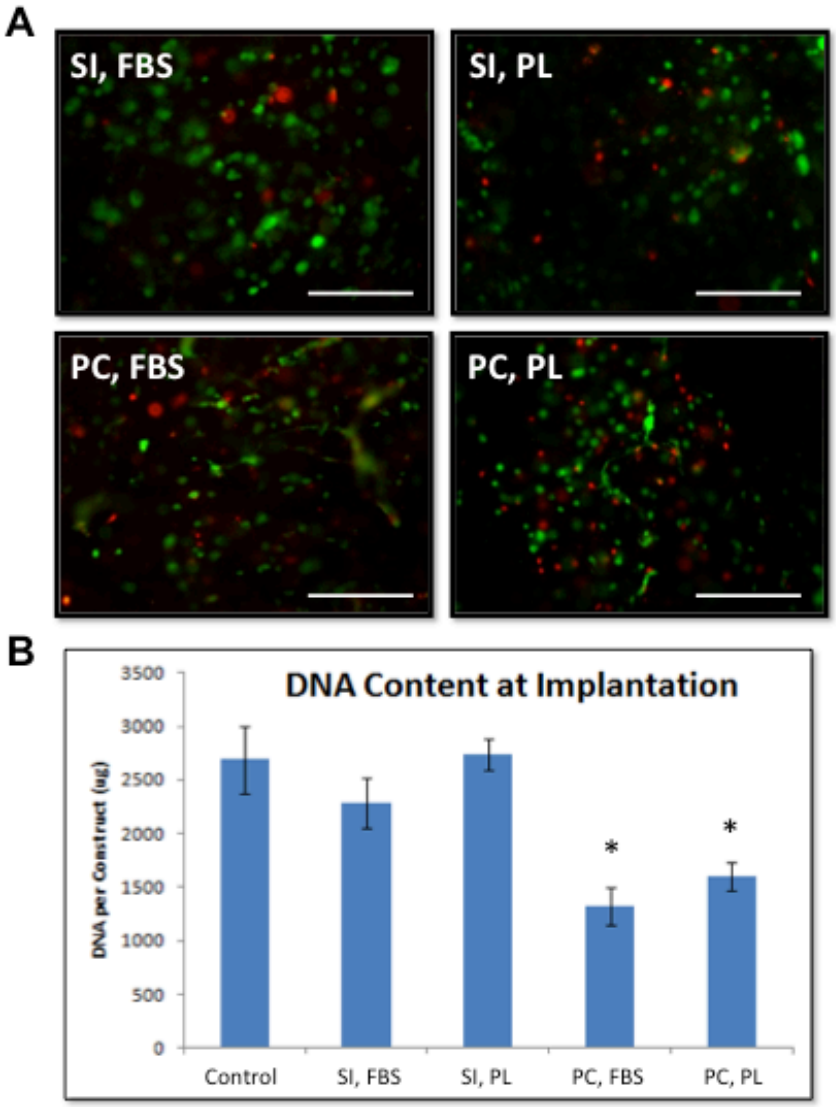

Figure 12: hMSC Viability within hPL Pre-Treatment Groups on Day 0 A) Embedded hMSCs (live = GFP (green); dead = ethidium homodimer (red)) displayed qualitatively reduced viability in the pre-cultured (PC) alginate/mesh constructs (scale bar = 150 μm). B) Measures of DNA content at the time of implantation were consistant microscopy observations, exhibiting decreased DNA in response to construct pre-culture (PC). No effect of expansion media type (FBS vs. PL) was observed.

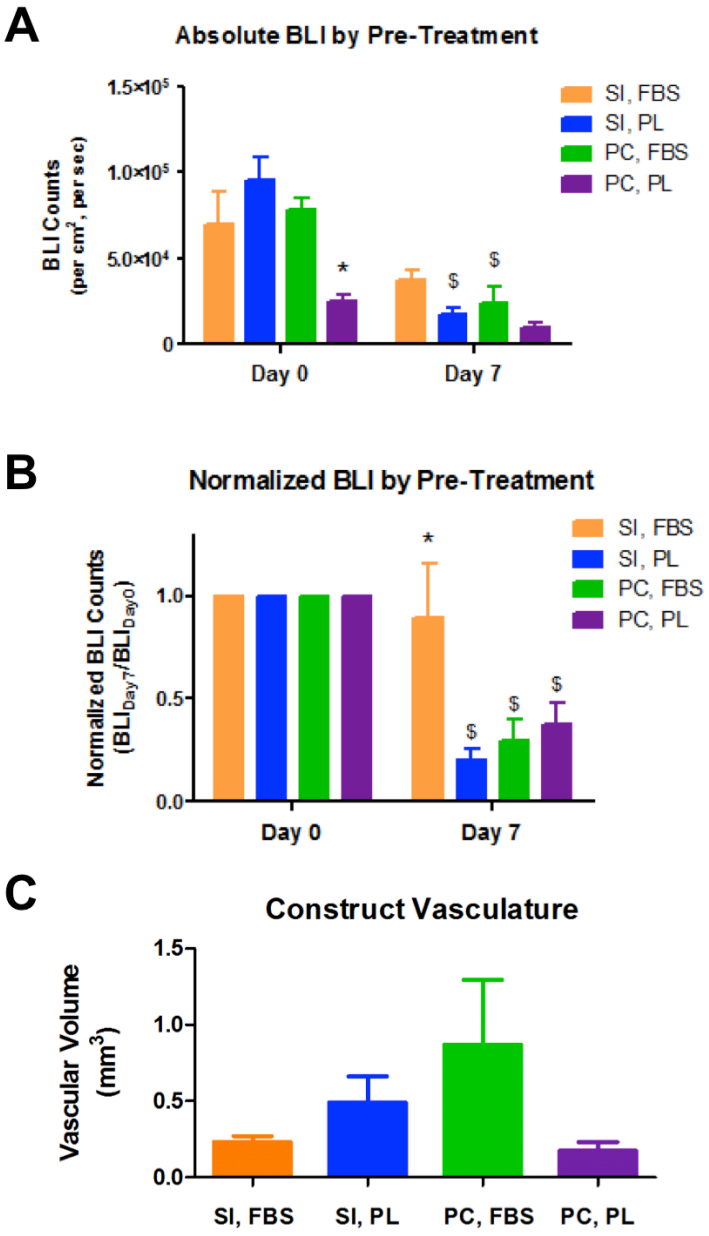

Figure 13: hMSC Survival and Construct Vasculature through Day 7 *In Vivo* A) Fewer viable hMSCs were delivered within the hPL-expanded, pre-cultured group (PC, PL) on Day 0. B) Delivery of FBS-expanded hMSCs within immediately implanted alginate/mesh constructs (SI, FBS) exhibited no decrease in hMSC surviving fraction *in vivo*, outperforming all other treatments strategies by Day 7. C) Pre-treatment strategy had no effect on construct vascular volume. (* = $p < 0.05$ within same timepoint vs. all other treatments; $ = $p < 0.05$ within same treatment vs. Day 0)

4.3.2 Addition of hPL to Hydrogels *In Vitro*

Having evaluated the effects of hPL pre-treatment, the potential utility of hPL co-delivery was explored. hPL (20% v/v) was incorporated into RGD-alginate hydrogels using a dual-syringe protocol. Resultant hydrogel was injected into PCL mesh tubes to form constructs and cultured over 7 days. Following an initial 48 hrs of culture, alginate-embedded hMSCs displayed a largely rounded morphology irrespective of whether hPL had been added to the hydrogel (Figure 14A). Persistence of incorporated hPL within the constructs was monitored by measurement of hPDGF-AB released into the surrounding media (Figure 14B). hPDGF-AB released by hPL-containing groups over one week was higher for the acellular constructs ($p<0.001$). Both acellular and hMSC-seeded constructs exhibited a burst release of growth factor, with roughly 70% and 95%, respectively, of measured hPDGF-AB release occurring during the first 12 hrs *in vitro*.

Addition of 20% hPL to hMSC-seeded constructs promoted an overall increase ($p<0.001$) in live cell number *in vitro*, as evaluated via absolute (Figure 14C) and normalized (Figure 14D) longitudinal BLI. Comparing within timepoints, signal for the hPL-containing hydrogels was significantly greater on Day 1, displaying an effect size of 32% (absolute BLI) or 66% (normalized BLI), depending on the BLI metric. Within treatment group, BLI recorded on each day was statistically distinct from all other timepoints.

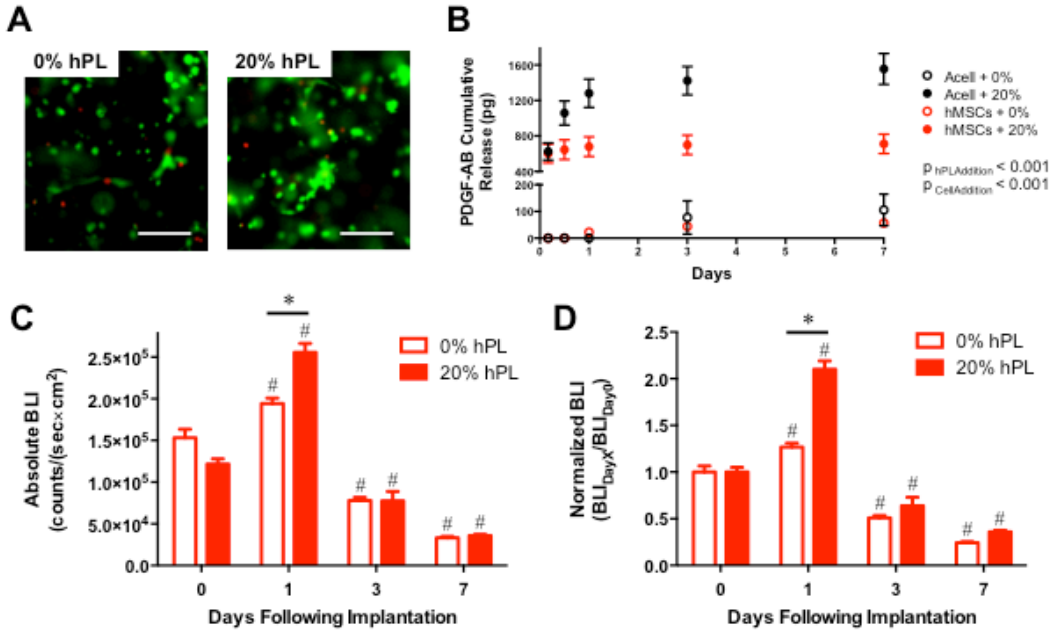

Figure 14: Addition of hPL to Hydrogels *In Vitro* A) Embedded hMSCs (live = GFP (green); dead = ethidium homodimer (red)) display similar rounded morphology at 48 hrs in culture irrespective of hPL addition (scale bar = 100 µm). B) The majority of hPDGF-AB release from hPL-containing constructs occurred by 12 hrs *in vitro*, with cumulative release over one week being greater for acellular constructs compared to hMSC-seeded. C) hPL addition enhanced hMSC live cell number in vitro ($p<0.001$), as evaluated via absolute BLI counts. D) hPL addition enhanced hMSC live cell number in vitro ($p<0.001$), as evaluated via normalized BLI counts. (* = $p < 0.05$ as indicated; # = $p < 0.05$ within same treatment vs. all other days)

4.3.3 Implantation of hPL Containing Constructs

hMSC-seeded and acellular constructs with or without incorporated hPL were implanted subcutaneously in Nude rats and monitored using BLI over 14 days. hPL incorporation was observed to have no impact on delivered cell number, as evaluated via absolute (Figure 15A) and normalized (Figure 15B) bioluminescent counts. Both treatment groups displayed 46-47% and 2% hMSC survival rates through Days 1 and 14, respectively.

To quantify the impact of hPL and hMSC delivery on construct vascularization, rats underwent vascular perfusion on Day 14 and explant vasculature was analyzed using μCT. Neither hPL incorporation ($p=0.354$) nor hMSC delivery ($p=0.199$) had a significant impact on construct vessel volume (Figure 15C). However, representative μCT reconstructions indicate that the distribution of vessels throughout the construct may have been altered as a function of treatment, with hPL-containing constructs exhibiting qualitatively enhanced infiltration of vessels towards the construct interior (Figure 15D).

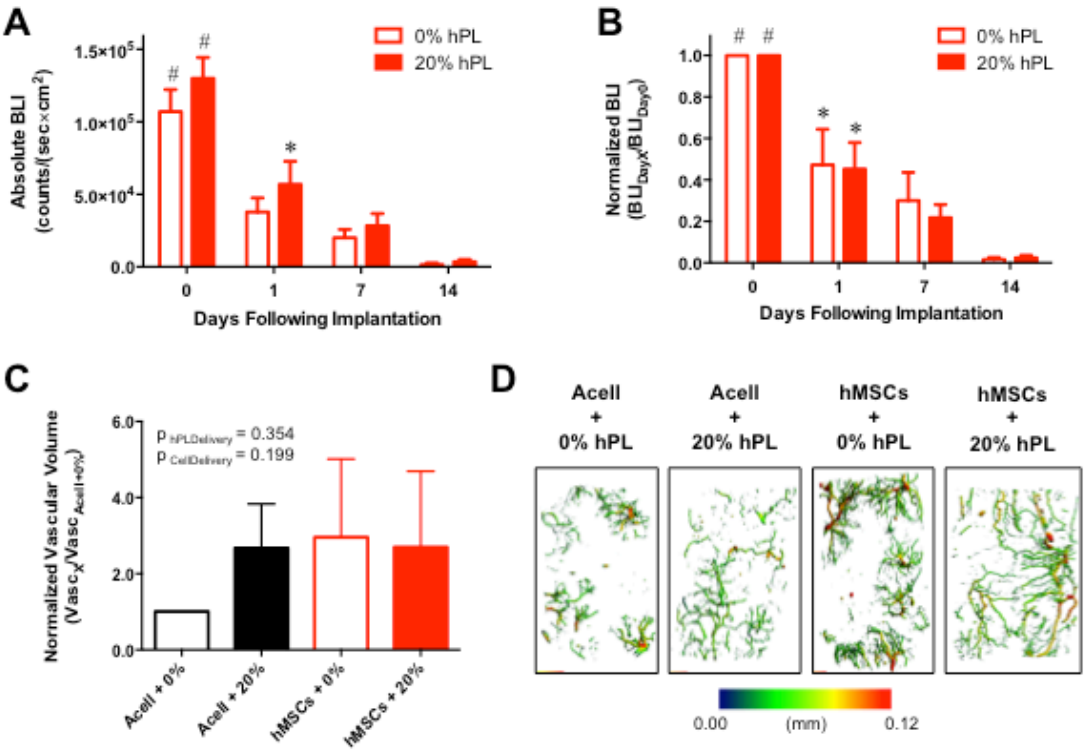

Figure 15: *In Vivo* Bioluminescent Imaging (BLI) and Construct Vasculature hMSC-seeded and acellular constructs with or without hPL were implanted subcutaneously in Nude rats and explanted on Day 14 following vascular perfusion. A) hPL co-delivery had no effect on hMSC live cell number in vivo (p=0.084), as evaluated via absolute BLI counts. B) Normalized BLI revealed no impact of hPL addition on hMSC survival in vivo (p=0.719), with <50% and 2% of cells remaining viable in either group on Days 1 and 14, respectively. C) Neither hPL addition (p=0.354) nor hMSC delivery (p=0.199) affected construct vascular volume. D) Representative vascular reconstructions illustrate that the spatial distribution of vessels may be altered as a function of treatment. (# = $p < 0.05$ within same treatment vs. all other days; * = $p < 0.05$ within same treatment vs. Day 14)

Tissue development and morphology at the construct interior were examined using H&E staining. Compared to all other treatments, acellular constructs lacking co-delivered hPL exhibited qualitatively reduced breakdown of alginate hydrogel and development of surrounding tissue (Figure 16A). In contrast, the development of tissue surrounding alginate pieces and the presence of central vasculature (denoted by green arrows) was observable in all treatment groups containing hMSCs and/or hPL (Figure 16B-D). Alginate-encased punctate staining was present only within the hMSC-seeded groups, suggesting this staining marked the remnants of delivered cells. To further investigate the effects of hPL incorporation on hMSC delivery, Masson's trichrome staining was used to visualize granulation tissue within and surrounding the constructs. hPL addition was found to have qualitatively no impact on fibrotic tissue development within the center of the constructs (Figure 16E, F). Similarly, no effect of hPL co-delivery on the extent of fibrous tissue lining the interior (INT) or exterior (EXT) of the PCL mesh (M) tubes demarcating the construct periphery was observed (Figure 16G, H).

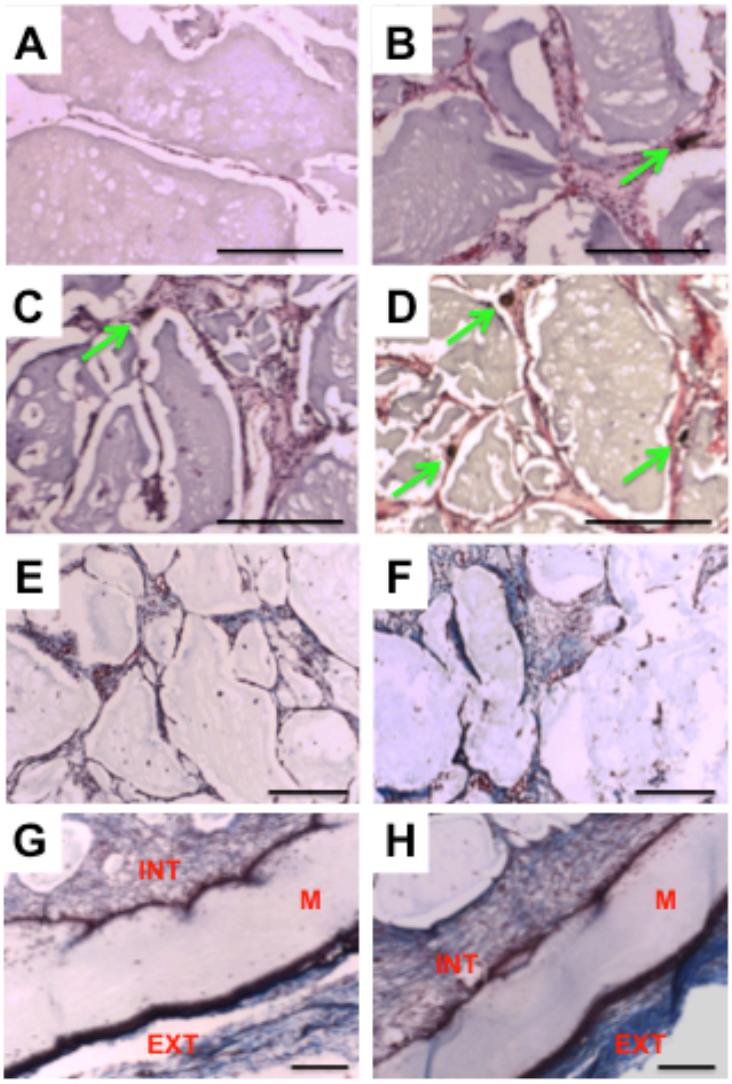

Figure 16: Tissue Development and Morphology on Day 14 Post Implantation A) Minimal breakdown of alginate pieces and development of surrounding tissue was observed within the acellular constructs lacking co-delivered hPL (H&E; scale bar = 250 μm). B-D) Delivery of hPL (B), hMSCs (C), or both (D) qualitatively increased tissue development, including vasculature, and alginate breakdown at the construct center (H&E; perfusion agent = black, indicated by green arrows; scale bar = 250 μm). E-H) hMSC-seeded constructs with (F,H) and without (E,G) co-delivered hPL contained a similar amount of granulation tissue present at the construct center as well as lining the PCL mesh (M) tube interior (INT) and exterior (EXT) (Masson's trichrome; scale bar = 250 μm).

4.3.4 Limitations of an Immunocompromised Rodent Animal Model

rMSCs were leveraged as a model rodent cell population in order to explore the response of rodent host cells to hPL exposure. Adhered hMSCs and rMSCs were introduced to media supplemented with FBS (16%), hPL (10%), hPL-HI (10%), or no serum over a 24-hr period *in vitro*. Little or no hMSC death was observed across all media treatments, as assessed via live/dead staining and fluorescent microscopy (Figure 17A). In contrast, a large degree of rMSC death was observed in the hPL media condition (Figure 17B). Unexpectedly, no serum culture elicited minimal death for either cell type. Qualitative findings were supported by the quantification of DNA content for each treatment (Figure 17C). DNA content increased for all serum-supplemented hMSC conditions (+40-55% compared to 0-hr measurement), with no statistical difference between groups. rMSCs cultured in FBS (+118%) and hPL-HI (+95%) media exhibited a greater increase in DNA compared to equivalent hMSC groups. Conversely, rMSCs cultured in hPL media had decreased DNA content (-47%). Culture of either cell type under serum-free conditions exhibited minimal change in DNA content (+1%).

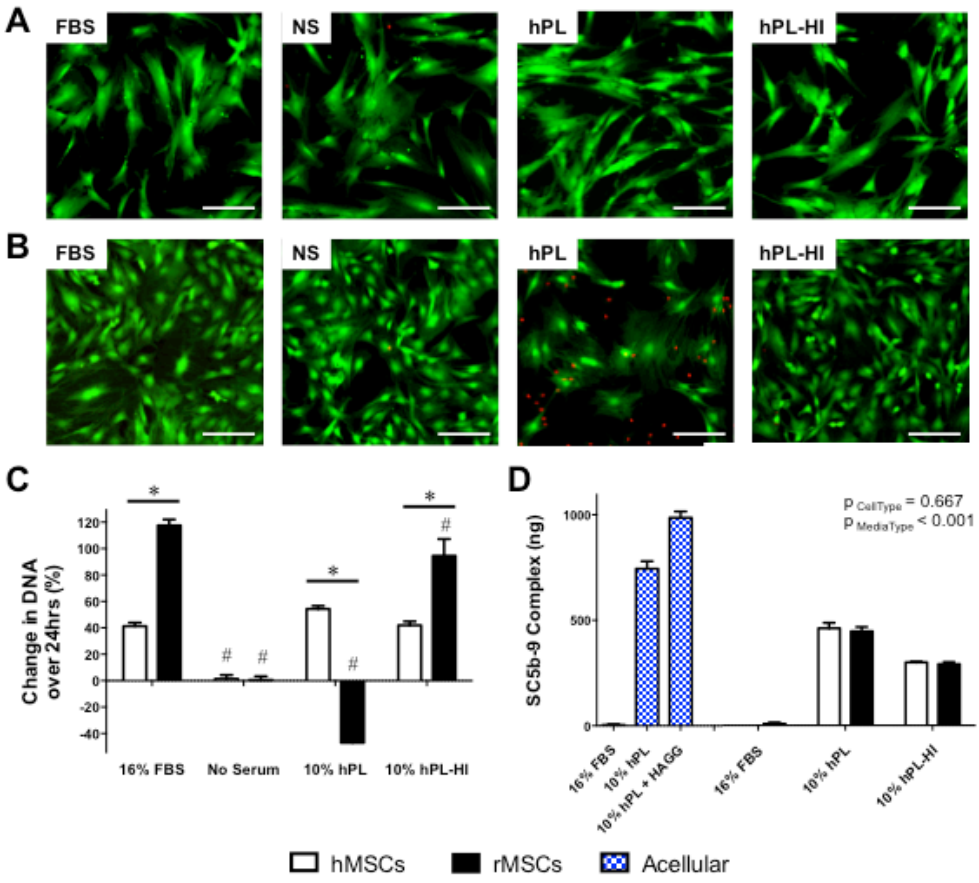

Figure 17: Limitations of an Immunocompromised Rodent Model Adhered hMSCs and rMSCs were introduced to media supplemented with FBS (16%), hPL (10%), hPL-HI (10%), or no serum over a 24-hr period in vitro. A) Little or no hMSC death was observed across all media treatments (live = GFP (green); dead = ethidium homodimer (red); scale bar = 100 μm). B) A large extent of rMSC death was observed for the hPL media condition only (scale bar = 100 μm). C) Quantification of DNA content supported qualitative microscopy observations, with hPL culture of rMSCs comprising the only serum-supplemented treatment to result in a DNA decrease. D) Similar concentrations of C5b-9 complement complex were measured for hMSCs and rMSCs ($p=0.667$) across all serum-supplemented media conditions. (* = $p < 0.05$ as indicated; # = $p < 0.05$ within same cell type vs. all other media conditions)

To determine whether the rescue in rMSC viability with hPL heat inactivation was due to the deactivation of complement proteins, the concentration of terminal complement complex (C5b-9) in each media condition at 24 hrs was measured (Figure 17D). Acellular data (collected in a parallel experiment) illustrated that C5b-9 complexes formed spontaneously in hPL-, but not FBS-, supplemented media and that complement was capable of being further activated with the addition of HAGG. Despite noted differences in cell viability, similar concentrations of C5b-9 complex were measured for hMSCs and rMSCs in each media condition ($p=0.667$), suggesting complement proteins were not the heat-inactivated component responsible for hPL-mediated rMSC death.

4.3.5 Limitations of a Syngeneic Rodent Animal Model

rPL was prepared from Lewis rats and analyzed *in vitro* to evaluate its similarity to the hPL product. hPL PDGF-AB content (56.4 pg/mL) was two orders of magnitude greater than that present in rPL (0.2 pg/mL), as measured via species-specific ELISA assays (Figure 18A). To observe whether differences in growth factor content may impact the response of MSCs to PL-supplemented culture, MSCs were expanded in same-species PL (5% or 10%) media over several passages (Figure 18B). Expansion of hMSCs in hPL culture promoted a dose-dependent decrease in cell DT by passage 4 compared to FBS (16%) expansion. In contrast, expansion of rMSCs in 5% rPL media increased cell DT at passages 4 and 5 in comparison to FBS and 10% rPL culture, which were statistically indistinguishable.

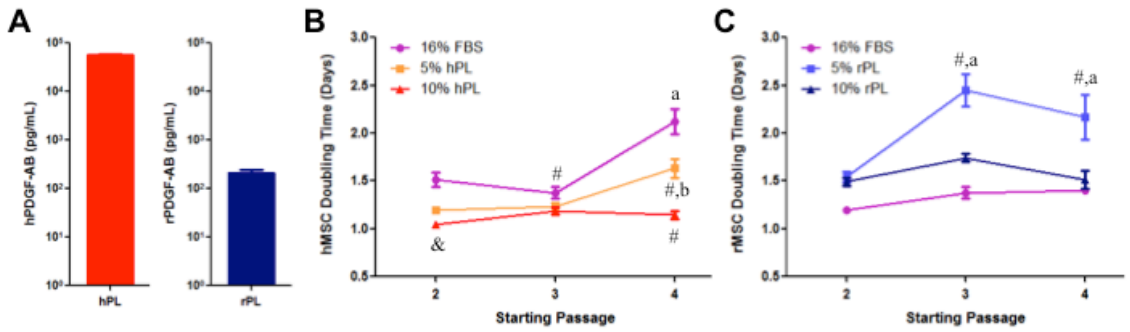

Figure 18: Limitations of a Syngeneic Rodent Model rPL was prepared from Lewis rats and analyzed in vitro to evaluate its similarity to the hPL product. A) PDGF-AB content was two orders of magnitude greater for hPL (56.4 pg/mL) vs. rPL (0.2 pg/mL), as measured via species-specific ELISA assay B) While expansion of hMSCs in hPL-supplemented media promoted a dose-dependent decrease in cell DT, culture of rMSCs in rPL-supplemented media produced an increase (5% rPL) or no change (10% rPL) in cell DT. (a = $p < 0.05$ within same media type vs. passage 2; b = $p < 0.05$ within same media type vs. passage 3; # = $p < 0.05$ within same passage vs. all other media conditions; & = $p < 0.05$ within same passage vs. 16% FBS)

4.4 Discussion

Given the multitude of growth factors, including mitogenic and angiogenic proteins, present in hPL, we expected its implementation as a pre-treatment or co-delivery strategy to improve delivered hMSC survival. We began this research using *in vitro* analyses and observed advantages of each utilization strategy. Culture of hMSCs in hPL-supplemented media led to a subsequent enhancement in cell expansion even under serum-starved, hypoxic conditions. Incorporation of hPL into hMSC-seeded alginate/mesh constructs improved viable cell number over time in culture. Yet despite these favorable outcomes *in vitro*, when challenged *in vivo*, neither hPL utilization approach served to better maintain delivered hMSC number through 7 or 14 days.

hPL was examined as a pre-treatment strategy for hMSCs embedded within immediately injected and pre-cultured constructs. The rationale for investigating construct pre-culture was to encourage hMSC attachment to the alginate matrix prior to delivery, thereby improving cell survival, in part, due to a reduction in anoikis-driven cell death following implantation (Gilmore 2005, Lee, Choi et al. 2015). However, we observed a negative effect of construct pre-culture on the number of viable cells delivered, particularly in the case of hPL culture. This result is consistent with what some others have seen for large volume constructs cultured *in vitro* (Griffith, Miller et al. 2005, Davis, Schroeder et al. 2007). If a pre-culture strategy were to be reevaluated in future studies, use of perfusion culture or a higher serum concentration (16% FBS and 5% hPL were examined here) may improve viable embedded-hMSC number during this pre-implantation period (Zhao and Ma 2005, Uzarski, Bijonowski et al. 2015).

Despite promising *in vitro* data, hPL expansion did not improve hMSC survival *in vivo*. This may in some part be attributed to challenges recapitulating the implantation

environment through culture conditions. Hypoxic culture in this aim leveraged a 5% oxygen concentration whereas the oxygen tension within our large volume constructs post-implantation was likely much lower (Davis, Schroeder et al. 2007). In response to 2D hypoxic culture, hMSCs exhibit enhanced proliferation associated with an alteration of cellular metabolism (Boutilier 2001, Grayson, Zhao et al. 2007, Dos Santos, Andrade et al. 2010). It's possible that hPL expansion impacts hMSC metabolic phenotype in a manner that impedes adaptation to severely hypoxic conditions (Griffiths, Baraniak et al. 2013).

The motivation to evaluate hPL as a co-delivery strategy was its capacity to provide both physical and biochemical cues. Within cell-contractible matrices, physical cues are known to impact many aspects of hMSC phenotype including proliferation and morphology (Guilak, Cohen et al. 2009, Khetan, Guvendiren et al. 2013, Lee, Abdeen et al. 2013, Zhang and Kilian 2013). The fibrinogen content of hPL allows it to form a hydrogel that has demonstrated advantages over the use of tissue culture plastic for hMSC expansion (Walenda, Hemeda et al. 2012). Our studies integrated hPL within an alginate hydrogel backbone in order to achieve the benefits of an hPL matrix while maintaining construct bulk, as preliminary studies had found the contractibility of pure hPL hydrogels to result in a severely reduced construct volume with hMSC culture (data not shown). However, although we anticipated the addition of a fibrin network to impact alginate-embedded hMSC morphology through promotion of cell spreading, we instead observed that cells were largely rounded in both treatment groups (Bensaid, Triffitt et al. 2003). We hypothesized this lack of morphological change could be due to a deficiency of hPL content (20% v/v) or calcium crosslinker. To explore whether the calcium sulfate

(80 mM) added to our hydrogels was sufficient to overwhelm the concentration of acid citrate dextrose, a calcium chelator, in order to crosslink both the alginate and hPL constituents, additional calcium was added during the crosslinking protocol (100 mM total). Increased calcium concentration did not result in an hPL-induced hMSC morphological change (data not shown), indicating that the low hPL concentration, rather than calcium content, may have been responsible for a lack of hMSC spreading.

Despite no evidence supporting a modulated physical environment with hPL co-delivery, achievement of biochemical manipulation was confirmed following a PDGF-AB release study. PDGF-AB underwent burst release, with greater than 50% release through 12 hrs in culture, from acellular and hMSC-seeded hPL-containing constructs. Cumulative PDGF-AB release from cell-containing hydrogels was lower, suggesting that hMSCs were metabolizing the incorporated growth factor. This finding is consistent with the known role PDGF signaling plays in various aspects of hMSC behavior including growth, migration, and differentiation (Ng, Boucher et al. 2008). Furthermore, the baseline activity of hMSC PDGF receptors may have been augmented due to VEGF-A present in the hPL (Ball, Shuttleworth et al. 2007, Italiano, Richardson et al. 2008, Baik, Lim et al. 2014). Unsurprisingly, as PDGF is only a minor component of the hMSC secretome, cell-seeded constructs without incorporated hPL failed to release substantial levels of PDGF-AB in this study (Kinnaird, Stabile et al. 2004, Ohnishi, Yasuda et al. 2007, Chiellini, Cochet et al. 2008).

In addition to hPL incorporation acting through the delivered hMSCs, we anticipated that an hPL-releasing therapeutic would drive a favorable host cell response as well. Due to its VEGF content, we hypothesized that hPL incorporation would

promote construct vasculature (Folkman 2007, Italiano, Richardson et al. 2008). Additionally, although we've previously identified no effect of cell delivery alone on construct vasculature within system, it was projected that hMSC delivery in conjunction with hPL may increase construct vasculature in a synergistic manner (Ball, Shuttleworth et al. 2007, Allen, Gazit et al. 2014). However, we saw no effect of either implanted component on construct vasculature volume. One potential explanation for this is the complex mixture of pro- and anti-angiogenic factors contained within hPL (Italiano, Richardson et al. 2008). The occurrence of hPL-elicited rMSC death, as identified by the *in vitro* studies discussed below, represents a likely contributing factor that was not yet recognized at the time of *in vivo* delivery.

To better isolate the potential interaction between delivered hPL and host cells, we studied the effect of hPL-culture on rMSCs *in vitro*. Strikingly, exposure of rMSCs to hPL produced dramatic cell death, a phenomenon attributable to a heat labile hPL component. It was suspected that membrane attack complex (MAC) formation was responsible for this effect due to the high concentration of complement proteins present in hPL (Romanella, Aminian et al. 1997, Blair and Flaumenhaft 2009, Rubio-Azpeitia and Andia 2014, Morgan 2015). However, MAC concentration was found to be similar across all hPL and hPL-HI culture conditions, indicating that complement-mediated cell lysis was not responsible for hPL-induced rMSC death. Complement-independent mechanisms that may have played a role in this xenogeneic response include cold agglutinin- and antithymocyte globulin-mediated processes (Salama, Gottsche et al. 1988, Zand, Vo et al. 2005). Irrespective of mechanism, rMSC death in response to hPL exposure *in vitro* indicated that an immunocompromised rodent model (Nude rats) was

not sufficient to ameliorate xenogeneic complications in the pre-clinical testing of hPL.

The potential for leveraging a syngeneic model (Lewis rats) for hPL therapeutic efficacy was subsequently explored. First, the hPL and rPL products were examined for growth factor quantity. The PDGF-AB content of rPL was found to be two orders of magnitude lower than that of hPL, rendering rPL a fundamentally distinct product. This observation is compatible with previously published data showing greater concentrations of PDGF-AA, PDGF-AB, PDGF-BB, and TGF-β in human platelet-rich plasma (PRP) compared to that derived from rat or goat (van den Dolder, Mooren et al. 2006). Secondly, the effect of rPL-supplemented culture on rMSC expansion was examined and shown not to produce the same beneficial effect on cell doubling time (DT) as observed for hPL-supplemented hMSC expansion. However, rMSC DT with increased rPL concentration (10% vs. 5% v/v) was comparable to that of FBS culture, suggesting no disadvantage of using rPL as a serum substitute to FBS culture. Overall, the heightened potency of human platelet-derived product may be physiologically rationalized by species variability in circulating platelet concentration, with rodents exhibiting a baseline quantity 5-fold that of humans (1000 vs. 200 $x10^6$ platelets/mL) (van den Dolder, Mooren et al. 2006).

To summarize the findings for this thesis aim, significant challenges in the pre-clinical testing of hPL as an hMSC-based delivery strategy were identified. Despite encouraging results in culture, the utility of hPL as either a pre-treatment or co-delivery strategy was investigated within an immunocompromised rodent model and found to serve no benefits regarding hMSC survival or construct vascularization. Upon follow-up inspection using a model rodent cell type *in vitro*, exposure of rMSCs to hPL-

supplemented media resulted in dramatic cell death, indicating a major limitation of delivering hPL to a rodent model, irrespective of immune system deficiency. In evaluating whether rPL could recapitulate the potential therapeutic efficacy of hPL delivery, rPL was found to be deficient in growth factor content as well as the capacity to potentiate rMSC expansion. These results highlight concerns of xenogenicity and interspecies variability that must be considered in the pre-clinical assessment of hPL.

CHAPTER 5 MESENCHYMAL STEM CELL AGGREGATION FOR LARGE BONE DEFECT REPAIR

5.1 Introduction

The repair of bone tissue is finely tuned to its local inflammatory environment. Injury stimulates an array of inflammatory signaling cascades, the factors and cytokines of which have been interrogated using knockout animal models and antagonist delivery (Mountziaris, Spicer et al. 2011, Thomas and Puleo 2011). These studies have highlighted the unique temporal role of inflammatory signals such as tumor necrosis factor alpha (TNF-α), interleukin 6 (IL-6), and prostaglandin E_2 (PGE2) during this regenerative period (Chambers, Fox et al. 1999, Mountziaris and Mikos 2008, Blanchard, Duplomb et al. 2009, Thomas and Puleo 2011).

While cell-based treatments for large bone defect repair hold promise, the long-term viability of these implants has proven difficult to maintain. It is possible that the potency of cell-based therapeutics could be improved by engineering delivered cells to secrete paracrine factors necessary for the healing process. Human mesenchymal stem cells (hMSCs) have inherent anti-inflammatory properties (Iyer and Rojas 2008, Ankrum, Ong et al. 2014). Recent work has found that this hMSC immunomodulatory potential can be augmented via the formation of these cells into three-dimensional aggregates (Bartosh, Ylostalo et al. 2010, Zimmermann and McDevitt 2014). Spheroid culture increased the production of immunomodulatory factors, including IL-6 and PGE2, in comparison to hMSCs cultured in monolayer. Additionally, exposure of hMSC spheroids to pro-inflammatory cytokines, as found within injured tissue, further enhanced this

factor secretion.

Aside from enriched anti-inflammatory capacity, MSC spheroids have demonstrated favorable survival, angiogenic, and osteogenic properties. Association of MSCs as spheroids has been shown to decrease cell apoptosis and increase angiogenic factor expression *in vitro* (Bhang, Cho et al. 2011, Murphy, Fang et al. 2014). In comparison to dissociated MSCs, cell aggregates exhibited improved osteogenic potential *in vitro* and *in vivo* (Wang, Itaka et al. 2009, Murphy, Fang et al. 2014, Yamaguchi, Ohno et al. 2014). However, although delivery of MSC aggregates demonstrated efficacy within one orthotopic bone repair model (a calvarial defect), this strategy had not been challenged within a large volume, critically-sized bone injury (Yamaguchi, Ohno et al. 2014).

The effects of MSC aggregation on angiogenic and osteogenic potential positions spheroid delivery as a promising cell-based platform for large bone defect repair. The objective of this aim was to quantify the effects of MSC aggregation on cell survival and cell-based bone regeneration. We hypothesized that delivery of MSC spheroids would potentiate MSC survival and guided bone regeneration in comparison to single cell delivery. To test this hypothesis, we evaluated the effects of MSC aggregation using alginate/mesh constructs delivered subcutaneously or to critically-sized femoral defects. Building on the discussion of pre-clinical testbeds prompted by our human platelet lysate (hPL) studies, we leveraged both immunocompromised and syngeneic rodent models.

5.2 Materials and Methods

5.2.1 MSC Culture and Aggregate Formation

Bone marrow-derived hMSCs were purchased from the Texas A&M University Health Science Center and cultured as previously described (Allen, Gazit et al. 2014). Briefly, two donor cell lines were expanded in Minimum Essential Medium alpha (αMEM) containing 16% v/v fetal bovine serum (FBS; Atlanta Biologicals; Lawrenceville, GA) and 100 units/mL penicillin/100 µg/mL streptomycin/2 mM L-glutamine (PSL; Invitrogen; Carlsbad, CA) at 37ºC and 5% CO_2. At passage 2, cells were detached using 0.25% trypsin-EDTA (Invitrogen) and combined 1:1 to form a pooled hMSC population. Lewis rat MSCs (rMSCs), characterized for multipotency, were purchased (Sciencell Research Laboratories; Carlsbad, CA) and expanded until passage 2 in similar culture conditions. Following expansion, MSCs to be used in bioluminescent imaging (BLI) studies were labeled via lentiviral co-transduction for constitutive expression of green fluorescent protein (GFP) and firefly luciferase (Luc) as previously reported (Sun, Lee et al. 2009, Sheyn, Kallai et al. 2011). To produce MSC aggregates, cells were seeded in 400-µm agarose micro-wells as described previously (Ungrin, Joshi et al. 2008, Zimmermann and McDevitt 2014). Briefly, MSCs were added to micro-well inserts, centrifuged for 5 minutes at 200g, and left to form aggregates (500 cells/spheroid) over 14-18 hrs. To characterize rMSC aggregate secretion and intracellular alkaline phosphatase (ALP) activity, a modified protocol to that conducted previously on hMSC aggregates was implemented (Zimmermann and McDevitt 2014). Culture media (n=6) at 24 hrs was collected from adherent "2D" rMSCs (1,300 cells/cm^2) as well as rMSC aggregates (0.3 x10^6 cells/100 mm dish) cultured on a rotary orbital shaker. Media

concentrations of rat interleukin 6 (IL-6) and prostaglandin E_2 (PGE2) were measured by ELISA assays (R&D Systems; Minneapolis, MN) and normalized to DNA content quantified via the Quant-iT PicoGreen dsDNA Kit (Molecular Probes; Eugene, OR). ALP activity (n=6) was measured by incubation of intracellular contents in 20mM phosphatase substrate (p-NPP; Sigma-Aldrich; St. Louis, MO).

5.2.2 Alginate Embedding of hMSCs

hMSCs were embedded within RGD-functionalized alginate hydrogel (2% w/v; FMC BioPolymer; Ewing, NJ) in either single cell and aggregate form using a dual-syringe mixing technique with subsequent calcium sulfate (8.4 mg/mL; Sigma-Aldrich) cross-linking (Allen, Gazit et al. 2014). To verify maintenance of cell viability and spheroid structure following alginate incorporation and syringe injection, hMSC aggregates were embedded at densities of 0.5 and 2.0 $x10^6$ cells/150 µL (n=3). Resultant hydrogel was stained using a LIVE/DEAD Kit (Invitrogen) and imaged by inverted microscope (Axio Observer; Carl Zeiss; Thornwood, NY). To evaluate BLI signal vs. cell number correlation, individual and aggregated GFP/Luc hMSCs were embedded at densities of 0, 0.5, and 1.0 $x10^6$ cells/150 µL (n=6) and imaged using an IVIS Lumina machine (Caliper Life Sciences; Hopkinton, MA). Beetle luciferin (Fisher Scientific; Hampton, NH) was added to the culture media (0.21 mg/mL) 20 minutes prior to image acquisition (5 second exposure; 12.5 cm field of view). Living Image software version 3.2 (Caliper Life Sciences) was used to demarcate a circular region of interest (ROI) centered over each well and BLI counts were normalized to exposure time and ROI area. A subset of aggregate-seeded hydrogels (n=3) were cultured over 1 week, sectioned using

a CryoStar NX70 cryostat (Fisher Scientific), stained with lactate dehydrogenase (LDH), and imaged (Zeiss).

5.2.3 Alginate Embedding of rMSCs

rMSC single cells or aggregates were similarly embedded within alginate hydrogel (2% w/v) along with added PBS (control) or perfluorotributylamine (10% w/v; PFTBA; Sigma-Aldrich) emulsion. Emulsions were prepared by sonication of PFTBA and phosphate-buffered saline (PBS; 2:3 ratio) or PBS alone with Lipoid E 80 (0.1 g/mL; Lipoid; Newark, NJ) using a Vibra-Cell VCX130PB (Sonics & Materials; Newtown, CT) for 2 minutes at 31%. Prior to alginate cross-linking, all rMSC groups and associated acellular controls received identical emulsion concentrations to produce 0% and 10% PFTBA hydrogels. GFP/Luc rMSC-seeded alginate with single or aggregated cells (0.5 $x10^6$ cells/150 μL) and 0% or 10% PFTBA was injected into electrospun, polycaprolactone (PCL) mesh tubes (150 μL/construct) and cultured over 4 days under hypoxic conditions (3% O_2). To quantify change in viable cell number, longitudinal BLI was performed on Days 0, 2, and 4 using the protocol described in sub-section 5.2.2 (n=8) with culture media (2 mL/well) replaced following each timepoint. In preparation for segmental defect delivery, singular or aggregated rMSCs were seeded at a density of 0 (acellular) or 1.0 $x10^6$ cells/150 μL, with or without PFTBA, and recombinant human BMP-2 (1.5 μg/150 μL; rhBMP-2). Resultant hydrogels (n=4) were cultured in mesh tubes with media collected and replaced on Days 1, 4, and 7. Conditioned media was measured for BMP-2 content using an ELISA assay (R&D Systems) and examined using a previously established ALP induction protocol (Wiemann, Rumpf et al. 2001, Priddy, Chaudhuri et al. 2014). Briefly, mouse clonal pre-osteoblasts (MC3T3-E1; American

Type Culture Collection; Manassas, VA) were plated at confluence (1,300 cells/cm^2) and culture in the construct-conditioned media. After 3 days, MC3T3-E1 cells were washed, fixed, and incubated in 7.6mM p-NPP to determine ALP activity. Normalized ALP activity was calculated using DNA content, measured as previously described in sub-section 5.2.1.

5.2.4 Subcutaneous Implantation

Surgical implantation was conducted in accordance with the Georgia Institute of Technology IACUC protocol #A13023 as described previously (Allen, Gazit et al. 2014). Alginate hydrogel seeded with singular or aggregated GFP/Luc hMSCs at a density of 0.5 $x10^6$ cells/150 μL (n=5) were stored at 4°C for 1-4 hrs prior to delivery, at which point hydrogel was injected into PCL tubes (150 μL/construct) and implanted within 11-week-old female, athymic Nude rats (Charles River Labs; Wilmington, MA). As previously described, two dorsal incisions were made to prepare four subcutaneous pockets per animal. rMSC-seeded hydrogels were implanted in a similar manner within 11-week-old male, inbred Lewis rats (Harlan Laboratories; Indianapolis, IN). GFP/Luc and unlabeled rMSCs were combined at a 2:1 ratio prior to alginate embedding. Constructs with singular or aggregated rMSCs at a density of 0 (acellular) or 0.5 $x10^6$ cells/150 μL and with or without PFTBA were delivered (n=7-10).

5.2.5 Subcutaneous BLI, Vascular, and Histological Analyses

Nude rats underwent longitudinal BLI at Days 0, 1, 3, 5, 7, and 14 post-operatively using a previously established protocol (Allen, Gazit et al. 2014). Anesthetized rats received a subcutaneous injection of 300 μL luciferin (21 mg/mL in saline) at a distance of 2-4 mm from each construct site. The animals were scanned on

either side 30 minutes post luciferin injection (10 second exposure; 12.5 cm field of view) and images were evaluated using a 4 cm^2 elliptical ROI. Following Day 14 BLI, Nude rats underwent vascular perfusion using serially applied saline (0.9% w/v), papaverin hydrochloride (0.4% w/v in saline), neutral buffered formalin (10% v/v), and the radiopaque contrast agent Microfil (Flow Tech; Carver, MA) solutions. Explants were excised and imaged via microcomputed tomography (μCT) scans on a MicroCT42 (Scanco Medical; Brüttisellen, Switzerland) at 55kVp, 145μA, and a 12μm voxel size. Acquired slices were contoured and segmented using a low-pass Gaussian filter (sigma=1.2, support=2) to evaluate vascular volume within the construct interior alone. Following μCT scans, explants were paraffin embedded, histologically sectioned via microtome (Microm; Walldorf, Germany), stained with Masson's trichrome or DAPI, and imaged (Zeiss). Lewis rats underwent similar examination with longitudinal BLI performed on Days 0, 1, 7, and 14 followed by takedown for vascular and histological analyses on Day 14.

5.2.6 Segmental Defect Implantation

Segmental defect surgeries were conducted in accordance with the Georgia Institute of Technology IACUC protocol #A14037. Due to a lengthened surgical timeline in comparison to subcutaneous implantation, the effect of 4°C syringe incubation on alginate-embedded MSC viability was examined prior to delivery. Single and spheroid MSCs at 1.0 $x10^6$ cells/150 μL alginate (n=3) were incubated for 0, 4, or 8 hrs at 4°C and subsequently injected, stained via LIVE/DEAD Kit (Invitrogen), and imaged (Zeiss). rMSC-seeded hydrogels containing emulsions were analyzed using a cell metabolic assay (n=3) due to imaging challenges resulting from altered gel opacity. Singular or

aggregated rMSC-seeded hydrogels containing no, PBS, or PFTBA emulsion and having undergone a 0- or 8-hr syringe incubation at 4°C were cultured for 48 hrs and assessed by CellTiter-Blue viability assay (Promega; Madison, WI) according to manufacturer recommendation. On each date of surgery, bilateral femoral defects were created in 13-week-old rats as previously described (Oest, Dupont et al. 2007, Kolambkar, Boerckel et al. 2011). Briefly, an 8-mm critically-sized defect was created in the mid-diaphysis of each femur following attachment of a polysulfone fixation plate to provide limb stabilization. Injuries were treated with a PCL mesh surrounding each defect followed by injection of alginate hydrogel (150 μL) incubated for 1-8 hrs at 4°C prior to delivery. Nude rats received acellular, single cell, or aggregated hMSC-seeded (1.0 $x10^6$ cells/150 μL) alginate containing a 2-μg dose of rhBMP-2. A treatment group containing hMSC aggregate-seeded alginate without rhBMP-2 was included as well. Lewis rat defects were treated with acellular, single cell, or aggregated rMSC-seeded (1.0 $x10^6$ cells/150 μL) alginate containing PBS or PFTBA emulsion and a 1.5-μg dose of rhBMP-2. A subset of Lewis rat defects received rMSCs labeled with DiI stain (Invitrogen) to facilitate downstream histological analysis.

5.2.7 Segmental Defect Radiography and μCT Analyses

Longitudinal bone regeneration for all rats was assessed qualitatively via radiography (Faxitron MX-20 Digital; Faxitron Bioptics; Tucson, AZ) at 4, 8, and 12 weeks post-operatively. At the same timepoints, Nude rats also received quantitative evaluation of bone formation by μCT (VivaCT40; Scanco Medical) at 55kVp, 145μA, and a 38.9μm voxel size (n=7-10). Regenerated bone volume was analyzed using a volume of interest (VOI) consisting of 100 slices within the defect center. Lewis rats

received *ex vivo* μCT evaluation due to their prohibitive size. Explanted femurs were scanned at 55kVp, 145μA, and a 21μm voxel size then evaluated using a VOI consisting of 280 slices (n=6-9).

5.2.8 Segmental Defect Biomechanical and Histological Analyses

Femurs were explanted at 12 week post-operatively and underwent torsional testing to failure as previously reported (Oest, Dupont et al. 2007). Briefly, bone ends were potted in Wood's metal (Alfa Aesar; Ward Hill, MA) following soft tissue and fixation plate removal. Using an ELF 3200 machine (Bose ElectroForce Systems Group; Eden Prairie, MN), samples were displaced at 3 °/s. Maximum torque and torsional stiffness were calculated for the Nude (n=5-7) and Lewis (n=6-9) rat explants. Following biomechanical testing, Lewis rat defects were removed, decalcified (Cal-ExII; Fisher Scientific), and paraffin embedded. Samples were sectioned via microtome (Microm), stained with safranin O (SafO), and imaged (Zeiss).

5.2.9 Statistical Analysis

Values are displayed as mean +/- standard error of mean (SEM) unless otherwise stated with statistical significance defined by $p<0.05$. Data were analyzed using two-way analyses of variance (ANOVA) with Tukey post hoc comparisons within the Minitab software (State College, PA).

5.3 Results

5.3.1 Subcutaneous Implantation of hMSC Aggregates in Nude Rats

In preparation for *in vivo* delivery, *in vitro* characterization of hMSC aggregates

incorporated into RGD-alginate hydrogels was performed. It was found that hMSCs aggregates maintained their viability and structure following the alginate cross-linking and syringe injection procedures (Figure 19A). Correlation of bioluminescent imaging (BLI) signal vs. viable cell number for GFP/Luc hMSC aggregates was observed to be linear ($r^2 = 0.75$) and statistically similar to that of GFP/Luc hMSCs embedded as single cells (Figure 19B). Culture of these constructs over 1 week illustrated the breakup of aggregate structure as hMSCs migrated within the alginate hydrogel as single cells (Figure 19C).

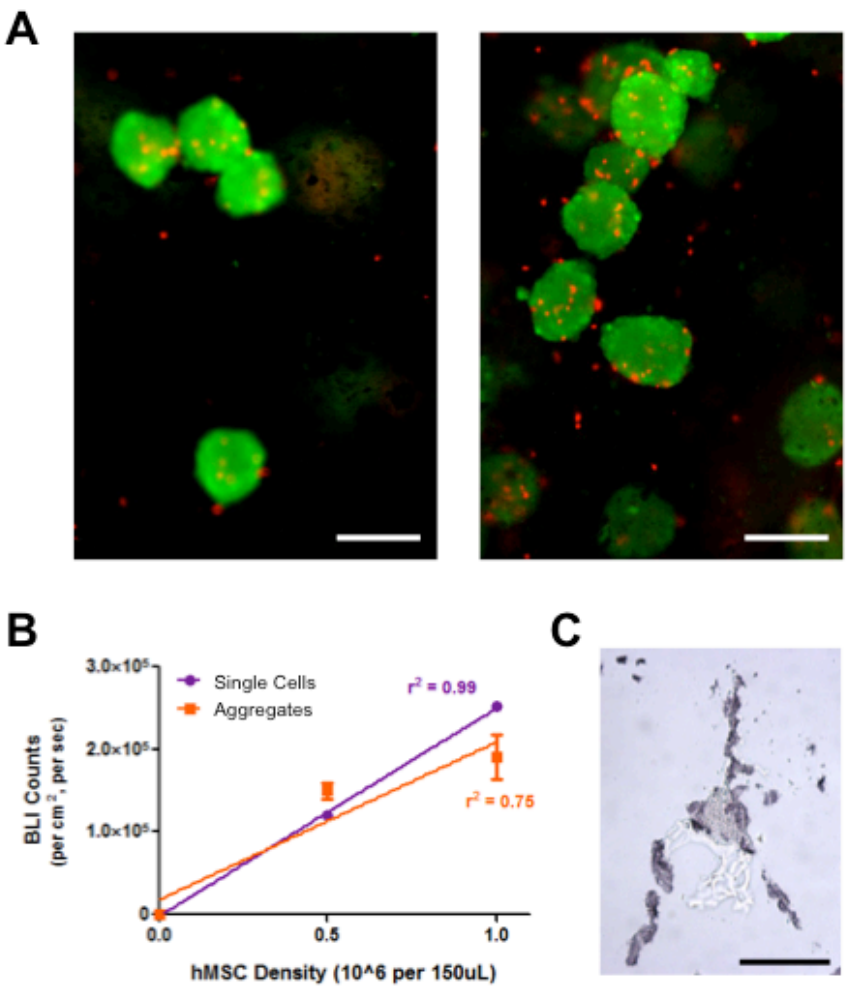

Figure 19: Embedding of hMSC Aggregates in Alginate Hydrogel A) hMSC aggregates (live = GFP (green); dead = ethidium homodimer (red)) maintained viability and structure following alginate embedding at densities of 0.5 (left) and 2.0 (right) x10^6 cells/150 µL (scale bar = 100 µm). B) *In vitro* BLI counts vs. viable cell number for aggregate-seeded hydrogels displayed a linear correlation (r^2 = 0.75) similar to that of constructs seeded with single hMSCs (r^2 = 0.99). C) Aggregated hMSCs migrated as single cells within the alginate hydrogel over 1 week of culture, as assessed by LDH staining (scale bar = 100 µm).

Alginate/mesh constructs seeded with dissociated or aggregated GFP/Luc hMSCs were implanted subcutaneously in Nude rats and monitored for cell survival via BLI. hMSC aggregation had no adverse effect on viable cell number, with both groups exhibiting 1-2% survival through 14 days post-operatively (Figure 20). On Day 14, vascular perfusion and histological analyses were performed to examine tissue development contiguous to the constructs. There was no effect of aggregate delivery on construct vascular volume (Figure 21A) or gross vessel morphology, as assessed qualitatively via representative μCT vasculature reconstructions (Figure 21B). Masson's trichrome staining revealed the presence of alginate pieces (dashed outline), fibrotic tissue (yellow arrows), and alginate-enclosed ECM pockets (green arrows) present within both treatment groups (Figure 21C). Morphology of ECM pockets embedded within the alginate pieces was observed to be qualitatively distinct between the treatment groups, with single cell delivery resulting in a more even distribution of pockets throughout the construct. In contrast, aggregate-seeded samples contained a more heterogeneous distribution of ECM pockets, including those that appeared to be branching (red arrows) or compromised of multiple nodes (pink arrows).

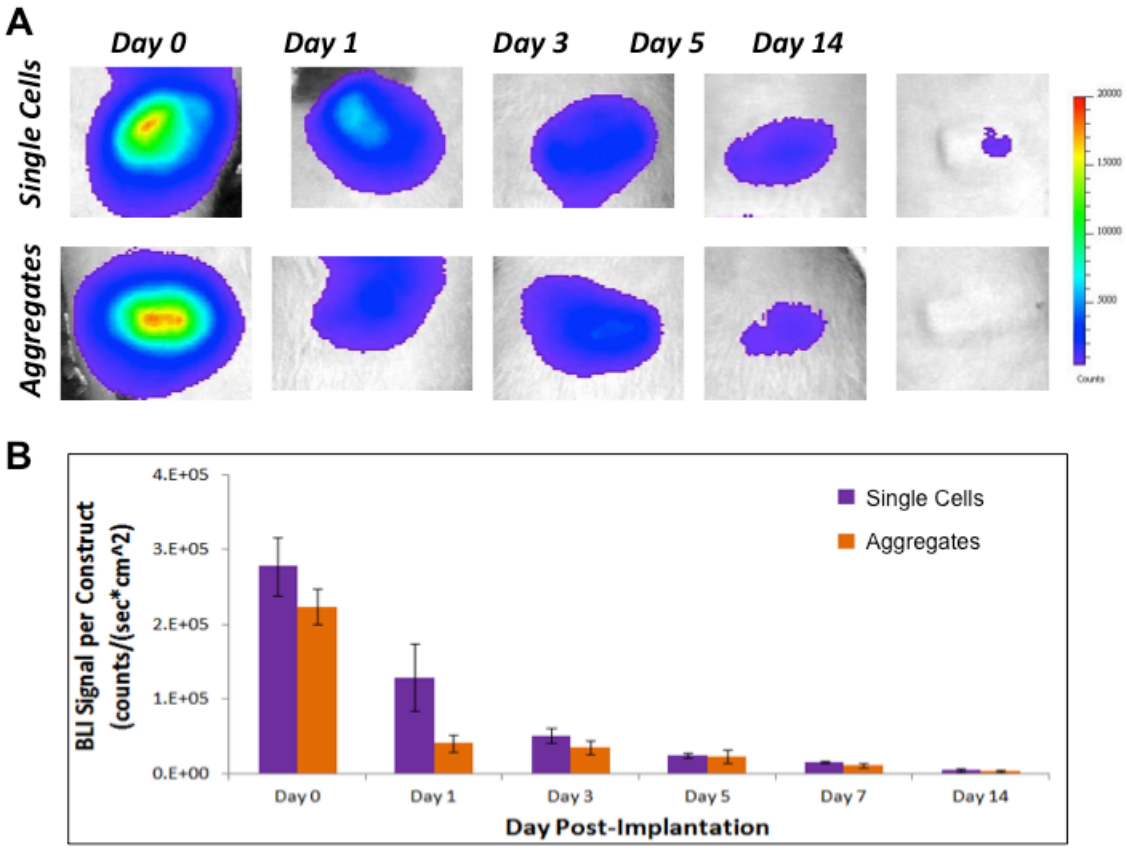

Figure 20: Effect of hMSC Aggregation on Viability through 14 Days *In Vivo* A) Representative BLI heatmaps illustrate similarly maintained viability for hMSCs delivered in single cell and aggregated form subcutaneously to Nude rats over 14 Days. B) Quantification of BLI signal found no significant effect of aggregate delivery on hMSC survival *in vivo*.

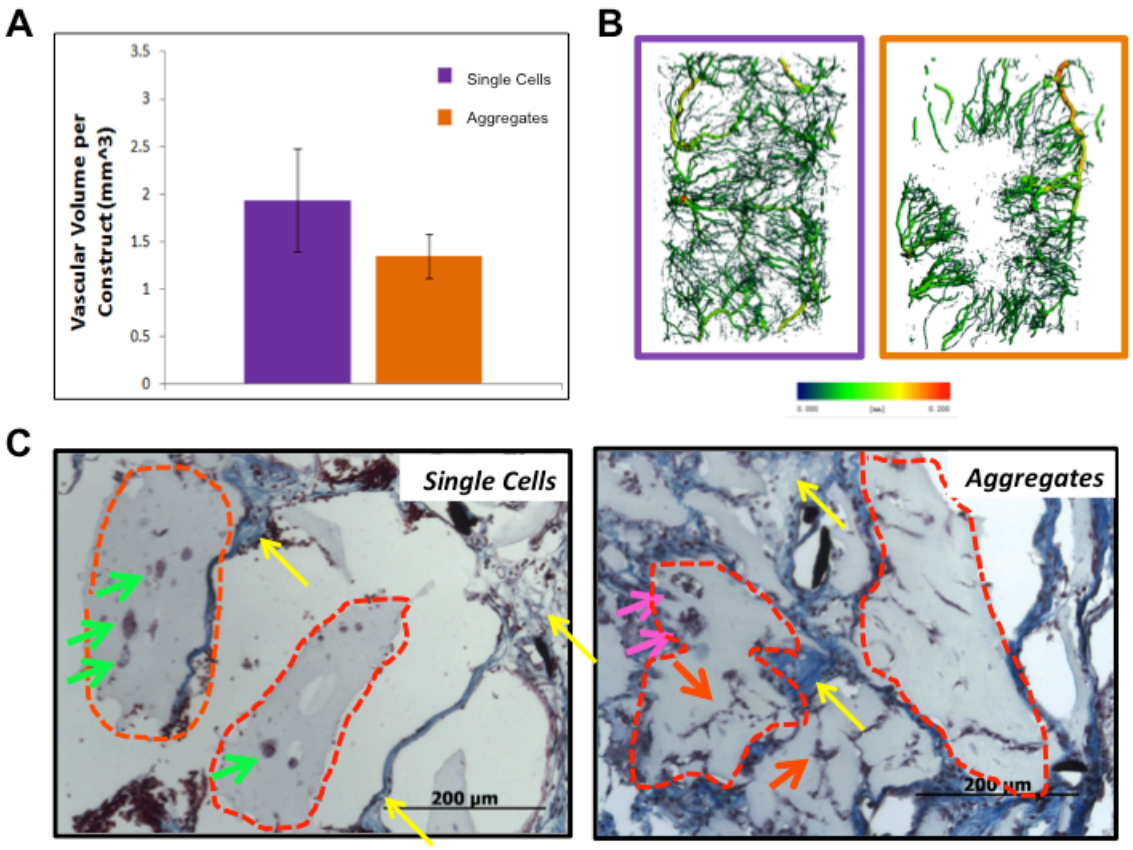

Figure 21: Effect of hMSC Aggregation on Construct Composition at 14 Days A) Construct vascular volume at Day 14 was unaffected by hMSC aggregation. B) Vascular reconstructions of representative single cell (left) and aggregate (right) samples colored to indicate vessel diameter demonstrate no qualitative difference in vessel morphology. C) Irrespective of treatment, explants contained alginate pieces (outlined in red, dashed lines) surrounded by fibrotic tissue (yellow arrows), as visualized using Masson's trichrome staining. Morphology of alginate-embedded ECM pockets differed between treatments, with single cell delivery resulting in a more qualitatively even distribution (green arrows) while aggregate samples contained multi-node (pink arrows) and branching (red arrows) pockets as well as regions void of ECM pockets (not shown).

5.3.2 hMSC Aggregation for Large Bone Defect Repair in Nude Rats

To examine the effect of hMSC aggregation on cell-based bone regeneration, bilateral critically-sized defects were created in Nude rats and treated with alginate/mesh constructs containing a 2-μg dose of BMP-2 and either no cells, single hMSCs, or aggregated hMSCs. Additionally, an aggregates treatment containing no BMP-2 was delivered to observe the extent of aggregate-mediated bone defect repair in the absence of co-delivered osteoinductive stimulus. Longitudinal *in vivo* μCT at 4, 8, and 12 weeks post-operatively revealed no difference in regenerated bone volume across BMP-2-containing treatments (Figure 22A). However, the absence of BMP-2 delivery was found to attenuate bone regeneration. Biomechanical testing data exhibited increased variability compared to bone volume results, with no significant effect of hMSC delivery or BMP-2 dose on maximum torque (Figure 22B) or torsional stiffness (Figure 22C) measurements.

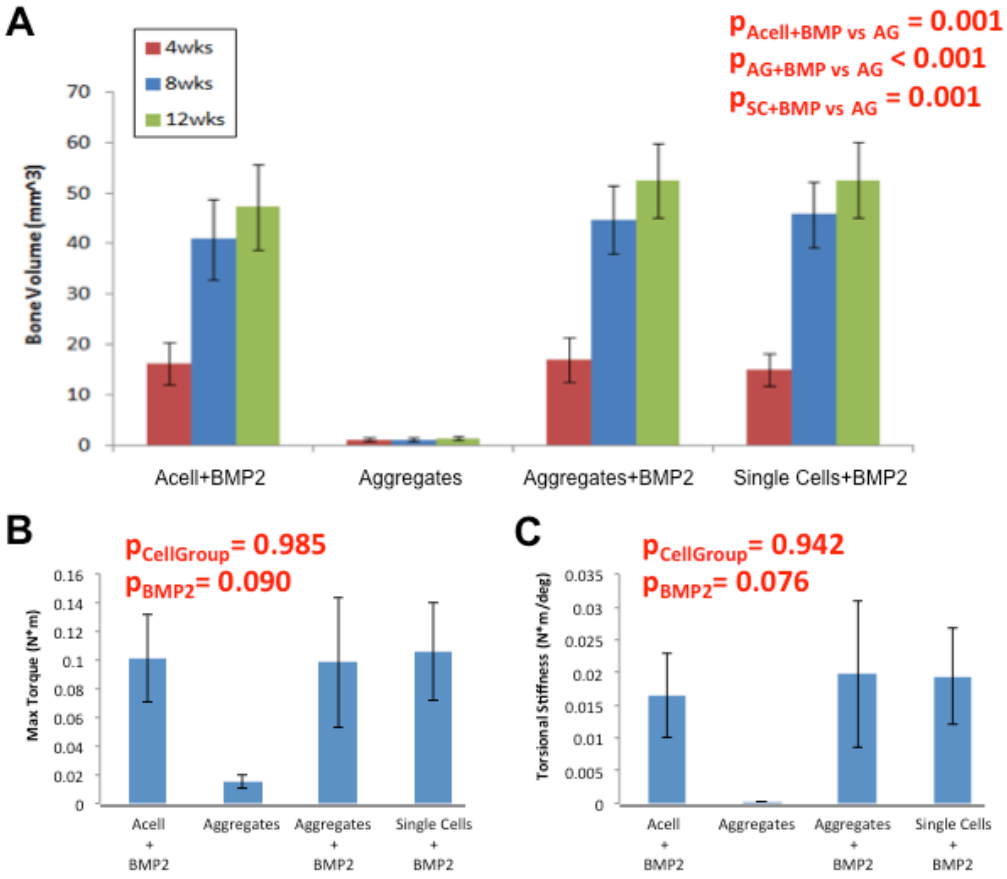

Figure 22: Effect of hMSC Delivery for Large Bone Defect Repair in Nude Rats A) Longitudinal µCT measurement revealed no effect of hMSC delivery, either as single cells or aggregates, on regenerate bone volume. However, the lack of a co-delivered BMP-2 alongside hMSC aggregates ("Aggregates" group) resulted in a significantly diminished amount of bone tissue. B) Maximum torque of the explanted femurs was highly variable and not significantly affected by method of hMSC delivery (p=0.985) nor BMP-2 treatment (p=0.090). C) Similarly, neither cell group (p=0.942) nor BMP-2 dose (p=0.076) impacted torsional stiffness.

Based on qualitative observations, a high degree of animal-to-animal variability was suspected in the aforementioned study. To explore this phenomenon, the average regenerated bone volume for each Nude rat receiving bilateral BMP-2-containing treatments was charted against the average BMP-2-mediated regenerated bone volume at each post-operative timepoint of 4, 8, and 12 weeks (Figure 23A-C). Qualitatively, subsets of animals were found to be either highly responsive or insensitive to BMP-2-mediated bone defect repair. To statistically analyze this finding, p-values for the "animal" and "treatment" variables were calculated for several data sets (Figure 23D). Applying this analysis to Nude rats receiving bilateral BMP-2-containing treatments (the illustrated data set), the "animal" variable alone was determined a significant predictor of regenerated bone volume. For historical comparison, identical analysis performed on results from a bilateral study in Sprague Dawley rats showed no significant effect of biological variability ($p=0.617$). The extent of biological variability observed within this Nude rat study motivated subsequent investigation of MSC aggregation within a syngeneic, Lewis rat model.

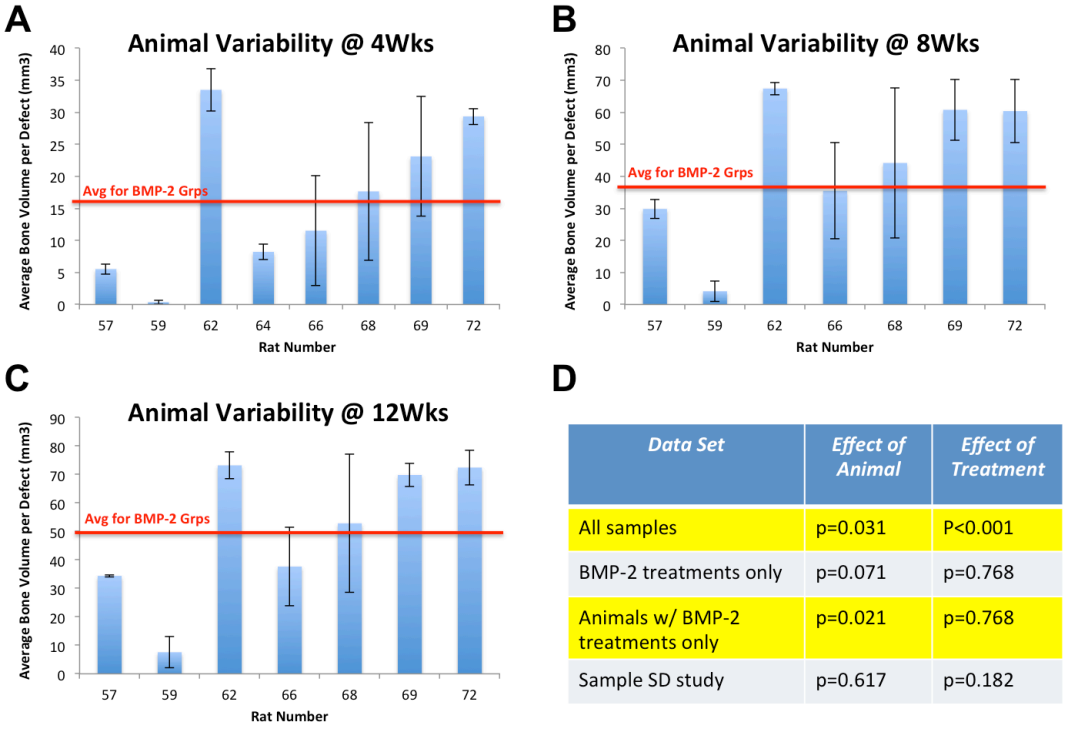

Data Set	Effect of Animal	Effect of Treatment
All samples	p=0.031	P<0.001
BMP-2 treatments only	p=0.071	p=0.768
Animals w/ BMP-2 treatments only	p=0.021	p=0.768
Sample SD study	p=0.617	p=0.182

Figure 23: Biological Variability within the Nude Rat Model A-C) The average regenerated bone volume (error bars = standard deviation) for Nude rats receiving bilateral BMP-2-containing treatments was charted against the overall regenerated bone volume average (excluding "Aggregates" group) at each post-operative timepoint of 4 (A), 8 (B), and 12 (C) weeks. Qualitatively, some animals appeared to be either highly responsive (#62, 72) or insensitive (#57, 59) to BMP-2-mediated defect repair. D) Statistical analysis via two-way ANOVA revealed a significant effect of animal (p=0.021), but not treatment (p=0.768), on regenerated bone volume for the aforementioned sample subset. In contrast, a similar bilateral segmental defect study performed in Sprague Dawley (SD) rodents had no significance of biological variability (p=0.617).

5.3.3 *In Vitro* Characterization of rMSC Aggregates

The same protocol employed for hMSC aggregate formation was effective to produce rMSC aggregates. Spheroids formed over 14 hrs when rMSCs were seeded in agar micro-wells (Figure 24A). Up-regulated immunomodulatory factor secretion, as previously observed for hMSC aggregates, arose with rMSC aggregation as well. rMSC aggregates exhibited increased production of IL-6 and PGE2 over 24 hrs in comparison to cells plated in 2D (Figure 24B). Additionally, intracellular ALP activity was potentiated by rMSC aggregation (Figure 24C).

Motivated by the nominal survival rate achieved with hMSC delivery (Figure 20), the effect of co-delivered PFTBA, a synthetic oxygen carrier, was explored for rMSC implantation. In preparation for *in vivo* delivery, the effect of PFTBA addition (10% w/v) to alginate/mesh constructs on embedded GFP/Luc rMSC survival was investigated *in vitro* under hypoxic conditions (3% O2). Quantification of viable cell number via longitudinal BLI revealed an effect of cell presentation (single cells vs. aggregates), but not PFTBA incorporation, on absolute BLI signal through 4 days (Figure 25A). Likewise, analysis of normalized BLI found improved maintenance of rMSC viability for single cell (SC) groups and no effect of PFTBA addition (Figure 25B). Given the differences between an *in vivo* vs. *in vitro* hypoxic environment and the finding that PFTBA co-delivery had no negative effect on embedded-rMSC viability, we chose to continue investigating PFTBA incorporation in subsequent experiments.

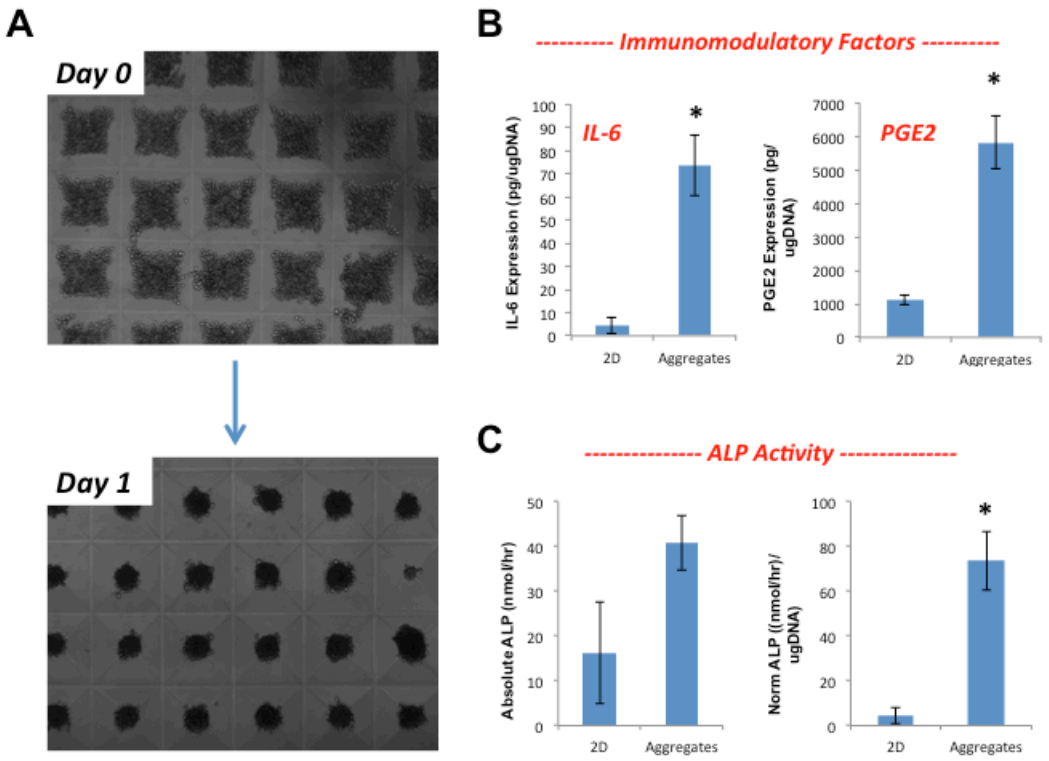

Figure 24: Formation and In Vitro Characterization of rMSC A) Similar to hMSCs, rMSCs seeded in agar micro-wells formed aggregates (500 cells/spheroid) over 14 hrs. B) rMSCs exhibited increased secretion of the immunomodulatory factors IL-6 and PGE2 over 24 hrs in comparison to rMSCs plated in 2D. C) Intracellular ALP activity normalized to DNA content was also enhanced with rMSC aggregation.

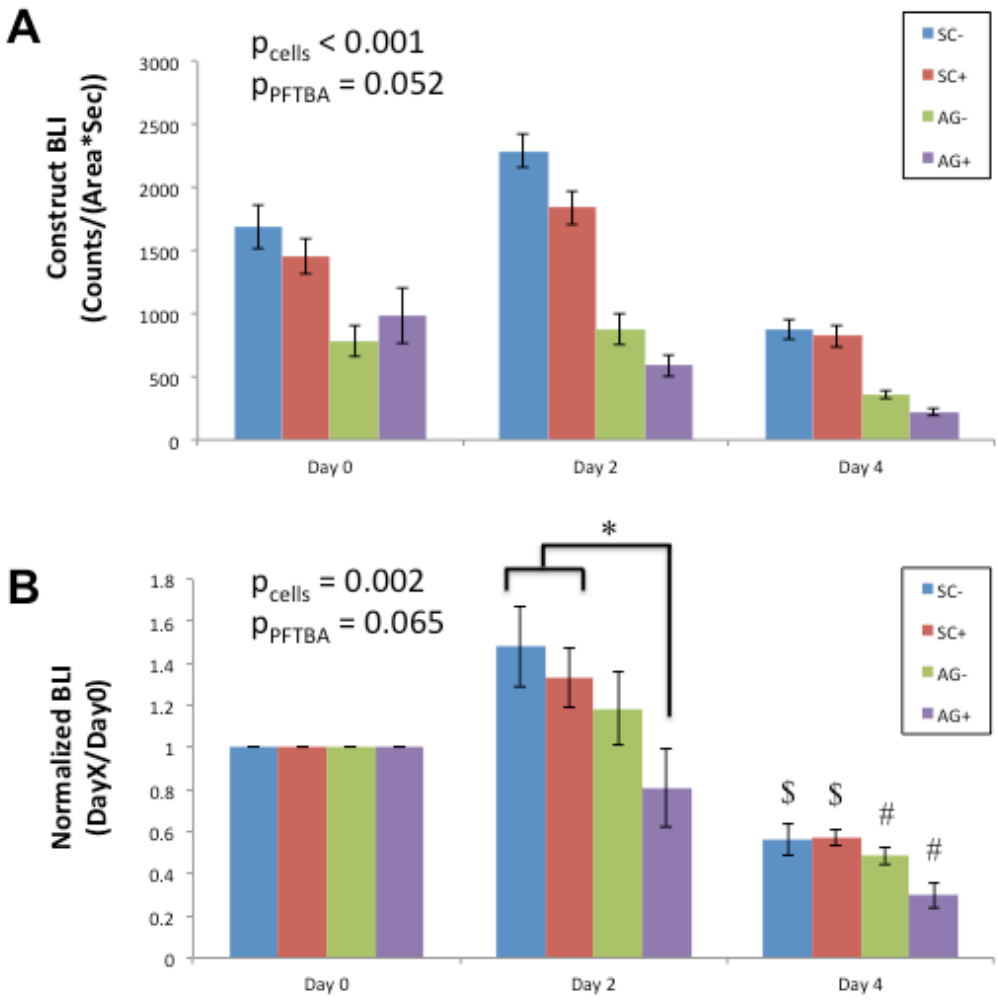

Figure 25: Hypoxic Culture of rMSCs within Alginate Hydrogels Single cell (SC) and aggregated (AG) rMSCs were embedded within alginate hydrogels with (+) or without (-) the synthetic oxygen carrier PFTBA. Longitudinal BLI was conducted to monitor cell viability throughout 4 days of culture at hypoxic (3% O_2) conditions. A) Absolute BLI signal demonstrated an overall effect of cell group (SC vs. AG), but not PFTBA incorporation, and no individual differences between treatments. B) Normalized BLI revealed better-maintained viability for single cell groups and no effect of PFTBA addition. (* = $p < 0.05$ as indicated; $ = $p < 0.05$ within treatment vs. Day 2; # = $p < 0.05$ within treatment vs. Days 0 and 2)

5.3.4 Subcutaneous Implantation of rMSC Aggregates in Lewis Rats

Single cell (SC) and aggregate (AG) seeded alginate/mesh constructs with (+) or without (-) PFTBA as well as acellular (Acell) controls were implanted subcutaneously in Lewis rats and monitored via BLI. Representative heatmaps illustrated a qualitative decrease in BLI signal for all rMSC delivery groups over 14 days post-implantation (Figure 26A). Constructs seeded with single rMSCs displayed a high degree of variability, with several samples exhibiting a marked increase in viable cell number between Days 0 and 1 (Figure 26B). Absolute BLI measurements showed that a similar number of viable cells were delivered across all rMSC-containing treatments (Figure 27A). Additionally, the negligible signal for acellular samples on Day 0 indicated minimal background noise arising from the BLI technique. Normalized BLI demonstrated a significant overall effect of cell presentation ($p_{SCvs.AG}$=0.009), but not PFTBA incorporation (p_{PFTBA}=0.075), on *in vivo* survival (Figure 27B). Single rMSC delivery in the absence of PFTBA (SC-) resulted in the greatest viable cell number on Day 1 post-operatively. Although the majority of acellular implants displayed negligible BLI signal throughout the study duration (Figure 28A), several Acell- constructs increased in BLI signal over time (Figure 28B). Interestingly, this phenomenon had not been observed in former hMSC delivery experiments and was not, in the present study, correlated to the BLI signal recorded from adjacent rMSC-seeded constructs (data not shown).

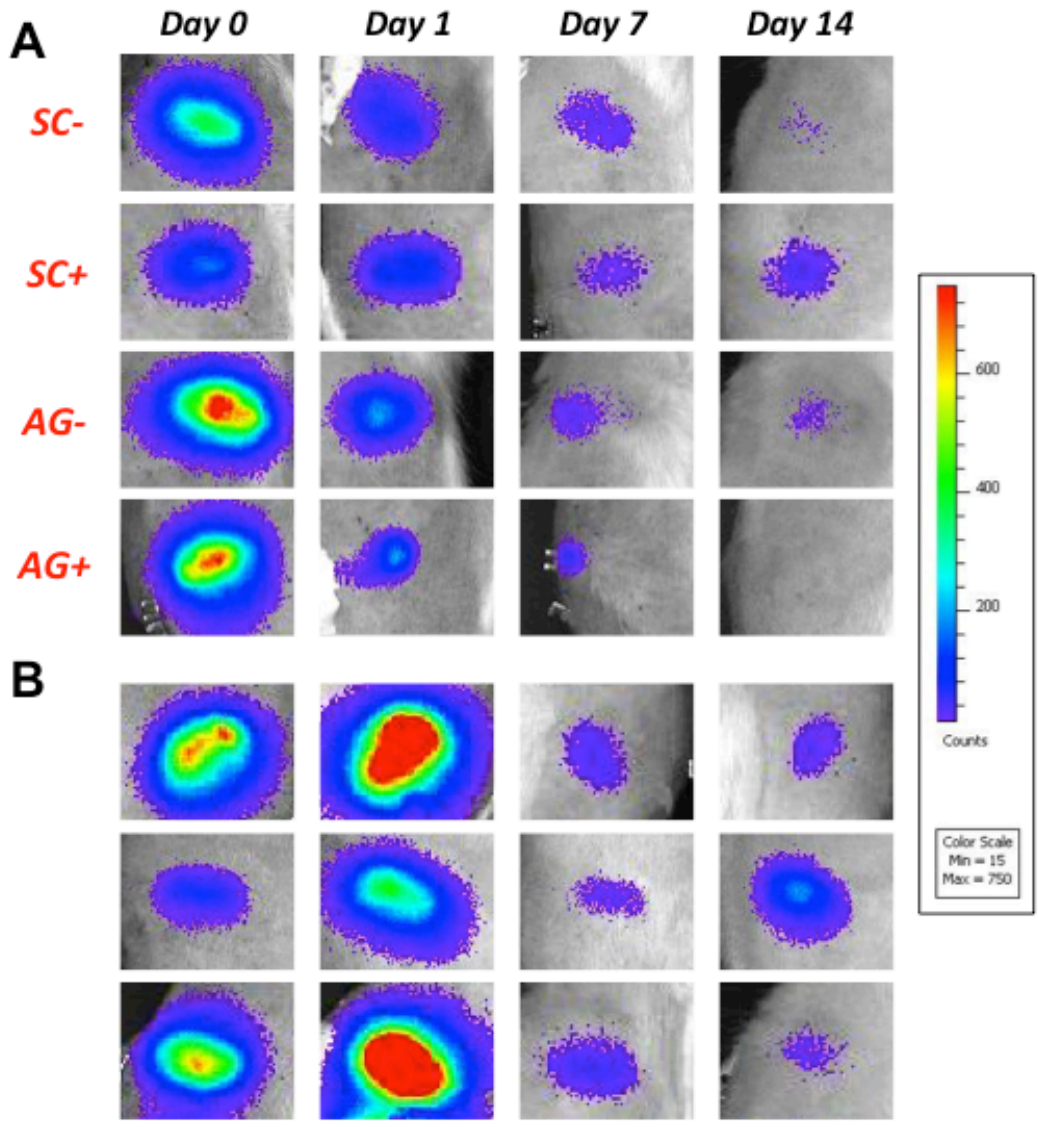

Figure 26: BLI Heatmaps of rMSCs Implanted Subcutaneously through 14 Days Single cell (SC) and aggregated (AG) rMSCs were delivered within alginate/mesh constructs with (+) or without (-) PFTBA oxygen carrier. A) All groups displayed a qualitative decrease in BLI signal through 14 days, indicative of a post-operative drop in viable cell number over time. B) Constructs seeded with single rMSCs exhibited high variability, with some samples increasing in signal between Days 0 and 1. Samples from the SC+ (top two rows) and SC- (bottom row) groups are shown.

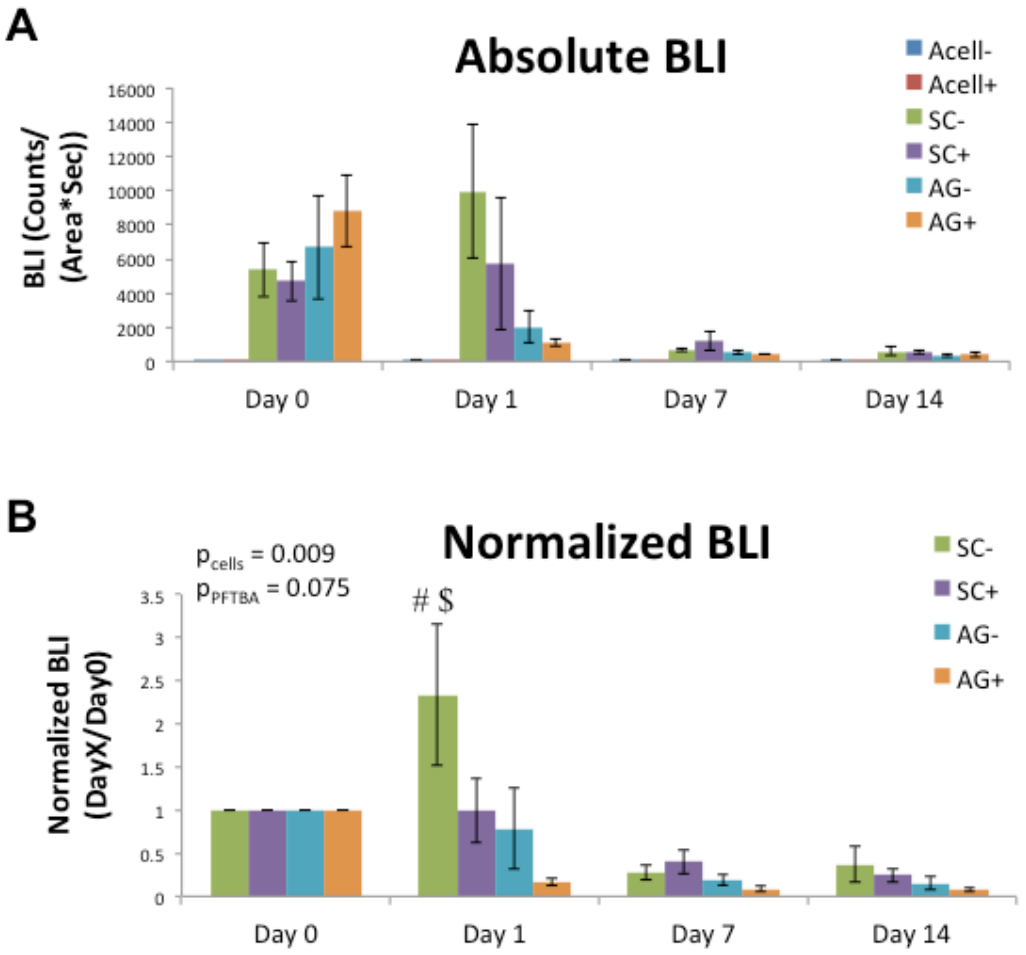

Figure 27: Longitudinal BLI of Subcutaneously Implanted rMSCs Acellular (Acell), single cell (SC), and aggregate (AG) treatments with (+) or without (-) PFTBA were delivered to Lewis rats and longitudinally monitored through 14 days using BLI. A) Absolute BLI measurements showed that a similar number of viable cells was delivered across all rMSC-containing treatments. Additionally, the low signal for acellular samples (Acell-, Acell+) on Day 0 indicated minimal background signal produced by the BLI technique. B) Normalized BLI demonstrated a significant effect of cell presentation ($p_{SCvs.AG}$=0.009), but not PFTBA incorporation (p_{PFTBA}=0.075), on *in vivo* survival. Individual comparisons between treatments and timepoints revealed an increase in viable cell number for the SC- treatment at Day 1. (# = $p < 0.05$ within timepoint vs. all other treatments; $ = $p < 0.05$ within treatment vs. Days 7 and 14)

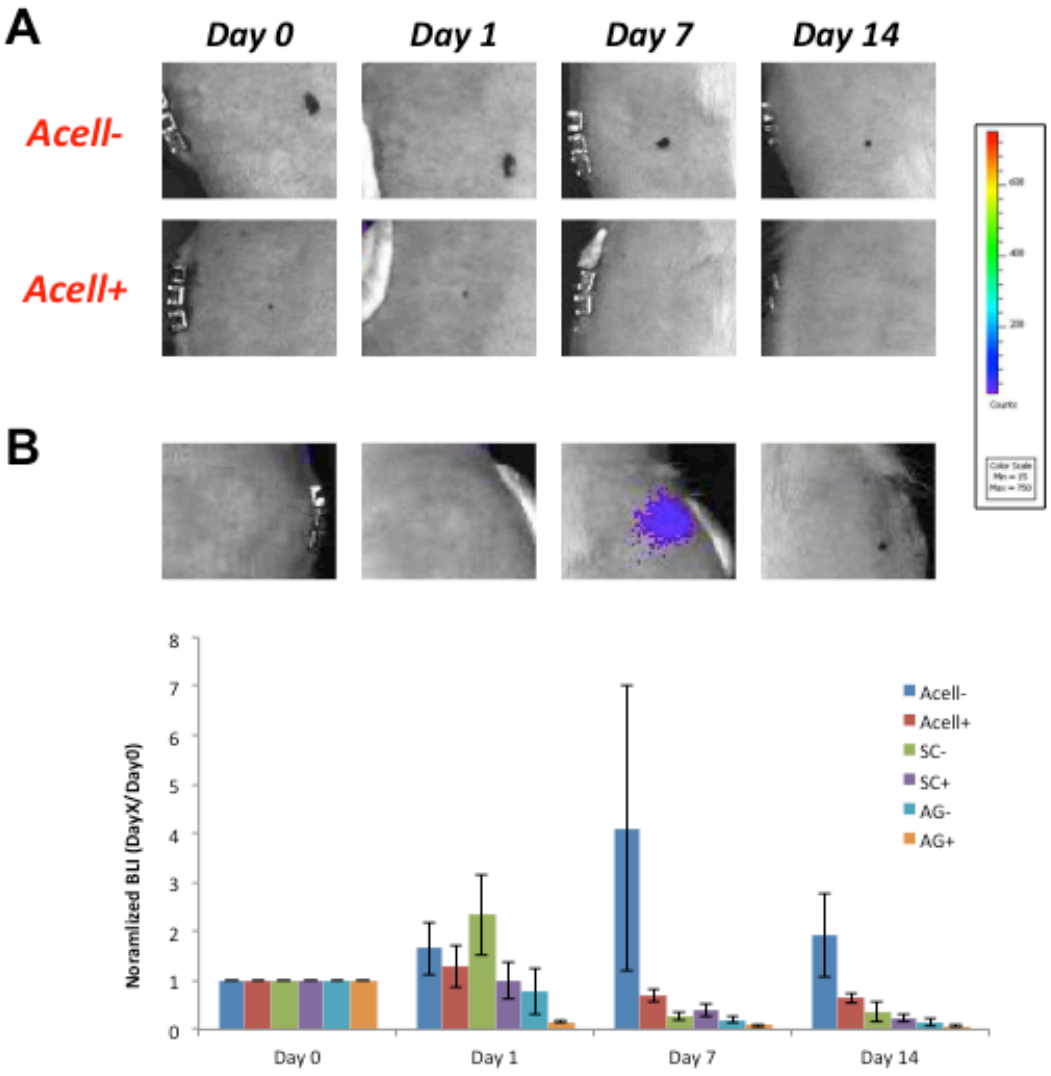

Figure 28: Longitudinal BLI of Acellular Constructs through 14 Days *In Vivo* A) Representative BLI heatmaps illustrate that the majority of acellular implants displayed negligible signal throughout the implantation duration. B) However, several acellular samples increased in BLI signal over time, as shown by heatmap images and normalized BLI signal (note Acell- value on Day 7). This behavior was not observed previously in Nude rat studies and no correlation was found between the BLI signal of Acell treatments vs. that of adjacent rMSC-seeded samples (data not shown).

Examining tissue composition within the subcutaneous explants, there was no qualitative effect of rMSC or PFTBA delivery on construct vessel size distribution or placement through the construct (Figure 29A). Upon quantification, these experimental parameters had no overall effect on construct vascular volume (Figure 29B). In comparing individual treatment groups, single rMSC seeded constructs without PFTBA (SC-) contained more vasculature than acellular, PFTBA-containing (Acell+) constructs. Histological examination via H&E staining revealed a similar extent of residual alginate pieces surrounded by granulation tissue across all experimental groups (Figure 30A). Consistent with bioluminescent data, fluorescence microscopy confirmed the retention of a delivered rMSC population within constructs initially seeded with singular and aggregated cells (Figure 30B). Aggregation may have promoted rMSC migration, as evidenced by single cells appearing to be retained within alginate pieces through 14 days despite delivered spheroids displaying an increase in cluster diameter over time.

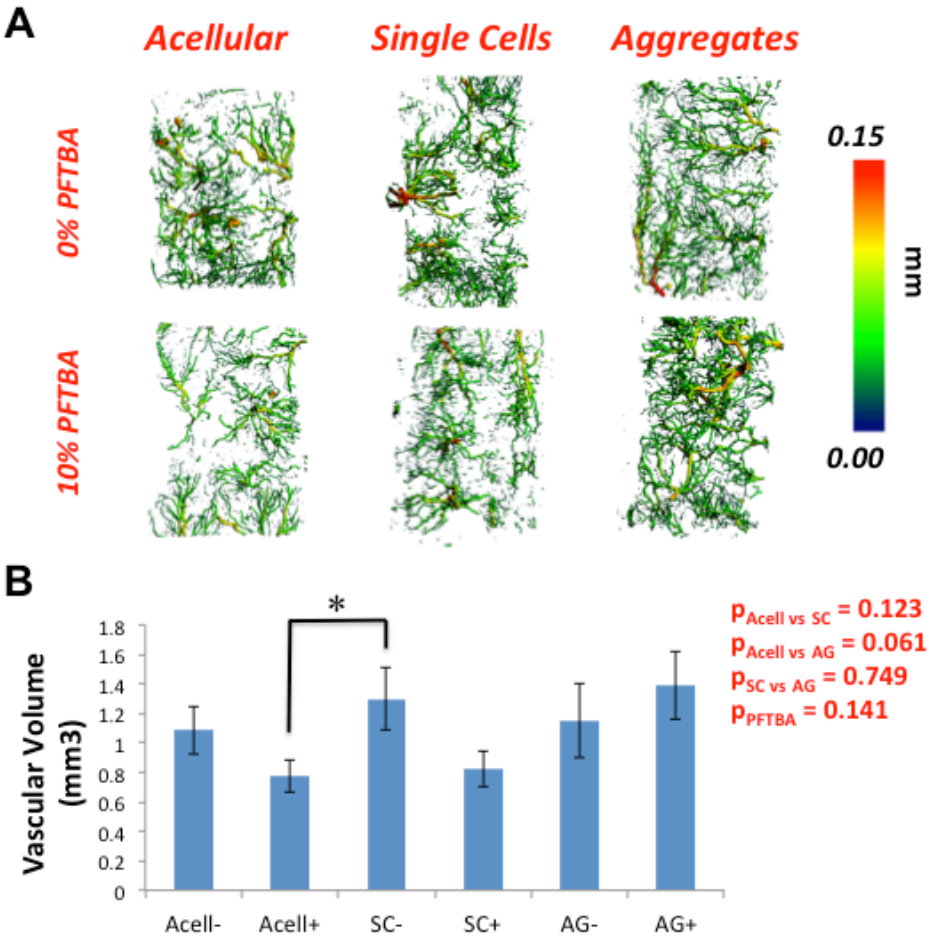

Figure 29: Effect of rMSC Aggregation on Construct Vasculature at 14 Days A) Vascular reconstructions illustrate vessel diameter distribution in representative images from each treatment group. Qualitatively, no gross effects of cell delivery group or PFTBA addition were apparent. B) Quantification of construct vascular volume found no overall effect of rMSC or PFTBA delivery. However, single cells constructs without co-delivered PFTBA had significantly more vasculature than acellular, PFTBA-containing constructs.

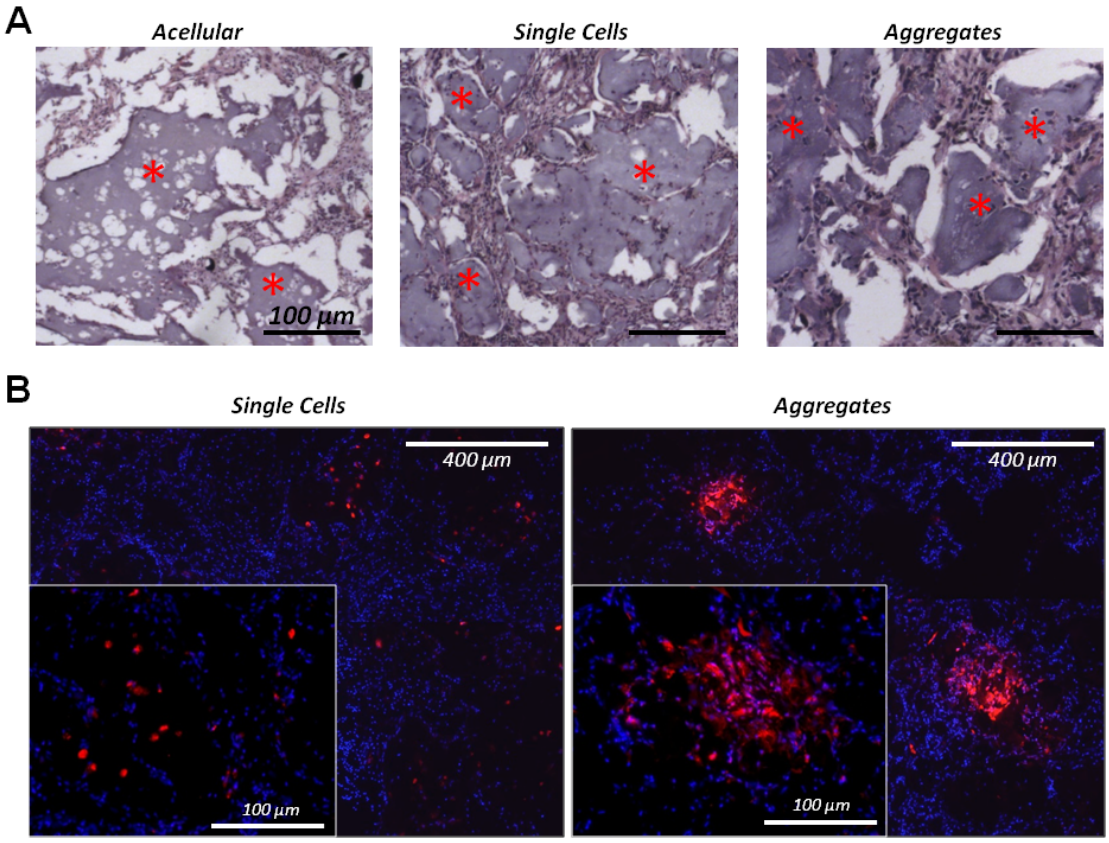

Figure 30: Effect of rMSC Aggregation on Construct Composition at 14 Days A) All treatment groups contained a similar extent of residual alginate pieces (red asterisks) surrounded by granulation tissue, as visualized through H&E staining (0% PFTBA groups shown). B) Fluorescent microscopy revealed the presence and distribution of delivered rMSCs (rMSCs = red (*DiI*); all nuclei = blue (*DAPI*)). Implanted single cells appeared to be retained within alginate pieces and away from regions of high cellularity. rMSCs delivered as spheroids remained clustered, although exhibiting a diameter greater than that of the initially implanted structures (~175 µm vs. ~100 µm), indicating the breakup of rMSC aggregates over time *in vivo*.

5.3.5 Release of BMP-2 from rMSC-Seeded Constructs *In Vitro*

In preparation to interrogate within the segmental defect model, the effect of rMSC and PFTBA incorporation on co-delivered BMP-2 release was quantified *in vitro*. Alginate/mesh constructs were prepared with no (Acell), singular (SC), or aggregated (AG) rMSCs, with (+) or without (-) PFTBA, and a 1.5-μg dose of BMP-2. Conditioned media was collected from cultured constructs on Days 1, 4, and 7 to measure (i) BMP-2 content and (ii) the capacity for ALP activity induction in a pre-osteoblast cell line (MC3T3-E1). Over the first 24 hrs of culture, constructs across all groups released comparable amounts of BMP-2 (Figure 31A). However, following this initial period, more BMP-2 was released from acellular constructs than those seeded with single ($p=0.002$) or aggregated ($p=0.046$) rMSCs. No effect of PFTBA incorporation was observed at any point in time. In contrast to BMP-2 release data, seeding of rMSCs considerably enriched the induction capacity of conditioned media on pre-osteoblast ALP activity (Figure 31B). Specifically, ALP activity for MC3T3-E1 cells treated with conditioned media from the first 24 hrs of construct culture was increased with rMSC-seeding and PFTBA addition. At all timepoints, media conditioned by aggregate-seeded constructs were most effective to induce ALP activity. To determine whether changes in induction capacity were attributed solely to MC3T3-E1 number, ALP activity was normalized to DNA content. Normalized data continued to show a benefit of rMSC and PFTBA delivery, indicating that enhancement of ALP activity was not due to perturbation of MC3T3-E1 cell number alone. In all, these promising *in vitro* results further encouraged challenging of the rMSC aggregation strategy within a bone defect model.

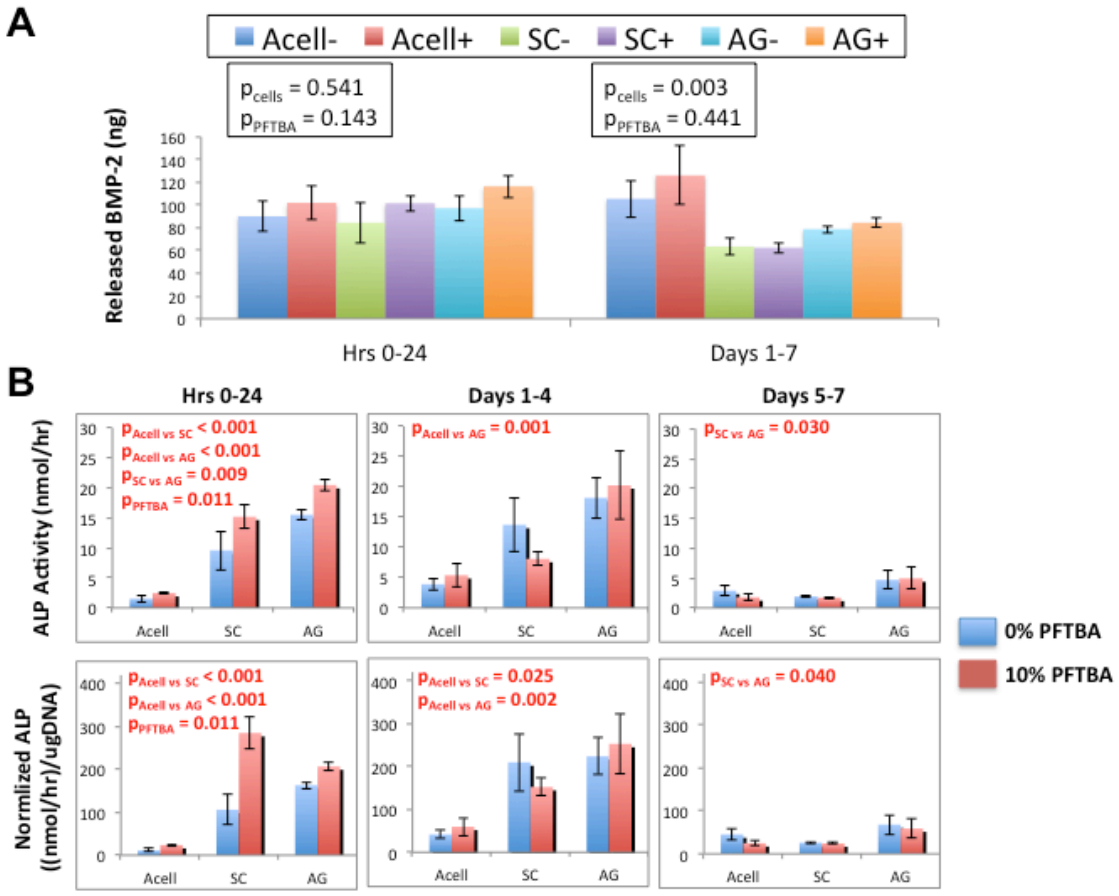

Figure 31: Effect of rMSC and PFTBA Delivery on *In Vitro* BMP-2 Release Acellular (Acell), single cell (SC), and aggregated (AG) rMSCs were embedded within alginate/mesh constructs with (+) or without (-) PFTBA and each containing a 1.5-µg dose of BMP-2. Constructs were cultured and conditioned media was collected over 7 days. A) BMP-2 released from the constructs was measured via ELISA. Over the first 24 hrs, all groups released similar amounts of BMP-2. However, following this initial period, acellular constructs released more BMP-2 than constructs seeded with single (p=0.002) or aggregated (p=0.046) rMSCs. There was no effect of PFTBA incorporation during either the first 24 hrs (p=0.143) or remaining (p=0.441) culture period. B) Despite BMP-2 release data, seeding of rMSCs led to increased induction of ALP activity in a pre-osteoblast cell line (MC3T3-E1) exposed to conditioned media. ALP activity was lower for acellular groups conditioned with media from the first 24 hrs in comparison to both rMSC-seeded groups (SC, AG). Media collected from aggregate-containing constructs at each timepoint induced ALP activity most strongly. Furthermore, PFTBA addition had an early positive effect (p=0.011). Normalized results indicate that changes in ALP activity were not due to altered MC3T3-E1 number alone.

5.3.6 rMSC Aggregate Delivery for Bone Defect Repair in Lewis Rats

To examine the effect of rMSC aggregation on cell-based bone regeneration, bilateral femoral defects created in Lewis rats were treated with alginate/mesh constructs containing a 1.5-μg dose of BMP-2, seeded with no cells, single rMSCs, or aggregated rMSCs, and comprised of 0 or 10% PFTBA. The effect of syringe incubation, as is necessary to facilitate delivery of alginate-embedded rMSC throughout each surgical day, on cell viability was first examined. rMSCs embedded as single cells and aggregates remained viable following 0-, 4-, and 8-hr syringe incubations at 4°C (Figure 32). To assess whether syringe incubation or the incorporation of emulsion (+/- PFTBA) incurred a delayed detriment to cell viability, rMSC-seeded hydrogels were culture 48 hrs and evaluated via metabolic rate assay. Neither syringe incubation ($p=0.170$) nor addition of emulsion ($p=0.129$) was found to adversely affect downstream rMSC viability (Figure 33).

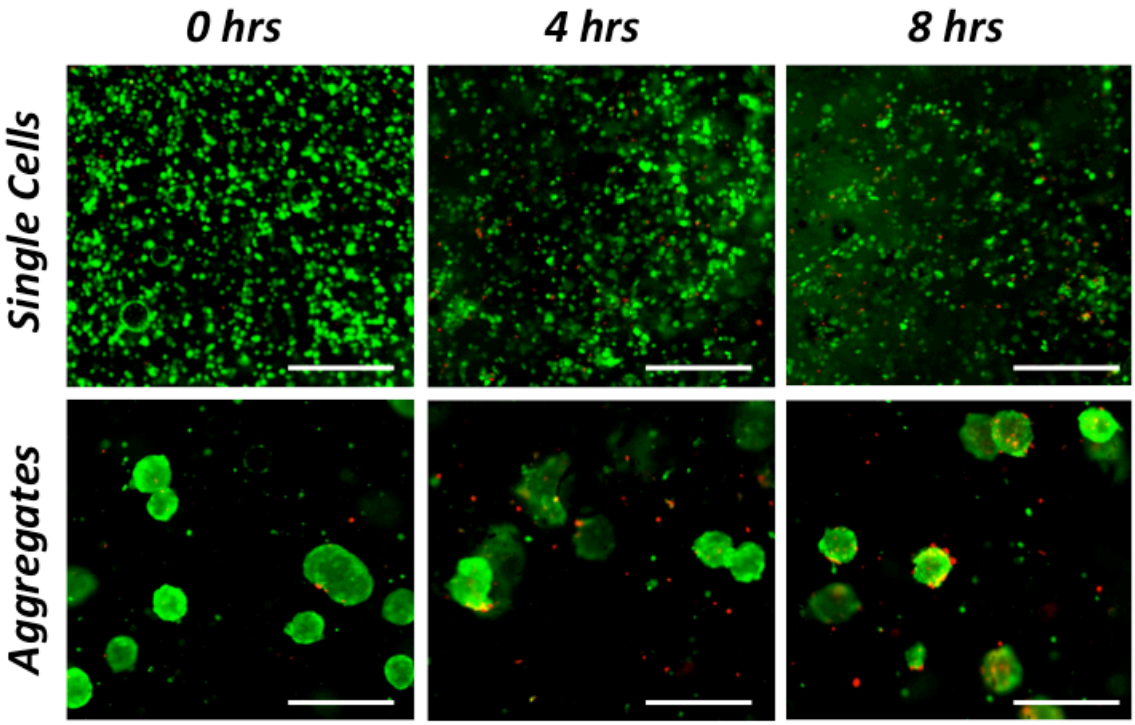

Figure 32: Viability of Alginate-Embedded rMSCs following Syringe Incubation Single cells and aggregates maintained viability (live = GFP (green); dead = ethidium homodimer (red)) following alginate embedding and syringe incubation at 4°C for 0, 4, or 8 hrs (scale bar = 200 μm).

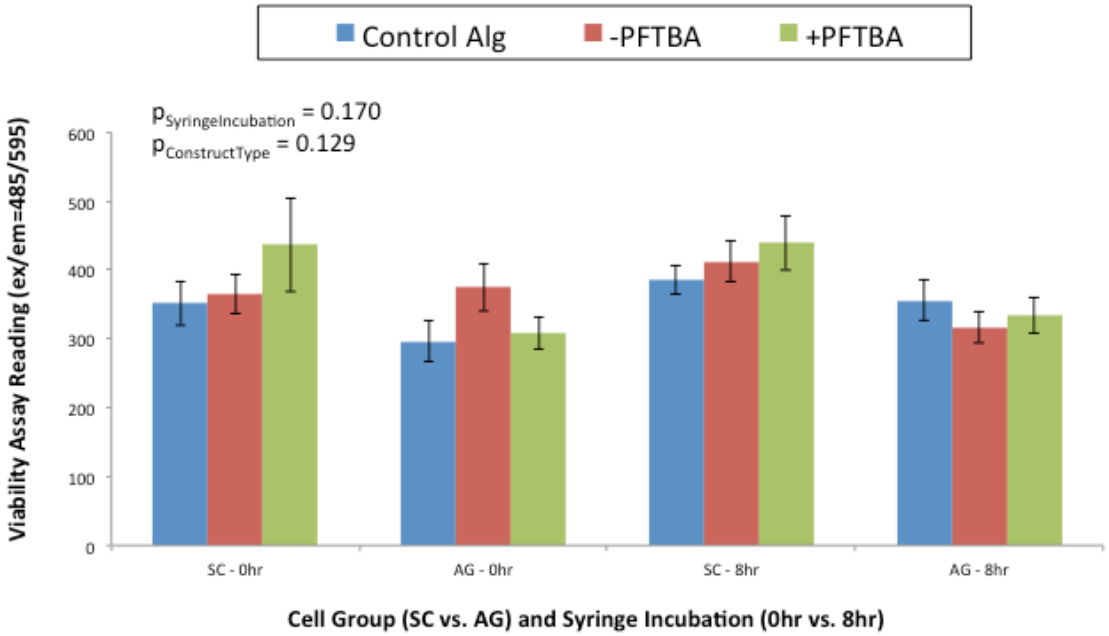

Figure 33: Embedded rMSC Viability Across Segmental Defect Treatments In preparation for segmental defect delivery, all cell-seeded treatments (single cell vs. aggregates +/- PFTBA) were cultured over 2 days following syringe incubation of 0 or 8 hrs at 4°C. Measurement using a metabolic rate assay indicated no adverse effect of syringe incubation (p=0.170) nor construct type (+/-PFTBA vs. alginate lacking emulsion; p=0.129) on rMSC viability (error bars = standard deviation).

Following *in vitro* validation of pre-surgical rMSC viability, alginate/mesh treatments were delivered to critically-sized bone defects created in Lewis rats. Longitudinal radiographs captured at 4, 8, and 12 weeks post-operatively showed a qualitative decrease in bone regeneration with rMSC or PFTBA delivery (Figure 34). In fact, only injuries treated by acellular constructs lacking PFTBA (Acell-) demonstrated defect bridging. Treated femurs were explanted and analyzed via μCT and torsional testing at 12 weeks. Representative mineral density heatmaps were consistent with radiograph observations, showing a qualitative attenuation of bone repair with rMSC or PFTBA delivery (Figure 35). Quantification of regenerated bone tissue properties revealed that bone volume was greatest with Acell- treatment and that rMSC or PFTBA addition attenuated regenerated bone volume in both an individual and additive manner (Figure 36A). Mean density was increased with cell ($p=0.025$), but not PFTBA ($p=0.172$), delivery (Figure 36B). Connectivity density varied with treatment group similarly to regenerated bone volume, with the addition of rMSCs ($p<0.001$) or PFTBA ($p=0.003$) resulting in a measure decrease (Figure 36C). Functional restoration of tissue function was accomplished to the greatest extent with Acell- treatment, as assessed by measurement of maximum torque (Figure 37A) and torsional stiffness (Figure 37B). The addition of rMSCs or PFTBA led to an overall decrease in either biomechanical metric.

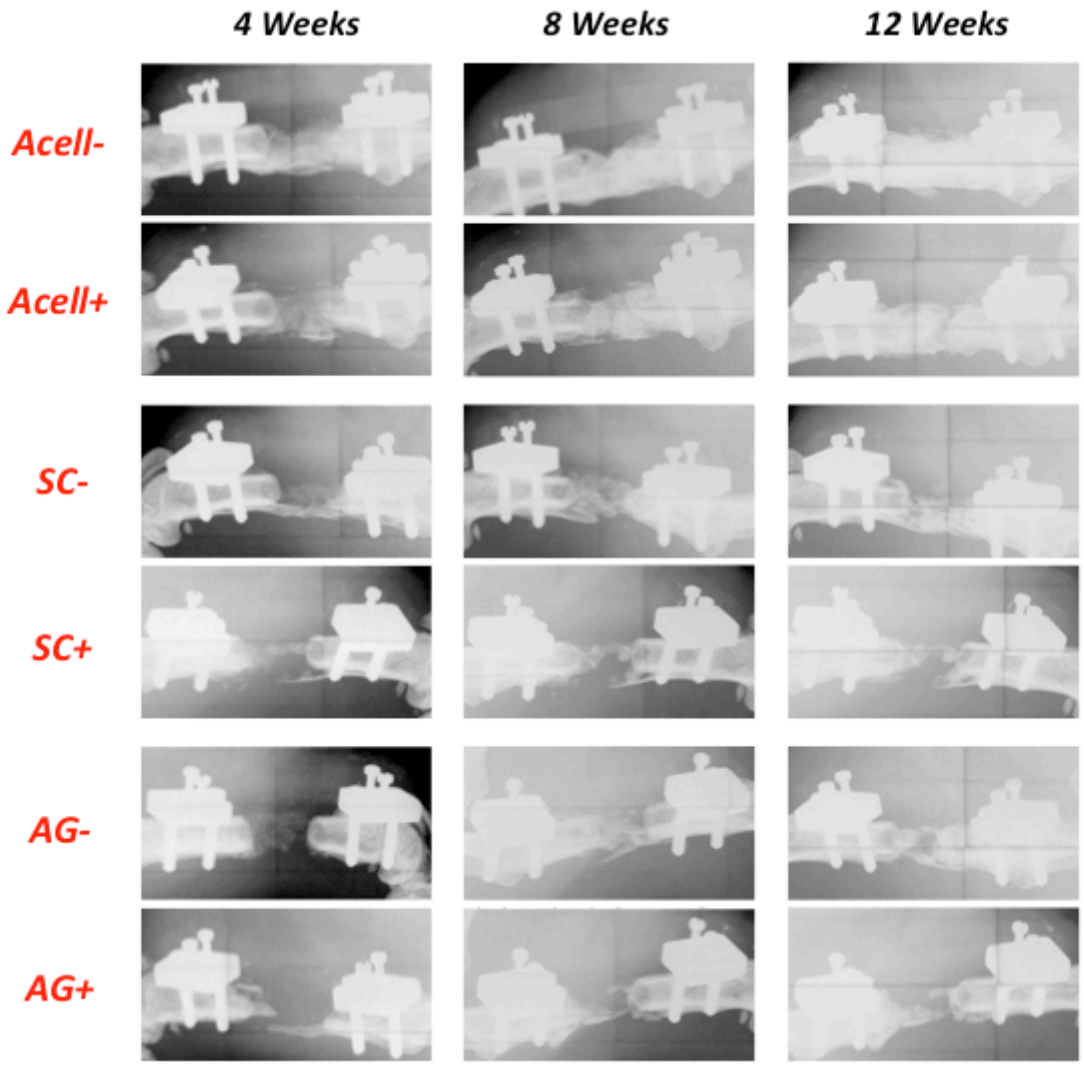

Figure 34: Radiographs of Large Bone Defect Repair in Lewis Rats Representative radiographs of critically-sized femoral defects treated with acellular (Acell), single cell (SC), and aggregate (AG) containing hydrogels with (+) or without (-) PFTBA show a qualitative decrease in bone regeneration with rMSC or PFTBA delivery. By 12 weeks, only samples in the Acell- treatment group exhibited bridging of the defect space.

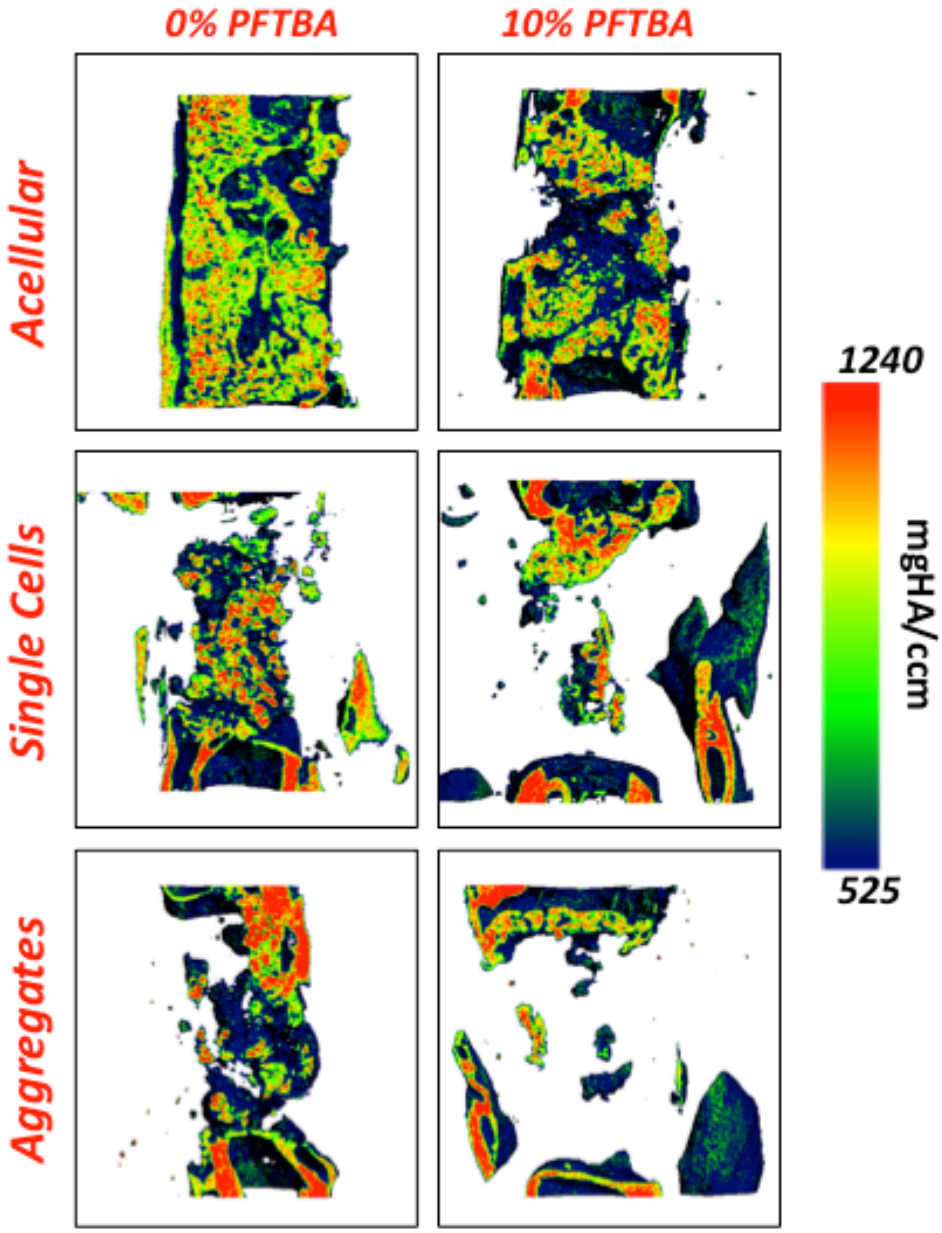

Figure 35: µCT Reconstruction of Bone Defect Repair in Lewis Rats at 12 Weeks Representative mineral density heatmaps of the defect space and native bone ends were generated from µCT data. rMSC and PFTBA delivery appeared to qualitatively reduce the amount of mineral present in the defect space. Consistent with radiograph observations, defect bridging occurred only with Acell- treatment.

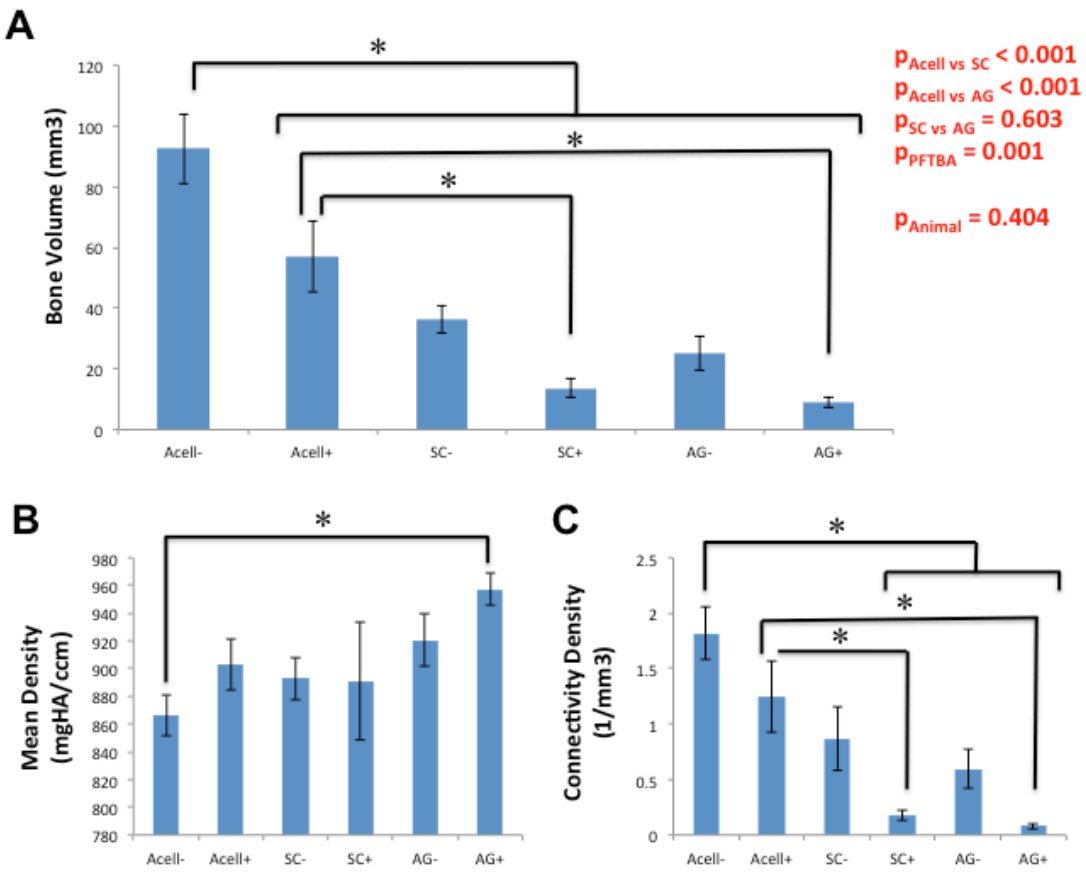

Figure 36: Properties of Regenerated Bone Tissue within Lewis Rat Defects A) Regenerated bone volume at 12 weeks was greatest for defects receiving acellular treatment lacking PFTBA (Acell-), as measured *ex vivo* via µCT. Treatment with rMSCs or PFTBA attenuated regenerated bone volume in both an individual and additive manner. B) Mean density exhibited an overall increase with cell ($p=0.025$), but not PFTBA ($p=0.172$), delivery. C) Connectivity density varied with treatment group similarly to regenerated bone volume, with the addition of rMSCs ($p<0.001$) or PFTBA ($p=0.003$) resulting in a decrease.

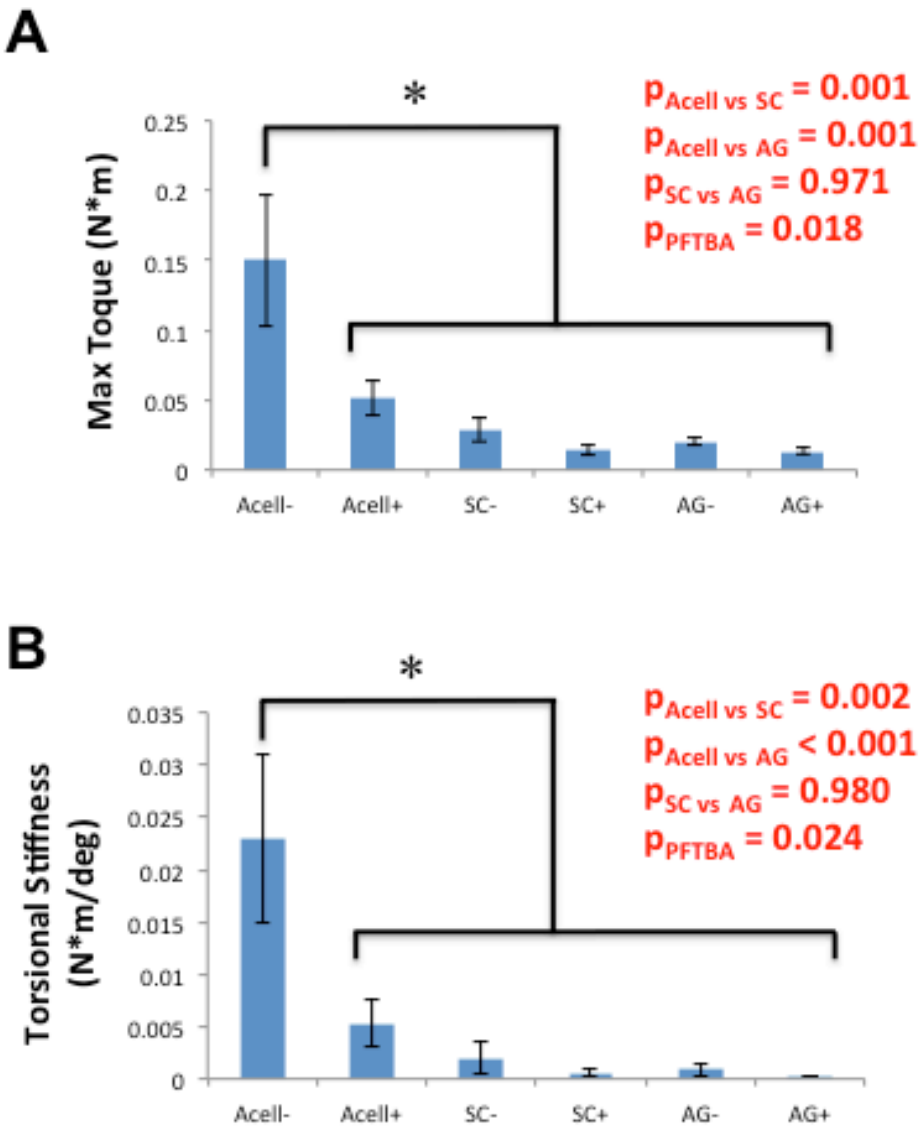

Figure 37: Biomechanical Testing of Lewis Rat Defects at 12 Weeks A) Maximum torque was significantly increased with Acell- treatment compared to all other groups. Addition of rMSCs (p_{SC}=0.001; p_{AG}=0.001) or PFTBA (p=0.018) each promoted an overall decrease in torque. B) Torsional stiffness values were similar to maximum torque data, with Acell- treatment resulting in the highest value and an observed detrimental effect of rMSC (p_{SC}=0.002; p_{AG}<0.001) or PFTBA (p=0.024) addition.

Tissue development within the defect space was examined histologically using a SafO stain and found to support μCT analysis (Figure 38). In the absence of rMSC or PFTBA delivery (Acell-), defects at 12 weeks contained organized bone tissue surrounding pieces of mineralized alginate. With the addition of cells or co-delivered PFTBA, mineralization within the injury space was qualitatively reduced and the presence of residual alginate increased.

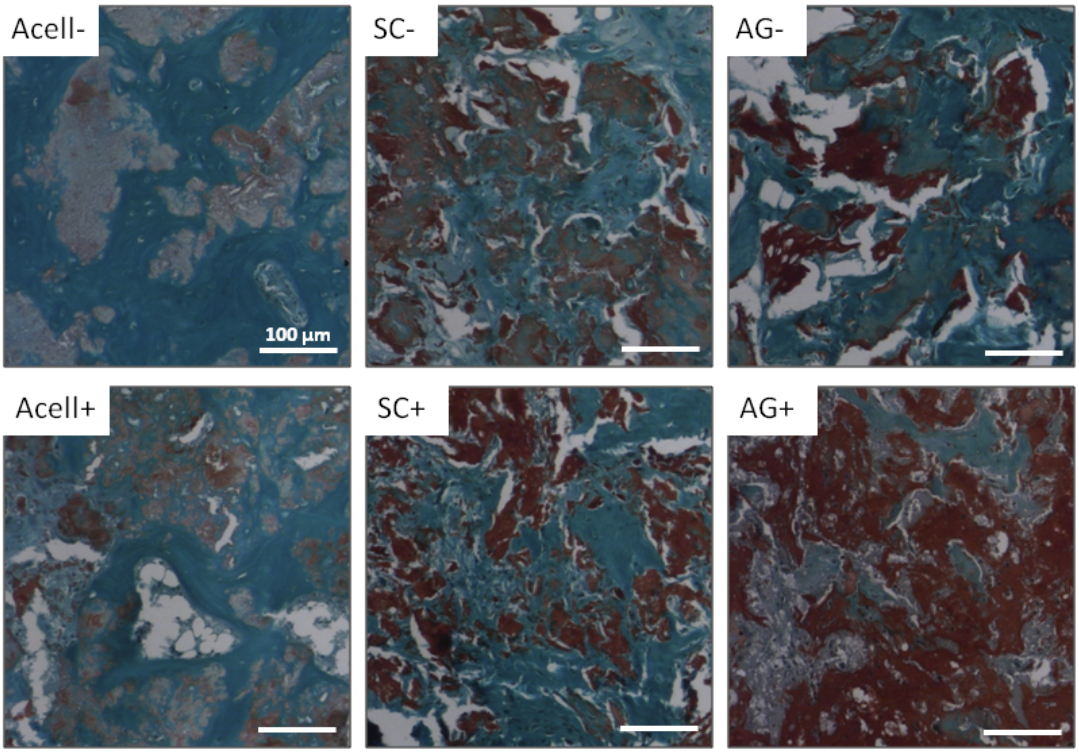

Figure 38: Histological Examination of Lewis Rat Defects at 12 Weeks Tissue development within the defect space varied with rMSC and PFTBA delivery, as visualized via SafO staining. Injuries treated with acellular hydrogel in the absence of co-delivered PFTBA (Acell-) contained the greatest extent of organized bone (blue) and mineralized alginate (pink) by 12 weeks. In contrast, delivery of rMSCs (singular (SC) or aggregated (AG)) or PFTBA (+) qualitatively decreased the extent of defect mineralization and increased the presence of residual alginate (red).

5.4 Discussion

Aggregation of MSCs is shown to engineer the cell secretome towards a pro-angiogenic and anti-inflammatory mixture of factors. Due to the interplay of regenerating bone tissue with its inflammatory and vascular environment, MSC aggregation was pursued as an approach to augment cell-based bone defect repair (Mountziaris, Spicer et al. 2011, Chim, Tickner et al. 2013, Krishnan, Willett et al. 2014). Using an immunocompromised rodent model, the effect of hMSC aggregation on cell survival and construct vasculature was first explored via a subcutaneous implantation study. Subsequently, the capacity of delivered hMSC spheroids to facilitate low dose BMP-2-mediated bone regeneration was evaluated within a critically-sized femoral defect.

hMSC aggregation produced comparable cell survival and construct vasculature when examined subcutaneously. Upon delivery to bone defects, hMSC single cell or aggregate delivery had no effect on regenerated bone volume or biomechanics in comparison to acellular treatment. However, within this animal model (Nude rats), biological variability was found to be a significant predictor of regenerative outcome. This finding motivated the continuation of aggregate delivery studies within a syngeneic animal model (Lewis rats).

In progression to the syngeneic model, *in vitro* characterization of rMSC spheroid immunomodulatory properties was first conducted. Consistent with hMSC findings, rMSC aggregation increased the secretion of IL-6 and PGE2 factors (Zimmermann and McDevitt 2014). Interestingly, aggregation also enhanced rMSC intracellular ALP activity. Although a known characteristic of MSC aggregates cultured under osteoinductive conditions, this had not previously investigated in the absence of

differentiation stimulus (Wang, Itaka et al. 2009, Frith, Thomson et al. 2010, Murphy, Fang et al. 2014, Yamaguchi, Ohno et al. 2014). Overall, similarities in the effect of MSC aggregation across cell species afforded pre-clinical relevance to testing spheroid delivery within the syngeneic rodent model.

In an effort to improve delivered rMSC survival, co-delivery of a synthetic oxygen carrier, PFTBA, was evaluated as well. Although perfluorocarbon addition to cell-seeded constructs has previously been shown to potentiate survival, our research did not observe this promotion of viable rMSC retention when tested under hypoxic culture or subcutaneously (Kimelman-Bleich, Pelled et al. 2009, Benjamin, Sheyn et al. 2013, Tamimi, Comeau et al. 2013). Given the extent of transport limitations imposed by our large volume alginate/mesh system, it's possible that the limited effect of perfluorocarbon incorporation was indiscernible experimentally (Goh, Gross et al. 2010). Despite the lack of efficacy observed in these studies, PFTBA incorporation may potentially hold promise in the case of hMSC delivery. rMSCs may be more resistant to hypoxic-induced death in comparison to hMSCs due to interspecies variability in apoptotic mechanism (Reed, Doctor et al. 2003). Within our alginate system, rMSCs displayed qualitatively superior maintenance of cell viability following prolonged syringe incubation compared to hMSCs. Additionally, subcutaneous delivery of rMSC-seeded constructs achieved an *in vivo* survival of 6 - 40% through day 14, whereas the survival rate for hMSC-seeded constructs (hPL incorporation study samples included) was 1.5 - 2.5%.

Despite no effect on embedded rMSC number, PFTBA incorporation facilitated a short-term enhancement of osteoinductive factor release, as examined using an ALP induction assay performed on pre-osteoblasts. However, more striking augmentation of

osteoinductive factor release, in terms of effect size and timeframe, was achieved with embedded rMSC aggregates. This effect may be attributable to any number of secreted factors acting in isolation or synergistically to promote osteogenesis. rMSC spheroids exhibit increased fibroblast growth factor (FGF) and decreased dickkopf 1 (Dkk-1) production, each serving to facilitate osteoblast differentiation (Marie 2003, Fujita and Janz 2007, Zhang, Cho et al. 2008, Sart, Ma et al. 2014). Although enhanced expression of PGE2 and IL-6 motivated the evaluation of aggregation for MSC-based bone repair, the osteoinductive effect observed in this assay was likely not due to these anti-inflammatory factors. IL-6 is shown to reduce ALP activity in the cell line studied here and PGE2 is considered to impact bone repair predominantly via immune cell signaling (Thomas and Puleo 2011, Kaneshiro, Ebina et al. 2014, Kovach, Dighe et al. 2015). In fact, similarly to IL-6 expression, aggregate-driven PGE2 signaling may have also acted counter to the observed effect, as increased PGE2 concentration is associated with a decrease in MC3T3-E1 ALP activity (Yokota, Kusaka et al. 1986, Suda, Tanaka et al. 1998, Dey, Lejeune et al. 2006).

In spite of the promising osteogenic properties *in vitro*, delivery of rMSC-seeded treatments to a critically-sized bone defect attenuated BMP-2-mediated repair. This discrepancy may have been due to the more complex cellular environment present at the orthotopic injury site, an intricate milieu not captured *in vitro*. Possible explanations for the hindered bone repair with rMSC delivery include a reduction in the co-delivered BMP-2 available to endogenous cell populations, unfavorable effects of rMSC waste or death-associated factors, and adverse disruption of the post-injury inflammatory phase (Mountziaris and Mikos 2008, Dosier, Uhrig et al. 2015). In the absence of intervention,

bone regeneration proceeds through an initial inflammatory period which acts to engage a host of cell types at the site of injury, including the eventual recruitment of MSCs, and has proven essential to functional tissue restoration (Thomas and Puleo 2011). Although serving to position an osteoprogenitor cell type within the defect space, immediate delivery of MSCs could instead obstruct the early TNF-α and interleukin 1 (IL-1) signaling necessary for endogenous cell homing (Barnes, Kostenuik et al. 1999, Dimitriou, Tsiridis et al. 2005, Ortiz, Dutreil et al. 2007).

This presented research falls short of relating delivered rMSC survival to regenerative efficacy, as there is no evidence suggesting PFTBA incorporation or cell aggregation modulated cell survival within our delivery system. However, the effect of PFTBA treatment independent from rMSC-related outcomes was successfully isolated, finding that PFTBA addition to alginate/mesh constructs reduced bone regeneration irrespective of co-delivered rMSCs. PFTBA has previously been found to improve cell-based mineralization, but had not been evaluated for its impact on acellular treatment strategy (Kimelman-Bleich, Pelled et al. 2009, Benjamin, Sheyn et al. 2013, Tamimi, Comeau et al. 2013). As PFTBA incorporation had no discernible effect on released BMP-2 quantity *in vitro*, we hypothesize that PFTBA-attenuated bone repair *in vivo* may have been due to differential release kinetics not captured by the *in vitro* timepoints selected or the consequence of modified alginate matrix properties, potentially perturbing the migration of endogenous cells into the defect region (White, Stoppel et al. 2013).

Overall, despite a multitude of *in vitro* evidence that MSC aggregation alters paracrine signaling, the present study observed no effect of spheroid delivery on cell-based bone regeneration. Furthermore, MSC delivery was observed to attenuate BMP-2-

mediated bone defect repair in comparison to acellular treatment. This latter finding was perhaps more unexpected, as several reports have demonstrated the efficacy of cell-based bone repair strategies *in vivo* (Ghantoji, Sail et al. 2010, Sheyn, Mizrahi et al. 2010, Dosier, Uhrig et al. 2015). We believe this discontinuity may be due to collective differences in the delivery vehicle (e.g. size and composition), stem cell type (e.g. source and extent of multipotency), and animal model (e.g. rodent strain and defect location) examined. In fact, previous work using alginate/mesh vehicles to induce ectopic mineralization identified a divergent effect of MSC delivery depending on cell source (Dosier, Uhrig et al. 2015).

This work highlighted the impact of animal model (immunocompromised vs. syngeneic) on the degree of biological variability present in a bone healing scenario. The effect of perfluorocarbon delivery on acellular BMP-2-mediated bone regeneration was also investigated which, to our knowledge, had not been previously pursued. Additional experiments, either through more sophisticated culture systems (e.g. co-culturing multiple cell types) or early timepoint analysis, are necessary to mechanistically probe the MSC- and PFTBA-attenuated bone repair observed in this study.

CHAPTER 6 CONCLUSIONS AND FUTURE DIRECTIONS

6.1 Summary

The objective of this research was to expose fundamental principles in developing an efficacious mesenchymal stem cell (MSC)-based therapeutic for the treatment of large bone defects. This effort was pursued through the investigation of two stem cell delivery strategies: utilization of platelet lysate (PL) and cell aggregation. The early and extensive death of stem cells following implantation is a well-established hurdle to development of volumetric tissue regeneration therapies. For this reason, we aimed to inspect the effect of MSC delivery strategy on implanted cell viability in addition to cell-based bone defect repair. Thus, our initial objective was the validation of a bioluminescent imaging (BLI) tracking protocol enabling the longitudinal monitoring of delivered MSCs *in vivo*.

Using an immunocompromised rodent model, we developed a BLI technique capable of monitoring viable hMSC number through 1 week *in vivo*. Luciferase-labeled hMSCs were delivered within hydrogel/mesh constructs of large volume (>200 mm^3), approaching the scale necessary to evaluate clinical applicability. Each hydrogel system tested, despite differences in signal magnitude, achieved a linear correlation between BLI signal and viable cell number immediately following implantation. Quantification of hMSCs present within alginate explants at 1 week using flow cytometry corroborated BLI data, demonstrating that a BLI signal vs. cell number correlation was retained, although of reduced correlative strength (r^2=0.912 vs. r^2=0.422). The observed decrease in correlation coefficient, suggestive of confounding variables present within the system, coincided with the development of contiguous fibrotic and vascular tissues. Overall, this

research developed an operational tool for the evaluation of cell-based delivery strategies while drawing attention to the potential impact of tissue development in its subsequent implementation.

Following development and characterization of BLI technique, this tool was used to evaluate the potential of human platelet lysate (hPL) as a pre-treatment or co-delivery strategy for improved hMSC survival following implantation. Although culture in hPL media produced long-lasting hMSC expansion benefits *in vitro*, application prior to *in vivo* delivery elicited a reduction in delivered cell survival at 1 week. Incorporation of hPL within alginate/mesh constructs was also examined and observed to have no effect on the maintenance of hMSC viability through 14 days post-operatively. The utility of rodent models to serve as a pre-clinical testing stage for hPL co-delivery was subsequently examined. Potential limitations of the immunocompromised model were first investigated by studying the interaction between hPL and rMSCs, selected as a model host cell type. Exposure to hPL-supplemented media resulted in rMSC death, a process deemed attributable to heat labile proteins, but not due to membrane attack complex (MAC) formation. Next, the capacity of a syngeneic model to inform pre-clinical decisions was examined through evaluation of interspecies variability for the PL product (hPL vs. rPL) and its effect on MSCs (hPL/hMSCs vs. rPL/rMSCs). The rodent system was found to be fundamentally distinct, with rPL having reduced growth factor content and stimulating no reduction in rMSC doubling time for the serum concentrations examined (5 and 10% v/v).

The pursued hPL studies were motivated predominantly by an effort to enhance hMSC survival upon delivery. In an alternative strategy for improved cell-based bone

regeneration therapeutics, the effect of delivered cell function was explored through MSC aggregation, an approach shown to modulate hMSC paracrine signaling *in vitro*. When tested in a Nude rat subcutaneous implant model, hMSC aggregation achieved *in vivo* cell survival and construct vasculature comparable to that of delivered single cells. Through successive testing within a critically-sized bone defect, all BMP-2 containing treatment groups realized similar bone repair irrespective of whether they were seeded with singular, aggregated, or no hMSCs. However, biological variability was found to significantly predict regenerative outcome, a discovery that motivated further investigation of MSC aggregation using a syngeneic rodent model. rMSC aggregates were first characterized *in vitro* and shown to exhibit anti-inflammatory properties similar to that of hMSC aggregates. Consistent with the immunocompromised study, there was no effect of rMSC aggregation on cell survival or construct vasculature upon subcutaneous delivery. However, when combined with a low dose of BMP-2 (1.5 μg/construct), aggregate-seeded alginate/mesh matrices showed encouraging results *in vitro*. Although incorporation of rMSC aggregates reduced the quantity of BMP-2 released over 1 week in culture, the overall osteoinductive potential of construct-released factors was shown to increase, as assessed using a pre-osteoblast ALP induction assay. Yet despite this promising performance *in vitro*, delivery of rMSC-seeded vehicles attenuated functional regeneration in comparison to acellular treatment when challenged within the femoral defect model.

This research aimed to elucidate fundamental principles for cell-based bone regeneration strategies through the investigation of hPL utilization and cell aggregation. Through this effort, the benefits and limitations of *in vitro* and rodent pre-clinical testbeds

were highlighted. Further attention was drawn to the selection of rodent strain in testing of biologic therapeutics (e.g. cells and blood-derived products). Using multiple implantation and *in vivo* monitoring techniques, survival and regenerative outcome measures were assessed for each MSC delivery strategy, serving to better understand how each variable may be perturbed and the extent of their interdependency within a large volume, cell delivery system. This work provides an experimental platform with which future cell-based therapeutic strategies could be tested.

6.2 Future Directions for hPL Utilization

Although limitations of hPL pre-clinical testing were identified for both immunocompromised and syngeneic animal models, the utility of a co-delivery strategy could be further challenged using heat-inactivated hPL. Deactivation of the heat labile proteins responsible for rMSC death observed *in vitro* may lead to a more favorable interaction between rat host cells and the hPL-releasing construct. Additionally, the percentage of incorporated hPL could be increased from that examined in these studies in an effort to potentiate the treatment effect size. The 20% v/v concentration tested in this research was selected on the basis of (i) necessitation of a non-hPL hydrogel backbone (hMSC-seeded 100% v/v hPL hydrogels were contracted down to qualitatively negligible construct volume when cultured over 2 days *in vitro*) and (ii) ease in adaptation of our present syringe mixing protocol (during which 3% w/v alginate hydrogel is diluted down to 2%, limiting the added volume of all other components to 50 μL/construct). Our mixing protocol has since been adapted to accommodate the PBS/PFTBA emulsion

volume delivered for rMSC aggregates studies, thus the barrier to implanting a vehicle of higher hPL concentration has already been reduced.

While hPL pre-treatment showed no benefit in our studies, its application towards expansion of hMSCs for large volume tissue regeneration may still hold translational promise. The hMSCs delivered in this study were at low (3-4) passage. However, more pronounced effects of hPL vs. FBS culture have been noted for hMSCs at higher (10-11) passage (Griffiths, Baraniak et al. 2013). In a clinical setting, delivery of autologous hMSCs can require *ex vivo* expansion to moderately high passage in order to reach necessary cell number. Thus, in a clinically motivated study, the pre-treatment strategies presented here could be reassessed using hMSCs of higher (e.g. 5) passage to observe whether efficacy is achieved.

6.3 Future Directions for MSC Aggregate Delivery

Despite the promising effect of rMSC-seeding, either as single or aggregated cells, on the osteoinductive capacity of construct-released factors *in vitro*, cell delivery went on to attenuate bone defect repair when challenged *in vivo*. Potential mechanisms for this include the engagement of alternative host cell populations (aside from the pre-osteoblast phenotype tested *in vitro*) and rMSC-produced factors that act on this more complex range of endogenous cell types, potentially in a manner counterproductive to injury resolution. Further, it is likely that embedded rMSCs may have functioned differently within the *in vivo* environment due to differences in oxygen, nutrients, and waste transport as well as the existence of delivered vs. host cell cross-talk, distinct from the scenario of one-way communication tested *in vitro*. To probe the mechanism behind a

lack of *in vivo* efficacy, the ALP induction *in vitro* experiment could be carried out under hypoxic or MC3T3-E1 co-culture conditions, two strategies aimed at better recapitulating the *in vivo* milieu. Using this experimental design, the effect of delivery strategy on previously untested cell populations, including osteoblasts, osteoclasts, fibroblasts, and inflammatory cells, could also be explored.

Although we did not observe the immunomodulatory potential of MSC aggregates translating to enhanced bone repair, our studies took only one approach to investigating their effect on BMP-2-mediated regeneration. Rather than evaluating MSC aggregation for the improvement of low dose BMP-2 delivery, future work could explore the potential for MSC aggregates to mitigate the complications associated with high dose BMP-2 treatment. Clinical application of BMP-2 often entails supra-physiologic dosing resulting in complications such as heterotopic bone formation and inflammation (Ratko, Belinson et al. 2010, Fu, Selph et al. 2013). Work in our lab has recently identified up-regulation of interferon gamma (IFN-γ) in the bone defect and adjacent muscle tissue (data not yet published) in response to high dose BMP-2 delivery. While MSCs have an inherent capacity to lower IFN-γ production from natural kill cells, this action is mediated by PGE2 and indoleamine 2,3-dioxygenase (IDO), two factors secreted in greater quantity with MSC aggregation (Spaggiari, Capobianco et al. 2008, Kode, Mukherjee et al. 2009, Zimmermann and McDevitt 2014).

6.4 Discussion of Cell Delivery for Volumetric Tissue Regeneration

Cell delivery strategies for volumetric tissue regeneration face numerous hurdles. Ideally, delivery approaches would be targeted towards advancement of cell survival as

well as function, be this engineered secretion of factors or guided cell differentiation. In the presented research, each of these outcome measures was evaluated using a large volume alginate/mesh delivery system. However, a sequential approach to this research challenge could prove more fruitful. For example, delivery strategies could first be screened on the basis of implanted cell function by means of a small volume construct for which nutrient and waste transport is less limited. Successful approaches could then be scaled up in size to observe their impact on cell survival within these large volume systems. If maintained viability is found insufficient, efforts to augment it could be implemented through modulated design parameters. An iterative process using the small volume system to validate preservation of desired cell function with each added survival-enhancing measure, followed by scale up to the large volume constructs, would constitute a logical workflow to isolate the collective potential of cell delivery techniques.

One specific approach that could be tested in conjunction with hPL or aggregation strategies for the improvement of delivered MSC survival and facilitated regeneration is modification of the hydrogel carrier. While alginate hydrogel has proven to be an advantageous material for osteoinductive protein delivery, it may not be best suited for cell-based treatments. Alternative carriers used in tissue engineering applications include a spectrum of synthetic and naturally-derived scaffold materials. Additionally, these materials can be engineered through the manipulation of intrinsic properties of the pre-existing backbone (e.g. structural properties) as well as the addition of controllable functional components (e.g. biological properties) (Lutolf and Hubbell 2005, Zhu 2010, Chan, Wippich et al. 2012). For example, functionalization of the poly(ethylene glycol) (PEG) synthetic hydrogel with the integrin-specific peptide GFOGER has been effective

to improve cell-based bone defect repair (Shekaran, Garcia et al. 2014). Alternatively, scaffolds sourced from mammalian, rather than plant, tissues could be investigated. Such matrices to be considered range from polymeric extracted proteins (e.g. collagen, gelatin, and fibrin) to native extracellular matrix (ECM) materials (e.g. amniotic membrane and small intestinal submucosa (SIS)) and represent highly attractive options due to their inherent bioactivity and amenability to remodeling by cells *in vivo* (Ruoslahti 2003, Erdbrugger, Konertz et al. 2006, Malafaya, Silva et al. 2007, Andree, Bar et al. 2013, Koob, Rennert et al. 2013, Murphy, McDevitt et al. 2014, Allen, Priddy et al. 2015). For example, use of a fibrin carrier has demonstrated efficacy of cell-based techniques for mineralized tissue formation within a variety of animal models (Sheyn, Kallai et al. 2011, Benjamin, Sheyn et al. 2013). Physical and biochemical cues of the biomaterial work in concert to drive embedded cell behavior including motility, proliferation, differentiation, and growth factor secretion (Marklein and Burdick 2010, Renth and Detamore 2012, Tejeda-Montes, Smith et al. 2012). Thus, despite the intrinsic functionality of naturally-derived mammalian materials in their raw form, structural and biofunctional augmentation techniques for these matrices have been explored in an effort to further cell-based regenerative potential (Haghi and Akbari 2007, Malafaya, Silva et al. 2007, Renth and Detamore 2012, Bajaj, Schweller et al. 2014, Allen, Priddy et al. 2015). Approaches including the use of composite materials, manipulation of mechanical properties, and addition of heparin-binding domains (HBD) or enzymatically cleavable sequences have demonstrated efficacy in modulating embedded cell function and facilitating cell-based bone tissue engineering (Engler, Sen et al. 2006, Choi, Lee et al. 2010, Fu, Wang et al. 2010, Feng, Zhu et al. 2014, Inzana, Olvera et al. 2014, Levato,

Visser et al. 2014). Overall, the investigatory space of carrier systems that may serve to potentiate cell-based bone regeneration is great and worthy of exploration.

Alternate or complementary to modifying the hydrogel carrier, implementation of construct pre-vascularization or addition of vascular constituents pre-implantation could be pursued. Efforts to accelerate early vascularization of large volume constructs have taken many forms, including the addition of vascular components (e.g. cells and vessel fragments) which have demonstrated the ability to inosculate with host vasculature following implantation (Rouwkema, Rivron et al. 2008, Zhou, Zhou et al. 2010, Novosel, Kleinhans et al. 2011, Laschke and Menger 2012, Krishnan, Chang et al. 2013, McFadden, Duffy et al. 2013). Such techniques aimed to improve early vascularization may prove effective for potentiating delivered cell survival within our alginate/mesh delivery system and potentially enable the benefit of hPL or aggregation strategies to be realized.

While efforts to enhance early construct vasculature may improve delivered cell survival, it should be noted that these system variables are unlikely to change in isolation. Work validating the BLI tracking protocol observed alteration of BLI profile contiguous with construct tissue development. Construct material properties, such as stiffness, have also been found to change with promotion of construct vasculature (Krishnan, Hoying et al. 2007). Interdependency of these therapeutic characteristics should not be overlooked, as construct vasculature could potentially be modified even in the absence of focused manipulation; for example, in selection of an animal model. Restructuring data from this thesis work to evaluate construct vascular volume as a function of delivered MSC species/strain (human, Lewis rat, or Sprague Dawley rat) and rodent model (Nude, Lewis,

or Sprague Dawley rat), there was no effect of the immunocompromised (n=53) vs. syngeneic (n=28) delivery on vascularization (Figure 39). However, seeding of constructs with Sprague Dawley-derived rMSCs may undergo strain-specific vascularization. As the sample size for these groups was small (n=4), further studies are necessary to determine whether these results are representative or a consequence of biological variability.

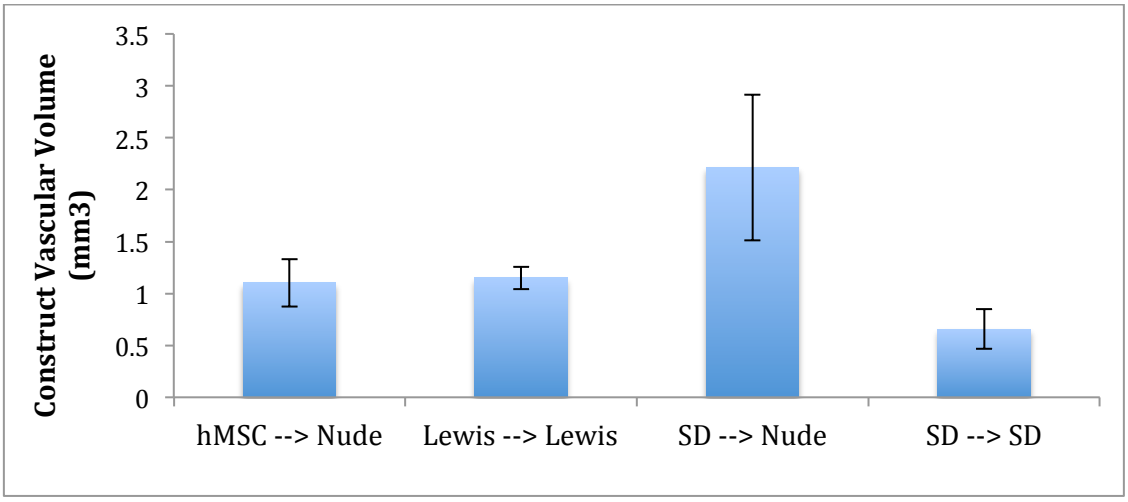

Figure 39: Construct Vascular Volume by Animal Model Construct vascular volume across all alginate/mesh subcutaneous MSC delivery samples presented in this thesis (hPL pre-treatment, hPL co-delivery, and single cell vs. aggregates studies) was not observed to differ as a function of immunocompromised (hMSC → Nude) or syngeneic (Lewis → Lewis) rodent model. However, delivery of Sprague Dawley (SD) rMSCs may promote construct vasculature in a rodent strain dependent manner (n=4). As each treatment was examined within a single animal, a larger sample size is needed to determine whether this is a representative effect of treatment or due to biological variability within this study.

6.5 Final Conclusions and Significance

We conclude that, while BLI may prove advantageous for informing large volume cell-based therapeutic design, care should be taken when implementing and drawing quantitative conclusions using this assessment technique. Furthermore, this thesis work highlights that two hydrogels of relatively similar material properties can exhibit divergent behavior under bioluminescent analysis. Overall, validation of BLI protocol and investigation of potentially confounding variables, such as vascular ingrowth and fibrosis, should be conducted on a system-by-system basis in order to draw representative conclusions in future analyses.

Although hPL utilization and MSC aggregation did not prove advantageous for maintenance of cell survival or facilitated bone regeneration in this body of work, these strategies may be efficacious in alternate, and perhaps more clinically relevant, delivery scenarios. As mentioned, hPL utilization could be investigated for improved high passage MSC delivery and a future direction of MSC aggregation may be to preclude high dose BMP-2 complications.

Importantly, this presented work draws attention to the critical task of animal model selection in developing a cell-based regenerative therapeutic. Both immunocompromised and syngeneic systems are with distinct benefits and limitations. It is necessary to acknowledge the utilities of each and select a model based on this knowledge. In the case of evaluating MSC-based delivery strategies, the extent of "immunological privilege" afforded to this cell type should not be overstated (Ankrum, Ong et al. 2014). Although dramatic hMSC death was observed in many of the presented experiments, viable delivered cells were consistently detectable through the study

conclusion (7 or 14 days) when delivered to Nude rats. In contrast, a pilot study conducted in Lewis rats detected no signal from GFP/Luc hMSCs past 5 and 7 days for aggregated and singular hMSCs, respectively (data not shown). Thus, challenging hMSC delivery approaches within an immunocompetent animal model is not a viable testbed for strategies aimed at achieving long-term cell survival.

Ultimately, the best approach for evaluating cell-based bone regeneration techniques may be the use of multiple rodent animal models. In addition to revealing the robustness of therapeutic strategy through evaluation within multiple test systems, dissimilarities in efficacy may provide valuable insight into therapeutic mechanism. Furthermore, recent studies have highlighted the meager reproducibility of published biomedical findings (Prinz, Schlange et al. 2011, Begley and Ellis 2012). Examination of a promising phenomenon within multiple animal models may confirm its fortitude and, where applicable, facilitate eventual clinical translation.

REFERENCES

Aarden, E. M., E. H. Burger and P. J. Nijweide (1994). "Function of osteocytes in bone." J Cell Biochem **55**(3): 287-299.

Aerssens, J., J. Dequeker and J. M. Mbuyi-Muamba (1994). "Bone tissue composition: biochemical anatomy of bone." Clin Rheumatol **13 Suppl 1**: 54-62.

Aggarwal, S. and M. F. Pittenger (2005). "Human mesenchymal stem cells modulate allogeneic immune cell responses." Blood **105**(4): 1815-1822.

Aguilar, S., E. Nye, J. Chan, M. Loebinger, B. Spencer-Dene, N. Fisk, G. Stamp, D. Bonnet and S. M. Janes (2007). "Murine but not human mesenchymal stem cells generate osteosarcoma-like lesions in the lung." Stem Cells **25**(6): 1586-1594.

Alivisatos, A. P., W. Gu and C. Larabell (2005). "Quantum dots as cellular probes." Annu Rev Biomed Eng **7**: 55-76.

Allen, A. B., Z. Gazit, S. Su, H. Y. Stevens and R. E. Guldberg (2014). "In vivo bioluminescent tracking of mesenchymal stem cells within large hydrogel constructs." Tissue Eng Part C Methods **20**(10): 806-816.

Allen, A. B., L. B. Priddy, M. T. Li and R. E. Guldberg (2015). "Functional augmentation of naturally-derived materials for tissue regeneration." Ann Biomed Eng **43**(3): 555-567.

Alsberg, E., H. J. Kong, Y. Hirano, M. K. Smith, A. Albeiruti and D. J. Mooney (2003). "Regulating bone formation via controlled scaffold degradation." J Dent Res **82**(11): 903-908.

Andree, B., A. Bar, A. Haverich and A. Hilfiker (2013). "Small intestinal submucosa segments as matrix for tissue engineering: review." Tissue Eng Part B Rev **19**(4): 279-291.

Anitua, E., I. Andia, B. Ardanza, P. Nurden and A. T. Nurden (2004). "Autologous platelets as a source of proteins for healing and tissue regeneration." Thromb Haemost **91**(1): 4-15.

Anitua, E. and G. Orive (2012). "Endogenous regenerative technology using plasma- and platelet-derived growth factors." J Control Release **157**(3): 317-320.

Ankrum, J. A., J. F. Ong and J. M. Karp (2014). "Mesenchymal stem cells: immune evasive, not immune privileged." Nat Biotechnol **32**(3): 252-260.

Arbab, A. S., L. A. Bashaw, B. R. Miller, E. K. Jordan, J. W. Bulte and J. A. Frank (2003). "Intracytoplasmic tagging of cells with ferumoxides and transfection agent for

cellular magnetic resonance imaging after cell transplantation: methods and techniques." Transplantation **76**(7): 1123-1130.

Aspenberg, P. and T. Turek (1996). "BMP-2 for intramuscular bone induction: effect in squirrel monkeys is dependent on implantation site." Acta Orthop Scand **67**(1): 3-6.

Au, P., J. Tam, D. Fukumura and R. K. Jain (2008). "Bone marrow-derived mesenchymal stem cells facilitate engineering of long-lasting functional vasculature." Blood **111**(9): 4551-4558.

Avanzini, M. A., M. E. Bernardo, A. M. Cometa, C. Perotti, N. Zaffaroni, F. Novara, L. Visai, A. Moretta, C. Del Fante, R. Villa, L. M. Ball, W. E. Fibbe, R. Maccario and F. Locatelli (2009). "Generation of mesenchymal stromal cells in the presence of platelet lysate: a phenotypic and functional comparison of umbilical cord blood- and bone marrow-derived progenitors." Haematologica **94**(12): 1649-1660.

Awad, H. A., M. Q. Wickham, H. A. Leddy, J. M. Gimble and F. Guilak (2004). "Chondrogenic differentiation of adipose-derived adult stem cells in agarose, alginate, and gelatin scaffolds." Biomaterials **25**(16): 3211-3222.

Azouna, N. B., L. Berraeis, Z. Regaya and F. Jenhani (2011). "Immunophenotyping of hematopoietic progenitor cells: Comparison between cord blood and adult mobilized blood grafts." World J Stem Cells **3**(11): 104-112.

Bago, J. R., E. Aguilar, M. Alieva, C. Soler-Botija, O. F. Vila, S. Claros, J. A. Andrades, J. Becerra, N. Rubio and J. Blanco (2013). "In vivo bioluminescence imaging of cell differentiation in biomaterials: a platform for scaffold development." Tissue Eng Part A **19**(5-6): 593-603.

Bahney, C. S., D. P. Hu, T. Miclau, 3rd and R. S. Marcucio (2015). "The multifaceted role of the vasculature in endochondral fracture repair." Front Endocrinol (Lausanne) **6**: 4.

Baik, S. Y., Y. A. Lim, S. J. Kang, S. H. Ahn, W. G. Lee and C. H. Kim (2014). "Effects of platelet lysate preparations on the proliferation of HaCaT cells." Ann Lab Med **34**(1): 43-50.

Bajaj, P., R. M. Schweller, A. Khademhosseini, J. L. West and R. Bashir (2014). "3D Biofabrication Strategies for Tissue Engineering and Regenerative Medicine." Annual Review of Biomedical Engineering **16**(1).

Ball, S. G., C. A. Shuttleworth and C. M. Kielty (2007). "Mesenchymal stem cells and neovascularization: role of platelet-derived growth factor receptors." J Cell Mol Med **11**(5): 1012-1030.

Banfi, A., A. Muraglia, B. Dozin, M. Mastrogiacomo, R. Cancedda and R. Quarto (2000). "Proliferation kinetics and differentiation potential of ex vivo expanded human

bone marrow stromal cells: Implications for their use in cell therapy." Exp Hematol **28**(6): 707-715.

Banwart, J. C., M. A. Asher and R. S. Hassanein (1995). "Iliac crest bone graft harvest donor site morbidity. A statistical evaluation." Spine (Phila Pa 1976) **20**(9): 1055-1060.

Barnes, G. L., P. J. Kostenuik, L. C. Gerstenfeld and T. A. Einhorn (1999). "Growth factor regulation of fracture repair." J Bone Miner Res **14**(11): 1805-1815.

Barry, F. P. and J. M. Murphy (2004). "Mesenchymal stem cells: clinical applications and biological characterization." Int J Biochem Cell Biol **36**(4): 568-584.

Bartholomew, A., C. Sturgeon, M. Siatskas, K. Ferrer, K. McIntosh, S. Patil, W. Hardy, S. Devine, D. Ucker, R. Deans, A. Moseley and R. Hoffman (2002). "Mesenchymal stem cells suppress lymphocyte proliferation in vitro and prolong skin graft survival in vivo." Exp Hematol **30**(1): 42-48.

Bartosh, T. J., J. H. Ylostalo, A. Mohammadipoor, N. Bazhanov, K. Coble, K. Claypool, R. H. Lee, H. Choi and D. J. Prockop (2010). "Aggregation of human mesenchymal stromal cells (MSCs) into 3D spheroids enhances their antiinflammatory properties." Proc Natl Acad Sci U S A **107**(31): 13724-13729.

Bastian, O., J. Pillay, J. Alblas, L. Leenen, L. Koenderman and T. Blokhuis (2011). "Systemic inflammation and fracture healing." J Leukoc Biol **89**(5): 669-673.

Beamer, B., C. Hettrich and J. Lane (2010). "Vascular endothelial growth factor: an essential component of angiogenesis and fracture healing." HSS J **6**(1): 85-94.

Becquart, P., A. Cambon-Binder, L. E. Monfoulet, M. Bourguignon, K. Vandamme, M. Bensidhoum, H. Petite and D. Logeart-Avramoglou (2012). "Ischemia is the prime but not the only cause of human multipotent stromal cell death in tissue-engineered constructs in vivo." Tissue Eng Part A **18**(19-20): 2084-2094.

Begley, C. G. and L. M. Ellis (2012). "Drug development: Raise standards for preclinical cancer research." Nature **483**(7391): 531-533.

Ben Azouna, N., F. Jenhani, Z. Regaya, L. Berraeis, T. Ben Othman, E. Ducrocq and J. Domenech (2012). "Phenotypical and functional characteristics of mesenchymal stem cells from bone marrow: comparison of culture using different media supplemented with human platelet lysate or fetal bovine serum." Stem Cell Res Ther **3**(1): 6.

Benglis, D., M. Y. Wang and A. D. Levi (2008). "A comprehensive review of the safety profile of bone morphogenetic protein in spine surgery." Neurosurgery **62**(5 Suppl 2): ONS423-431; discussion ONS431.

Benjamin, S., D. Sheyn, S. Ben-David, A. Oh, I. Kallai, N. Li, D. Gazit and Z. Gazit (2013). "Oxygenated environment enhances both stem cell survival and osteogenic differentiation." Tissue Eng Part A **19**(5-6): 748-758.

Bensaid, W., J. T. Triffitt, C. Blanchat, K. Oudina, L. Sedel and H. Petite (2003). "A biodegradable fibrin scaffold for mesenchymal stem cell transplantation." Biomaterials **24**(14): 2497-2502.

Berger, F., R. Paulmurugan, S. Bhaumik and S. S. Gambhir (2008). "Uptake kinetics and biodistribution of 14C-D-luciferin--a radiolabeled substrate for the firefly luciferase catalyzed bioluminescence reaction: impact on bioluminescence based reporter gene imaging." Eur J Nucl Med Mol Imaging **35**(12): 2275-2285.

Bernardo, M. E., M. A. Avanzini, C. Perotti, A. M. Cometa, A. Moretta, E. Lenta, C. Del Fante, F. Novara, A. de Silvestri, G. Amendola, O. Zuffardi, R. Maccario and F. Locatelli (2007). "Optimization of in vitro expansion of human multipotent mesenchymal stromal cells for cell-therapy approaches: further insights in the search for a fetal calf serum substitute." J Cell Physiol **211**(1): 121-130.

Bernardo, M. E., A. M. Cometa, D. Pagliara, L. Vinti, F. Rossi, R. Cristantielli, G. Palumbo and F. Locatelli (2011). "Ex vivo expansion of mesenchymal stromal cells." Best Pract Res Clin Haematol **24**(1): 73-81.

Bernardo, M. E., N. Zaffaroni, F. Novara, A. M. Cometa, M. A. Avanzini, A. Moretta, D. Montagna, R. Maccario, R. Villa, M. G. Daidone, O. Zuffardi and F. Locatelli (2007). "Human bone marrow derived mesenchymal stem cells do not undergo transformation after long-term in vitro culture and do not exhibit telomere maintenance mechanisms." Cancer Res **67**(19): 9142-9149.

Berner, A., J. D. Boerckel, S. Saifzadeh, R. Steck, J. Ren, C. Vaquette, J. Q. Zhang, M. Nerlich, R. E. Guldberg, D. W. Hutmacher and M. A. Woodruff (2012). "Biomimetic tubular nanofiber mesh and platelet rich plasma-mediated delivery of BMP-7 for large bone defect regeneration." Cell Tissue Res **347**(3): 603-612.

Berrey, B. H., Jr., C. F. Lord, M. C. Gebhardt and H. J. Mankin (1990). "Fractures of allografts. Frequency, treatment, and end-results." J Bone Joint Surg Am **72**(6): 825-833.

Berridge, M. V., N. O'Kech, L. J. McNeilage, B. F. Heslop and R. Moore (1979). "Rat mutant (NZNU) showing "nude" characteristics." Transplantation **27**(6): 410-413.

Bessa, P. C., M. Casal and R. L. Reis (2008). "Bone morphogenetic proteins in tissue engineering: the road from laboratory to clinic, part II (BMP delivery)." J Tissue Eng Regen Med **2**(2-3): 81-96.

Bhang, S. H., S. W. Cho, W. G. La, T. J. Lee, H. S. Yang, A. Y. Sun, S. H. Baek, J. W. Rhie and B. S. Kim (2011). "Angiogenesis in ischemic tissue produced by spheroid grafting of human adipose-derived stromal cells." Biomaterials **32**(11): 2734-2747.

Bhang, S. H., S. Lee, J. Y. Shin, T. J. Lee and B. S. Kim (2012). "Transplantation of cord blood mesenchymal stem cells as spheroids enhances vascularization." Tissue Eng Part A.

Bieback, K., S. Kern, H. Kluter and H. Eichler (2004). "Critical parameters for the isolation of mesenchymal stem cells from umbilical cord blood." Stem Cells **22**(4): 625-634.

Bittira, B., D. Shum-Tim, A. Al-Khaldi and R. C. Chiu (2003). "Mobilization and homing of bone marrow stromal cells in myocardial infarction." Eur J Cardiothorac Surg **24**(3): 393-398.

Blair, J. M., H. Zhou, M. J. Seibel and C. R. Dunstan (2006). "Mechanisms of disease: roles of OPG, RANKL and RANK in the pathophysiology of skeletal metastasis." Nat Clin Pract Oncol **3**(1): 41-49.

Blair, P. and R. Flaumenhaft (2009). "Platelet alpha-granules: basic biology and clinical correlates." Blood Rev **23**(4): 177-189.

Blanchard, F., L. Duplomb, M. Baud'huin and B. Brounais (2009). "The dual role of IL-6-type cytokines on bone remodeling and bone tumors." Cytokine Growth Factor Rev **20**(1): 19-28.

Boerckel, J. D., Y. M. Kolambkar, K. M. Dupont, B. A. Uhrig, E. A. Phelps, H. Y. Stevens, A. J. Garcia and R. E. Guldberg (2011). "Effects of protein dose and delivery system on BMP-mediated bone regeneration." Biomaterials **32**(22): 5241-5251.

Boerckel, J. D., B. A. Uhrig, N. J. Willett, N. Huebsch and R. E. Guldberg (2011). "Mechanical regulation of vascular growth and tissue regeneration in vivo." Proc Natl Acad Sci U S A **108**(37): E674-680.

Boland, T., V. Mironov, A. Gutowska, E. A. Roth and R. R. Markwald (2003). "Cell and organ printing 2: fusion of cell aggregates in three-dimensional gels." Anat Rec A Discov Mol Cell Evol Biol **272**(2): 497-502.

Boskey, A. L. and A. S. Posner (1984). "Bone structure, composition, and mineralization." Orthop Clin North Am **15**(4): 597-612.

Boutilier, R. G. (2001). "Mechanisms of cell survival in hypoxia and hypothermia." J Exp Biol **204**(Pt 18): 3171-3181.

Bruder, S. P. and B. S. Fox (1999). "Tissue engineering of bone. Cell based strategies." Clin Orthop Relat Res(367 Suppl): S68-83.

Bruder, S. P., N. Jaiswal, N. S. Ricalton, J. D. Mosca, K. H. Kraus and S. Kadiyala (1998). "Mesenchymal stem cells in osteobiology and applied bone regeneration." Clin Orthop Relat Res(355 Suppl): S247-256.

Buckwalter, J. A. and R. R. Cooper (1987). "Bone structure and function." Instr Course Lect **36**: 27-48.

Bulte, J. W., T. Douglas, B. Witwer, S. C. Zhang, B. K. Lewis, P. van Gelderen, H. Zywicke, I. D. Duncan and J. A. Frank (2002). "Monitoring stem cell therapy in vivo using magnetodendrimers as a new class of cellular MR contrast agents." Acad Radiol **9 Suppl 2**: S332-335.

Burdick, J. A. (2012). "Injectable gels for tissue/organ repair." Biomed Mater **7**(2): 020201.

Calori, G. M., W. Albisetti, A. Agus, S. Iori and L. Tagliabue (2007). "Risk factors contributing to fracture non-unions." Injury **38 Suppl 2**: S11-18.

Calori, G. M., E. Mazza, M. Colombo and C. Ripamonti (2011). "The use of bone-graft substitutes in large bone defects: any specific needs?" Injury **42 Suppl 2**: S56-63.

Campagnoli, C., I. A. Roberts, S. Kumar, P. R. Bennett, I. Bellantuono and N. M. Fisk (2001). "Identification of mesenchymal stem/progenitor cells in human first-trimester fetal blood, liver, and bone marrow." Blood **98**(8): 2396-2402.

Canalis, E. (1993). "Insulin like growth factors and the local regulation of bone formation." Bone **14**(3): 273-276.

Cao, J., B. Luo, H. Lin and S. Chen (2011). "Photocatalytic activity of novel AgBr/WO3 composite photocatalyst under visible light irradiation for methyl orange degradation." J Hazard Mater **190**(1-3): 700-706.

Cao, L., G. Liu, Y. Gan, Q. Fan, F. Yang, X. Zhang, T. Tang and K. Dai (2012). "The use of autologous enriched bone marrow MSCs to enhance osteoporotic bone defect repair in long-term estrogen deficient goats." Biomaterials **33**(20): 5076-5084.

Caplan, A. I. (1991). "Mesenchymal stem cells." J Orthop Res **9**(5): 641-650.

Caplan, A. I. (2005). "Review: mesenchymal stem cells: cell-based reconstructive therapy in orthopedics." Tissue Eng **11**(7-8): 1198-1211.

Caplan, A. I. (2007). "Adult mesenchymal stem cells for tissue engineering versus regenerative medicine." J Cell Physiol **213**(2): 341-347.

Caplan, A. I. (2009). "New era of cell-based orthopedic therapies." Tissue Eng Part B Rev **15**(2): 195-200.

Caplan, A. I. and D. Correa (2011). "PDGF in bone formation and regeneration: new insights into a novel mechanism involving MSCs." J Orthop Res **29**(12): 1795-1803.

Carrade, D. D. and D. L. Borjesson (2013). "Immunomodulation by mesenchymal stem cells in veterinary species." Comp Med **63**(3): 207-217.

Carrancio, S., N. Lopez-Holgado, F. M. Sanchez-Guijo, E. Villaron, V. Barbado, S. Tabera, M. Diez-Campelo, J. Blanco, J. F. San Miguel and M. C. Del Canizo (2008).

"Optimization of mesenchymal stem cell expansion procedures by cell separation and culture conditions modification." Exp Hematol **36**(8): 1014-1021.

Chambers, T. J., S. Fox, C. J. Jagger, J. M. Lean and J. W. Chow (1999). "The role of prostaglandins and nitric oxide in the response of bone to mechanical forces." Osteoarthritis Cartilage **7**(4): 422-423.

Chan, B. K., C. C. Wippich, C. J. Wu, P. M. Sivasankar and G. Schmidt (2012). "Robust and semi-interpenetrating hydrogels from poly(ethylene glycol) and collagen for elastomeric tissue scaffolds." Macromol Biosci **12**(11): 1490-1501.

Chan, R. K., P. Liu, D. H. Lew, S. I. Ibrahim, R. Srey, C. R. Valeri, H. B. Hechtman and D. P. Orgill (2005). "Expired liquid preserved platelet releasates retain proliferative activity." J Surg Res **126**(1): 55-58.

Chaudhary, L. R. and L. V. Avioli (1997). "Activation of extracellular signal-regulated kinases 1 and 2 (ERK1 and ERK2) by FGF-2 and PDGF-BB in normal human osteoblastic and bone marrow stromal cells: differences in mobility and in-gel renaturation of ERK1 in human, rat, and mouse osteoblastic cells." Biochem Biophys Res Commun **238**(1): 134-139.

Chiellini, C., O. Cochet, L. Negroni, M. Samson, M. Poggi, G. Ailhaud, M. C. Alessi, C. Dani and E. Z. Amri (2008). "Characterization of human mesenchymal stem cell secretome at early steps of adipocyte and osteoblast differentiation." BMC Mol Biol **9**: 26.

Chim, S. M., J. Tickner, S. T. Chow, V. Kuek, B. Guo, G. Zhang, V. Rosen, W. Erber and J. Xu (2013). "Angiogenic factors in bone local environment." Cytokine Growth Factor Rev **24**(3): 297-310.

Choi, Y. J., J. Y. Lee, J. H. Park, J. B. Park, J. S. Suh, Y. S. Choi, S. J. Lee, C. P. Chung and Y. J. Park (2010). "The identification of a heparin binding domain peptide from bone morphogenetic protein-4 and its role on osteogenesis." Biomaterials **31**(28): 7226-7238.

Ciapetti, G., D. Granchi and N. Baldini (2012). "The combined use of mesenchymal stromal cells and scaffolds for bone repair." Curr Pharm Des **18**(13): 1796-1820.

Colnot, C. (2009). "Skeletal cell fate decisions within periosteum and bone marrow during bone regeneration." J Bone Miner Res **24**(2): 274-282.

Cramer, D. V. (2000). "Natural antibodies and the host immune responses to xenografts." Xenotransplantation **7**(2): 83-92.

Crane, J. L. and X. Cao (2014). "Function of matrix IGF-1 in coupling bone resorption and formation." J Mol Med (Berl) **92**(2): 107-115.

da Silva Meirelles, L., A. I. Caplan and N. B. Nardi (2008). "In search of the in vivo identity of mesenchymal stem cells." Stem Cells **26**(9): 2287-2299.

da Silva Meirelles, L., P. C. Chagastelles and N. B. Nardi (2006). "Mesenchymal stem cells reside in virtually all post-natal organs and tissues." J Cell Sci **119**(Pt 11): 2204-2213.

Dallari, D., M. Fini, C. Stagni, P. Torricelli, N. Nicoli Aldini, G. Giavaresi, E. Cenni, N. Baldini, A. Cenacchi, A. Bassi, R. Giardino, P. M. Fornasari and A. Giunti (2006). "In vivo study on the healing of bone defects treated with bone marrow stromal cells, platelet-rich plasma, and freeze-dried bone allografts, alone and in combination." J Orthop Res **24**(5): 877-888.

Davis, B. H., T. Schroeder, P. S. Yarmolenko, F. Guilak, M. W. Dewhirst and D. A. Taylor (2007). "An in vitro system to evaluate the effects of ischemia on survival of cells used for cell therapy." Ann Biomed Eng **35**(8): 1414-1424.

de Almeida, P. E., J. R. van Rappard and J. C. Wu (2011). "In vivo bioluminescence for tracking cell fate and function." Am J Physiol Heart Circ Physiol **301**(3): H663-671.

De Bari, C., F. Dell'Accio, F. Vandenabeele, J. R. Vermeesch, J. M. Raymackers and F. P. Luyten (2003). "Skeletal muscle repair by adult human mesenchymal stem cells from synovial membrane." J Cell Biol **160**(6): 909-918.

de Boer, J., C. van Blitterswijk and C. Lowik (2006). "Bioluminescent imaging: emerging technology for non-invasive imaging of bone tissue engineering." Biomaterials **27**(9): 1851-1858.

de Jong, W. H., P. A. Steerenberg, P. S. Ursem, A. D. Osterhaus, J. G. Vos and E. J. Ruitenberg (1980). "The athymic nude rat. III. Natural cell-mediated cytotoxicity." Clin Immunol Immunopathol **17**(2): 163-172.

De Long, W. G., Jr., T. A. Einhorn, K. Koval, M. McKee, W. Smith, R. Sanders and T. Watson (2007). "Bone grafts and bone graft substitutes in orthopaedic trauma surgery. A critical analysis." J Bone Joint Surg Am **89**(3): 649-658.

De Miguel, M. P., S. Fuentes-Julian, A. Blazquez-Martinez, C. Y. Pascual, M. A. Aller, J. Arias and F. Arnalich-Montiel (2012). "Immunosuppressive properties of mesenchymal stem cells: advances and applications." Curr Mol Med **12**(5): 574-591.

De Ugarte, D. A., K. Morizono, A. Elbarbary, Z. Alfonso, P. A. Zuk, M. Zhu, J. L. Dragoo, P. Ashjian, B. Thomas, P. Benhaim, I. Chen, J. Fraser and M. H. Hedrick (2003). "Comparison of multi-lineage cells from human adipose tissue and bone marrow." Cells Tissues Organs **174**(3): 101-109.

Dey, I., M. Lejeune and K. Chadee (2006). "Prostaglandin E2 receptor distribution and function in the gastrointestinal tract." Br J Pharmacol **149**(6): 611-623.

Dhurat, R. and M. Sukesh (2014). "Principles and Methods of Preparation of Platelet-Rich Plasma: A Review and Author's Perspective." J Cutan Aesthet Surg **7**(4): 189-197.

Dimitriou, R., E. Tsiridis and P. V. Giannoudis (2005). "Current concepts of molecular aspects of bone healing." Injury **36**(12): 1392-1404.

Dobnig, H., F. Kainer, V. Stepan, R. Winter, R. Lipp, M. Schaffer, A. Kahr, S. Nocnik, G. Patterer and G. Leb (1995). "Elevated parathyroid hormone-related peptide levels after human gestation: relationship to changes in bone and mineral metabolism." J Clin Endocrinol Metab **80**(12): 3699-3707.

Dohan Ehrenfest, D. M., L. Rasmusson and T. Albrektsson (2009). "Classification of platelet concentrates: from pure platelet-rich plasma (P-PRP) to leucocyte- and platelet-rich fibrin (L-PRF)." Trends Biotechnol **27**(3): 158-167.

Dominici, M., K. Le Blanc, I. Mueller, I. Slaper-Cortenbach, F. Marini, D. Krause, R. Deans, A. Keating, D. Prockop and E. Horwitz (2006). "Minimal criteria for defining multipotent mesenchymal stromal cells. The International Society for Cellular Therapy position statement." Cytotherapy **8**(4): 315-317.

Dos Santos, F., P. Z. Andrade, J. S. Boura, M. M. Abecasis, C. L. da Silva and J. M. Cabral (2010). "Ex vivo expansion of human mesenchymal stem cells: a more effective cell proliferation kinetics and metabolism under hypoxia." J Cell Physiol **223**(1): 27-35.

Dosier, C. R., B. A. Uhrig, N. J. Willett, L. Krishnan, M. T. Li, H. Y. Stevens, Z. Schwartz, B. D. Boyan and R. E. Guldberg (2015). "Effect of cell origin and timing of delivery for stem cell-based bone tissue engineering using biologically functionalized hydrogels." Tissue Eng Part A **21**(1-2): 156-165.

Doucet, C., I. Ernou, Y. Zhang, J. R. Llense, L. Begot, X. Holy and J. J. Lataillade (2005). "Platelet lysates promote mesenchymal stem cell expansion: a safety substitute for animal serum in cell-based therapy applications." J Cell Physiol **205**(2): 228-236.

Dozza, M., L. Chiari, R. J. Peterka, C. Wall and F. B. Horak (2011). "What is the most effective type of audio-biofeedback for postural motor learning?" Gait Posture **34**(3): 313-319.

Drury, J. L. and D. J. Mooney (2003). "Hydrogels for tissue engineering: scaffold design variables and applications." Biomaterials **24**(24): 4337-4351.

Dupont, K. M., J. D. Boerckel, H. Y. Stevens, T. Diab, Y. M. Kolambkar, M. Takahata, E. M. Schwarz and R. E. Guldberg (2012). "Synthetic scaffold coating with adeno-associated virus encoding BMP2 to promote endogenous bone repair." Cell Tissue Res **347**(3): 575-588.

Dupont, K. M., K. Sharma, H. Y. Stevens, J. D. Boerckel, A. J. Garcia and R. E. Guldberg (2010). "Human stem cell delivery for treatment of large segmental bone defects." Proc Natl Acad Sci U S A **107**(8): 3305-3310.

Duvall, C. L., W. R. Taylor, D. Weiss and R. E. Guldberg (2004). "Quantitative microcomputed tomography analysis of collateral vessel development after ischemic injury." Am J Physiol Heart Circ Physiol **287**(1): H302-310.

Egana, J. T., S. Danner, M. Kremer, D. H. Rapoport, J. A. Lohmeyer, J. F. Dye, U. Hopfner, S. Lavandero, C. Kruse and H. G. Machens (2009). "The use of glandular-derived stem cells to improve vascularization in scaffold-mediated dermal regeneration." Biomaterials **30**(30): 5918-5926.

Einhorn, T. A. (2003). "Clinical applications of recombinant human BMPs: early experience and future development." J Bone Joint Surg Am **85-A Suppl 3**: 82-88.

El-Sharkawy, H., A. Kantarci, J. Deady, H. Hasturk, H. Liu, M. Alshahat and T. E. Van Dyke (2007). "Platelet-rich plasma: growth factors and pro- and anti-inflammatory properties." J Periodontol **78**(4): 661-669.

Engler, A. J., S. Sen, H. L. Sweeney and D. E. Discher (2006). "Matrix elasticity directs stem cell lineage specification." Cell **126**(4): 677-689.

Erdbrugger, W., W. Konertz, P. M. Dohmen, S. Posner, H. Ellerbrok, O. E. Brodde, H. Robenek, D. Modersohn, A. Pruss, S. Holinski, M. Stein-Konertz and G. Pauli (2006). "Decellularized xenogenic heart valves reveal remodeling and growth potential in vivo." Tissue Eng **12**(8): 2059-2068.

Fehrer, C. and G. Lepperdinger (2005). "Mesenchymal stem cell aging." Exp Gerontol **40**(12): 926-930.

Feltsan, T., J. Mracna and D. Holly (2011). "Use of thrombocyte concentrates in treatment of bone defects." Bratisl Lek Listy **112**(11): 655-657.

Feng, Q., M. Zhu, K. Wei and L. Bian (2014). "Cell-Mediated Degradation Regulates Human Mesenchymal Stem Cell Chondrogenesis and Hypertrophy in MMP-Sensitive Hyaluronic Acid Hydrogels." PLoS One **9**(6): e99587.

Festing, M. F., D. May, T. A. Connors, D. Lovell and S. Sparrow (1978). "An athymic nude mutation in the rat." Nature **274**(5669): 365-366.

Filvaroff, E. H. (2003). "VEGF and bone." J Musculoskelet Neuronal Interact **3**(4): 304-307; discussion 320-301.

Finkemeier, C. G. (2002). "Bone-grafting and bone-graft substitutes." J Bone Joint Surg Am **84-A**(3): 454-464.

Flemming, A., K. Schallmoser, D. Strunk, M. Stolk, H. D. Volk and M. Seifert (2011). "Immunomodulative efficacy of bone marrow-derived mesenchymal stem cells cultured in human platelet lysate." J Clin Immunol **31**(6): 1143-1156.

Folkman, J. (2007). "Angiogenesis: an organizing principle for drug discovery?" Nat Rev Drug Discov **6**(4): 273-286.

Freyman, T., G. Polin, H. Osman, J. Crary, M. Lu, L. Cheng, M. Palasis and R. L. Wilensky (2006). "A quantitative, randomized study evaluating three methods of mesenchymal stem cell delivery following myocardial infarction." Eur Heart J **27**(9): 1114-1122.

Friedenstein, A. J., S. Piatetzky, II and K. V. Petrakova (1966). "Osteogenesis in transplants of bone marrow cells." J Embryol Exp Morphol **16**(3): 381-390.

Frith, J. E., B. Thomson and P. G. Genever (2010). "Dynamic three-dimensional culture methods enhance mesenchymal stem cell properties and increase therapeutic potential." Tissue Eng Part C Methods **16**(4): 735-749.

Fu, J., Y. K. Wang, M. T. Yang, R. A. Desai, X. Yu, Z. Liu and C. S. Chen (2010). "Mechanical regulation of cell function with geometrically modulated elastomeric substrates." Nat Methods **7**(9): 733-736.

Fu, R., S. Selph, M. McDonagh, K. Peterson, A. Tiwari, R. Chou and M. Helfand (2013). "Effectiveness and harms of recombinant human bone morphogenetic protein-2 in spine fusion: a systematic review and meta-analysis." Ann Intern Med **158**(12): 890-902.

Fujita, K. and S. Janz (2007). "Attenuation of WNT signaling by DKK-1 and -2 regulates BMP2-induced osteoblast differentiation and expression of OPG, RANKL and M-CSF." Mol Cancer **6**: 71.

Fukuda, J., Y. Sakai and K. Nakazawa (2006). "Novel hepatocyte culture system developed using microfabrication and collagen/polyethylene glycol microcontact printing." Biomaterials **27**(7): 1061-1070.

Gafni, Y., G. Pelled, Y. Zilberman, G. Turgeman, F. Apparailly, H. Yotvat, E. Galun, Z. Gazit, C. Jorgensen and D. Gazit (2004). "Gene therapy platform for bone regeneration using an exogenously regulated, AAV-2-based gene expression system." Mol Ther **9**(4): 587-595.

Gaston, M. S. and A. H. Simpson (2007). "Inhibition of fracture healing." J Bone Joint Surg Br **89**(12): 1553-1560.

Gautschi, O. P., S. P. Frey and R. Zellweger (2007). "Bone morphogenetic proteins in clinical applications." ANZ J Surg **77**(8): 626-631.

Gerstenfeld, L. C., T. J. Cho, T. Kon, T. Aizawa, A. Tsay, J. Fitch, G. L. Barnes, D. T. Graves and T. A. Einhorn (2003). "Impaired fracture healing in the absence of TNF-alpha signaling: the role of TNF-alpha in endochondral cartilage resorption." J Bone Miner Res **18**(9): 1584-1592.

Geuze, R. E., H. J. Prins, F. C. Oner, Y. J. van der Helm, L. S. Schuijff, A. C. Martens, M. C. Kruyt, J. Alblas and W. J. Dhert (2010). "Luciferase labeling for multipotent stromal cell tracking in spinal fusion versus ectopic bone tissue engineering in mice and rats." Tissue Eng Part A **16**(11): 3343-3351.

Ghantoji, S. S., K. Sail, D. R. Lairson, H. L. DuPont and K. W. Garey (2010). "Economic healthcare costs of Clostridium difficile infection: a systematic review." J Hosp Infect **74**(4): 309-318.

Giannoni, P., S. Scaglione, A. Daga, C. Ilengo, M. Cilli and R. Quarto (2010). "Short-time survival and engraftment of bone marrow stromal cells in an ectopic model of bone regeneration." Tissue Eng Part A **16**(2): 489-499.

Giannoudis, P. V., T. A. Einhorn and D. Marsh (2007). "Fracture healing: a harmony of optimal biology and optimal fixation?" Injury **38 Suppl 4**: S1-2.

Gilmore, A. P. (2005). "Anoikis." Cell Death Differ **12 Suppl 2**: 1473-1477.

Goh, F., J. D. Gross, N. E. Simpson and A. Sambanis (2010). "Limited beneficial effects of perfluorocarbon emulsions on encapsulated cells in culture: experimental and modeling studies." J Biotechnol **150**(2): 232-239.

Gorny, G., A. Shaw and M. J. Oursler (2004). "IL-6, LIF, and TNF-alpha regulation of GM-CSF inhibition of osteoclastogenesis in vitro." Exp Cell Res **294**(1): 149-158.

Goulet, J. A., L. E. Senunas, G. L. DeSilva and M. L. Greenfield (1997). "Autogenous iliac crest bone graft. Complications and functional assessment." Clin Orthop Relat Res(339): 76-81.

Grayson, W. L., F. Zhao, B. Bunnell and T. Ma (2007). "Hypoxia enhances proliferation and tissue formation of human mesenchymal stem cells." Biochem Biophys Res Commun **358**(3): 948-953.

Grieshaber, S. E., T. Nie, C. Yan, S. Zhong, S. S. Teller, R. J. Clifton, D. J. Pochan, K. L. Kiick and X. Jia (2011). "Assembly Properties of an Alanine-Rich, Lysine-Containing Peptide and the Formation of Peptide/Polymer Hybrid Hydrogels." Macromol Chem Phys **212**(3): 229-239.

Griffith, C. K., C. Miller, R. C. Sainson, J. W. Calvert, N. L. Jeon, C. C. Hughes and S. C. George (2005). "Diffusion limits of an in vitro thick prevascularized tissue." Tissue Eng **11**(1-2): 257-266.

Griffiths, S., P. R. Baraniak, I. B. Copland, R. M. Nerem and T. C. McDevitt (2013). "Human platelet lysate stimulates high-passage and senescent human multipotent mesenchymal stromal cell growth and rejuvenation in vitro." Cytotherapy **15**(12): 1469-1483.

Guilak, F., D. M. Cohen, B. T. Estes, J. M. Gimble, W. Liedtke and C. S. Chen (2009). "Control of stem cell fate by physical interactions with the extracellular matrix." Cell Stem Cell **5**(1): 17-26.

Haack-Sorensen, M., S. K. Hansen, L. Hansen, M. Gaster, P. Hyttel, A. Ekblond and J. Kastrup (2012). "Mesenchymal Stromal Cell Phenotype is not Influenced by Confluence during Culture Expansion." Stem Cell Rev.

Haghi, A. K. and M. Akbari (2007). "Trends in electrospinning of natural nanofibers." Physica Status Solidi a-Applications and Materials Science **204**(6): 1830-1834.

Hara, M., T. Murakami and E. Kobayashi (2008). "In vivo bioimaging using photogenic rats: fate of injected bone marrow-derived mesenchymal stromal cells." J Autoimmun **30**(3): 163-171.

Harrison, P. and E. M. Cramer (1993). "Platelet alpha-granules." Blood Rev **7**(1): 52-62.

Hart, C. E., M. Bailey, D. A. Curtis, S. Osborn, E. Raines, R. Ross and J. W. Forstrom (1990). "Purification of PDGF-AB and PDGF-BB from human platelet extracts and identification of all three PDGF dimers in human platelets." Biochemistry **29**(1): 166-172.

Herschman, H. R. (2004). "Noninvasive imaging of reporter gene expression in living subjects." Adv Cancer Res **92**: 29-80.

Hollinger, J. O., J. Brekke, E. Gruskin and D. Lee (1996). "Role of bone substitutes." Clin Orthop Relat Res(324): 55-65.

Hollinger, J. O., C. E. Hart, S. N. Hirsch, S. Lynch and G. E. Friedlaender (2008). "Recombinant human platelet-derived growth factor: biology and clinical applications." J Bone Joint Surg Am **90 Suppl 1**: 48-54.

Honigman, A., E. Zeira, P. Ohana, R. Abramovitz, E. Tavor, I. Bar, Y. Zilberman, R. Rabinovsky, D. Gazit, A. Joseph, A. Panet, E. Shai, A. Palmon, M. Laster and E. Galun (2001). "Imaging transgene expression in live animals." Mol Ther **4**(3): 239-249.

Huang, S. and Z. Wang (2012). "Platelet-rich plasma-derived growth factors promote osteogenic differentiation of rat muscle satellite cells: in vitro and in vivo studies." Cell Biol Int **36**(12): 1195-1205.

Huang, Y. Z., J. Q. Cai, F. J. Lv, H. L. Xie, Z. M. Yang, Y. C. Huang and L. Deng (2013). "Species variation in the spontaneous calcification of bone marrow-derived mesenchymal stem cells." Cytotherapy **15**(3): 323-329.

Hutmacher, D. W. (2000). "Scaffolds in tissue engineering bone and cartilage." Biomaterials **21**(24): 2529-2543.

Hutmacher, D. W., J. T. Schantz, C. X. Lam, K. C. Tan and T. C. Lim (2007). "State of the art and future directions of scaffold-based bone engineering from a biomaterials perspective." J Tissue Eng Regen Med **1**(4): 245-260.

Ide, C., Y. Nakai, N. Nakano, T. B. Seo, Y. Yamada, K. Endo, T. Noda, F. Saito, Y. Suzuki, M. Fukushima and T. Nakatani (2010). "Bone marrow stromal cell transplantation for treatment of sub-acute spinal cord injury in the rat." Brain Res **1332**: 32-47.

In 't Anker, P. S., S. A. Scherjon, C. Kleijburg-van der Keur, W. A. Noort, F. H. Claas, R. Willemze, W. E. Fibbe and H. H. Kanhai (2003). "Amniotic fluid as a novel source of mesenchymal stem cells for therapeutic transplantation." Blood **102**(4): 1548-1549.

Inoue, Y., S. Kiryu, M. Watanabe, A. Tojo and K. Ohtomo (2010). "Timing of imaging after d-luciferin injection affects the longitudinal assessment of tumor growth using in vivo bioluminescence imaging." Int J Biomed Imaging **2010**: 471408.

Inzana, J. A., D. Olvera, S. M. Fuller, J. P. Kelly, O. A. Graeve, E. M. Schwarz, S. L. Kates and H. A. Awad (2014). "3D printing of composite calcium phosphate and collagen scaffolds for bone regeneration." Biomaterials **35**(13): 4026-4034.

Italiano, J. E., Jr., J. L. Richardson, S. Patel-Hett, E. Battinelli, A. Zaslavsky, S. Short, S. Ryeom, J. Folkman and G. L. Klement (2008). "Angiogenesis is regulated by a novel mechanism: pro- and antiangiogenic proteins are organized into separate platelet alpha granules and differentially released." Blood **111**(3): 1227-1233.

Iyer, S. S. and M. Rojas (2008). "Anti-inflammatory effects of mesenchymal stem cells: novel concept for future therapies." Expert Opin Biol Ther **8**(5): 569-581.

Jackson, W. M., L. J. Nesti and R. S. Tuan (2012). "Concise review: clinical translation of wound healing therapies based on mesenchymal stem cells." Stem Cells Transl Med **1**(1): 44-50.

Jager, M., X. Michalet and S. Weiss (2005). "Protein-protein interactions as a tool for site-specific labeling of proteins." Protein Sci **14**(8): 2059-2068.

Janicki, P. and G. Schmidmaier (2011). "What should be the characteristics of the ideal bone graft substitute? Combining scaffolds with growth factors and/or stem cells." Injury **42 Suppl 2**: S77-81.

Jenkins, D. E., Y. Oei, Y. S. Hornig, S. F. Yu, J. Dusich, T. Purchio and P. R. Contag (2003). "Bioluminescent imaging (BLI) to improve and refine traditional murine models of tumor growth and metastasis." Clin Exp Metastasis **20**(8): 733-744.

Jin, Q. M., O. Anusaksathien, S. A. Webb, R. B. Rutherford and W. V. Giannobile (2003). "Gene therapy of bone morphogenetic protein for periodontal tissue engineering." J Periodontol **74**(2): 202-213.

Johnson, E. E., M. R. Urist and G. A. Finerman (1992). "Resistant nonunions and partial or complete segmental defects of long bones. Treatment with implants of a composite of human bone morphogenetic protein (BMP) and autolyzed, antigen-extracted, allogeneic (AAA) bone." Clin Orthop Relat Res(277): 229-237.

Jones, A. L., R. W. Bucholz, M. J. Bosse, S. K. Mirza, T. R. Lyon, L. X. Webb, A. N. Pollak, J. D. Golden and A. Valentin-Opran (2006). "Recombinant human BMP-2 and allograft compared with autogenous bone graft for reconstruction of diaphyseal tibial fractures with cortical defects. A randomized, controlled trial." J Bone Joint Surg Am **88**(7): 1431-1441.

Jones, E. and X. Yang (2011). "Mesenchymal stem cells and bone regeneration: current status." Injury **42**(6): 562-568.

Jones, S. J., C. Gray and A. Boyde (1994). "Simulation of bone resorption-repair coupling in vitro." Anat Embryol (Berl) **190**(4): 339-349.

Kadiyala, S., R. G. Young, M. A. Thiede and S. P. Bruder (1997). "Culture expanded canine mesenchymal stem cells possess osteochondrogenic potential in vivo and in vitro." Cell Transplant **6**(2): 125-134.

Kaneshiro, S., K. Ebina, K. Shi, C. Higuchi, M. Hirao, M. Okamoto, K. Koizumi, T. Morimoto, H. Yoshikawa and J. Hashimoto (2014). "IL-6 negatively regulates osteoblast differentiation through the SHP2/MEK2 and SHP2/Akt2 pathways in vitro." J Bone Miner Metab **32**(4): 378-392.

Kawada, H., J. Fujita, K. Kinjo, Y. Matsuzaki, M. Tsuma, H. Miyatake, Y. Muguruma, K. Tsuboi, Y. Itabashi, Y. Ikeda, S. Ogawa, H. Okano, T. Hotta, K. Ando and K. Fukuda (2004). "Nonhematopoietic mesenchymal stem cells can be mobilized and differentiate into cardiomyocytes after myocardial infarction." Blood **104**(12): 3581-3587.

Keramaris, N. C., G. M. Calori, V. S. Nikolaou, E. H. Schemitsch and P. V. Giannoudis (2008). "Fracture vascularity and bone healing: a systematic review of the role of VEGF." Injury **39 Suppl 2**: S45-57.

Khetan, S., M. Guvendiren, W. R. Legant, D. M. Cohen, C. S. Chen and J. A. Burdick (2013). "Degradation-mediated cellular traction directs stem cell fate in covalently crosslinked three-dimensional hydrogels." Nat Mater **12**(5): 458-465.

Kim, J., J. M. Shin, Y. J. Jeon, H. M. Chung and J. I. Chae (2012). "Proteomic validation of multifunctional molecules in mesenchymal stem cells derived from human bone marrow, umbilical cord blood and peripheral blood." PLoS One **7**(5): e32350.

Kim, S., H. Y. Kang, E. H. Nam, M. S. Choi, X. F. Zhao, C. S. Hong, J. W. Lee, J. H. Lee and Y. K. Park (2010). "TMPRSS4 induces invasion and epithelial-mesenchymal transition through upregulation of integrin alpha5 and its signaling pathways." Carcinogenesis **31**(4): 597-606.

Kimelman-Bleich, N., G. Pelled, D. Sheyn, I. Kallai, Y. Zilberman, O. Mizrahi, Y. Tal, W. Tawackoli, Z. Gazit and D. Gazit (2009). "The use of a synthetic oxygen carrier-enriched hydrogel to enhance mesenchymal stem cell-based bone formation in vivo." Biomaterials **30**(27): 4639-4648.

King, S. M. and G. L. Reed (2002). "Development of platelet secretory granules." Semin Cell Dev Biol **13**(4): 293-302.

Kinnaird, T., E. Stabile, M. S. Burnett, C. W. Lee, S. Barr, S. Fuchs and S. E. Epstein (2004). "Marrow-derived stromal cells express genes encoding a broad spectrum of arteriogenic cytokines and promote in vitro and in vivo arteriogenesis through paracrine mechanisms." Circ Res **94**(5): 678-685.

Kode, J. A., S. Mukherjee, M. V. Joglekar and A. A. Hardikar (2009). "Mesenchymal stem cells: immunobiology and role in immunomodulation and tissue regeneration." Cytotherapy **11**(4): 377-391.

Kolambkar, Y. M., J. D. Boerckel, K. M. Dupont, M. Bajin, N. Huebsch, D. J. Mooney, D. W. Hutmacher and R. E. Guldberg (2011). "Spatiotemporal delivery of bone morphogenetic protein enhances functional repair of segmental bone defects." Bone **49**(3): 485-492.

Kolambkar, Y. M., K. M. Dupont, J. D. Boerckel, N. Huebsch, D. J. Mooney, D. W. Hutmacher and R. E. Guldberg (2011). "An alginate-based hybrid system for growth factor delivery in the functional repair of large bone defects." Biomaterials **32**(1): 65-74.

Kolambkar, Y. M., A. Peister, A. K. Ekaputra, D. W. Hutmacher and R. E. Guldberg (2010). "Colonization and osteogenic differentiation of different stem cell sources on electrospun nanofiber meshes." Tissue Eng Part A **16**(10): 3219-3230.

Kon, T., T. J. Cho, T. Aizawa, M. Yamazaki, N. Nooh, D. Graves, L. C. Gerstenfeld and T. A. Einhorn (2001). "Expression of osteoprotegerin, receptor activator of NF-kappaB ligand (osteoprotegerin ligand) and related proinflammatory cytokines during fracture healing." J Bone Miner Res **16**(6): 1004-1014.

Koob, T. J., R. Rennert, N. Zabek, M. Massee, J. J. Lim, J. S. Temenoff, W. W. Li and G. Gurtner (2013). "Biological properties of dehydrated human amnion/chorion composite graft: implications for chronic wound healing." Int Wound J **10**(5): 493-500.

Kopen, G. C., D. J. Prockop and D. G. Phinney (1999). "Marrow stromal cells migrate throughout forebrain and cerebellum, and they differentiate into astrocytes after injection into neonatal mouse brains." Proc Natl Acad Sci U S A **96**(19): 10711-10716.

Kostura, L., D. L. Kraitchman, A. M. Mackay, M. F. Pittenger and J. W. Bulte (2004). "Feridex labeling of mesenchymal stem cells inhibits chondrogenesis but not adipogenesis or osteogenesis." NMR Biomed **17**(7): 513-517.

Kovach, T. K., A. S. Dighe, P. I. Lobo and Q. Cui (2015). "Interactions between MSCs and immune cells: implications for bone healing." J Immunol Res **2015**: 752510.

Kricka, L. J. (1999). "Human anti-animal antibody interferences in immunological assays." Clin Chem **45**(7): 942-956.

Krishnan, L., C. C. Chang, S. S. Nunes, S. K. Williams, J. A. Weiss and J. B. Hoying (2013). "Manipulating the microvasculature and its microenvironment." Crit Rev Biomed Eng **41**(2): 91-123.

Krishnan, L., J. B. Hoying, H. Nguyen, H. Song and J. A. Weiss (2007). "Interaction of angiogenic microvessels with the extracellular matrix." Am J Physiol Heart Circ Physiol **293**(6): H3650-3658.

Krishnan, L., N. J. Willett and R. E. Guldberg (2014). "Vascularization strategies for bone regeneration." Ann Biomed Eng **42**(2): 432-444.

Kronenberg, H. M. (2003). "Developmental regulation of the growth plate." Nature **423**(6937): 332-336.

Kunz-Schughart, L. A., J. P. Freyer, F. Hofstaedter and R. Ebner (2004). "The use of 3-D cultures for high-throughput screening: the multicellular spheroid model." J Biomol Screen **9**(4): 273-285.

Laschke, M. W. and M. D. Menger (2012). "Vascularization in tissue engineering: angiogenesis versus inosculation." Eur Surg Res **48**(2): 85-92.

Leddy, H. A., H. A. Awad and F. Guilak (2004). "Molecular diffusion in tissue-engineered cartilage constructs: effects of scaffold material, time, and culture conditions." J Biomed Mater Res B Appl Biomater **70**(2): 397-406.

Lee, E. J., S. J. Park, S. K. Kang, G. H. Kim, H. J. Kang, S. W. Lee, H. B. Jeon and H. S. Kim (2012). "Spherical bullet formation via E-cadherin promotes therapeutic potency of mesenchymal stem cells derived from human umbilical cord blood for myocardial infarction." Mol Ther **20**(7): 1424-1433.

Lee, J., A. A. Abdeen, D. Zhang and K. A. Kilian (2013). "Directing stem cell fate on hydrogel substrates by controlling cell geometry, matrix mechanics and adhesion ligand composition." Biomaterials **34**(33): 8140-8148.

Lee, K. B., C. E. Taghavi, S. S. Murray, K. J. Song, G. Keorochana and J. C. Wang (2012). "BMP induced inflammation: A comparison of rhBMP-7 and rhBMP-2." J Orthop Res.

Lee, K. Y. and D. J. Mooney (2012). "Alginate: properties and biomedical applications." Prog Polym Sci **37**(1): 106-126.

Lee, S., E. Choi, M. J. Cha and K. C. Hwang (2015). "Cell adhesion and long-term survival of transplanted mesenchymal stem cells: a prerequisite for cell therapy." Oxid Med Cell Longev **2015**: 632902.

Levato, R., J. Visser, J. A. Planell, E. Engel, J. Malda and M. A. Mateos-Timoneda (2014). "Biofabrication of tissue constructs by 3D bioprinting of cell-laden microcarriers." Biofabrication **6**(3): 035020.

Levenberg, S., J. Rouwkema, M. Macdonald, E. S. Garfein, D. S. Kohane, D. C. Darland, R. Marini, C. A. van Blitterswijk, R. C. Mulligan, P. A. D'Amore and R. Langer (2005). "Engineering vascularized skeletal muscle tissue." Nat Biotechnol **23**(7): 879-884.

Lieberman, J. R., A. Daluiski, S. Stevenson, L. Wu, P. McAllister, Y. P. Lee, J. M. Kabo, G. A. Finerman, A. J. Berk and O. N. Witte (1999). "The effect of regional gene therapy with bone morphogenetic protein-2-producing bone-marrow cells on the repair of segmental femoral defects in rats." J Bone Joint Surg Am **81**(7): 905-917.

Liu, J., J. Hilderink, T. A. Groothuis, C. Otto, C. A. van Blitterswijk and J. de Boer (2013). "Monitoring nutrient transport in tissue-engineered grafts." J Tissue Eng Regen Med.

Lodewyckx, L. and R. J. Lories (2009). "WNT Signaling in osteoarthritis and osteoporosis: what is the biological significance for the clinician?" Curr Rheumatol Rep **11**(1): 23-30.

Lodie, T. A., C. E. Blickarz, T. J. Devarakonda, C. He, A. B. Dash, J. Clarke, K. Gleneck, L. Shihabuddin and R. Tubo (2002). "Systematic analysis of reportedly distinct populations of multipotent bone marrow-derived stem cells reveals a lack of distinction." Tissue Eng **8**(5): 739-751.

Logeart-Avramoglou, D., K. Oudina, M. Bourguignon, L. Delpierre, M. A. Nicola, M. Bensidhoum, E. Arnaud and H. Petite (2010). "In vitro and in vivo bioluminescent quantification of viable stem cells in engineered constructs." Tissue Eng Part C Methods **16**(3): 447-458.

Lohmann, M., G. Walenda, H. Hemeda, S. Joussen, W. Drescher, S. Jockenhoevel, G. Hutschenreuter, M. Zenke and W. Wagner (2012). "Donor age of human platelet lysate affects proliferation and differentiation of mesenchymal stem cells." PLoS One **7**(5): e37839.

Lou, J., F. Xu, K. Merkel and P. Manske (1999). "Gene therapy: adenovirus-mediated human bone morphogenetic protein-2 gene transfer induces mesenchymal progenitor cell proliferation and differentiation in vitro and bone formation in vivo." J Orthop Res **17**(1): 43-50.

Lovett, M., K. Lee, A. Edwards and D. L. Kaplan (2009). "Vascularization strategies for tissue engineering." Tissue Eng Part B Rev **15**(3): 353-370.

Lutolf, M. P. and J. A. Hubbell (2005). "Synthetic biomaterials as instructive extracellular microenvironments for morphogenesis in tissue engineering." Nat Biotechnol **23**(1): 47-55.

Macher, S., S. Sipurzynski-Budrass, K. Rosskopf, E. Rohde, A. Griesbacher, A. Groselj-Strele, G. Lanzer and K. Schallmoser (2010). "Function and activation state of platelets in vitro depend on apheresis modality." Vox Sang **99**(4): 332-340.

Mackenzie, T. C. and A. W. Flake (2001). "Human mesenchymal stem cells persist, demonstrate site-specific multipotential differentiation, and are present in sites of wound healing and tissue regeneration after transplantation into fetal sheep." Blood Cells Mol Dis **27**(3): 601-604.

Maguire, P. B. and D. J. Fitzgerald (2003). "Platelet proteomics." J Thromb Haemost **1**(7): 1593-1601.

Malafaya, P. B., G. A. Silva and R. L. Reis (2007). "Natural-origin polymers as carriers and scaffolds for biomolecules and cell delivery in tissue engineering applications." Adv Drug Deliv Rev **59**(4-5): 207-233.

Mamidi, M. K., K. G. Nathan, G. Singh, S. T. Thrichelvam, N. A. My, N. A. Fakharuzi, Z. Zakaria, R. Bhonde, A. K. Das and A. S. Majumdar (2012). "Comparative cellular and molecular analyses of pooled bone marrow multipotent mesenchymal stromal cells during continues passaging and after successive cryopreservation." J Cell Biochem.

Maraldi, T., M. Riccio, E. Resca, A. Pisciotta, G. B. La Sala, A. Ferrari, G. Bruzzesi, A. Motta, C. Migliaresi, L. Marzona and A. De Pol (2011). "Human amniotic fluid stem cells seeded in fibroin scaffold produce in vivo mineralized matrix." Tissue Eng Part A **17**(21-22): 2833-2843.

Marie, P. J. (2003). "Fibroblast growth factor signaling controlling osteoblast differentiation." Gene **316**: 23-32.

Marklein, R. A. and J. A. Burdick (2010). "Controlling stem cell fate with material design." Adv Mater **22**(2): 175-189.

Marotti, G. (1996). "The structure of bone tissues and the cellular control of their deposition." Ital J Anat Embryol **101**(4): 25-79.

Marsh, D. R. and G. Li (1999). "The biology of fracture healing: optimising outcome." Br Med Bull **55**(4): 856-869.

Marx, R. E., E. R. Carlson, R. M. Eichstaedt, S. R. Schimmele, J. E. Strauss and K. R. Georgeff (1998). "Platelet-rich plasma: Growth factor enhancement for bone grafts." Oral Surg Oral Med Oral Pathol Oral Radiol Endod **85**(6): 638-646.

Mauney, J. R., V. Volloch and D. L. Kaplan (2005). "Role of adult mesenchymal stem cells in bone tissue engineering applications: current status and future prospects." Tissue Eng **11**(5-6): 787-802.

McFadden, T. M., G. P. Duffy, A. B. Allen, H. Y. Stevens, S. M. Schwarzmaier, N. Plesnila, J. M. Murphy, F. P. Barry, R. E. Guldberg and F. J. O'Brien (2013). "The delayed addition of human mesenchymal stem cells to pre-formed endothelial cell networks results in functional vascularization of a collagen-glycosaminoglycan scaffold in vivo." Acta Biomater **9**(12): 9303-9316.

McKibbin, B. (1978). "The biology of fracture healing in long bones." J Bone Joint Surg Br **60-B**(2): 150-162.

Meirelles Lda, S. and N. B. Nardi (2003). "Murine marrow-derived mesenchymal stem cell: isolation, in vitro expansion, and characterization." Br J Haematol **123**(4): 702-711.

Metz, L. N., R. B. Martin and A. S. Turner (2003). "Histomorphometric analysis of the effects of osteocyte density on osteonal morphology and remodeling." Bone **33**(5): 753-759.

Meza-Zepeda, L. A., A. Noer, J. A. Dahl, F. Micci, O. Myklebost and P. Collas (2008). "High-resolution analysis of genetic stability of human adipose tissue stem cells cultured to senescence." J Cell Mol Med **12**(2): 553-563.

Miki, H., M. Hirose, N. Ogonuki, K. Inoue, F. Kezuka, A. Honda, K. Mekada, K. Hanaki, H. Iwafune, A. Yoshiki, F. Ishino and A. Ogura (2009). "Efficient production of androgenetic embryos by round spermatid injection." Genesis **47**(3): 155-160.

Mirabella, T., M. Cilli, S. Carlone, R. Cancedda and C. Gentili (2011). "Amniotic liquid derived stem cells as reservoir of secreted angiogenic factors capable of stimulating neo-arteriogenesis in an ischemic model." Biomaterials **32**(15): 3689-3699.

Monaco, E., M. Bionaz, S. Rodriguez-Zas, W. L. Hurley and M. B. Wheeler (2012). "Transcriptomics comparison between porcine adipose and bone marrow mesenchymal stem cells during in vitro osteogenic and adipogenic differentiation." PLoS One **7**(3): e32481.

Monteiro, B. S., R. J. Del Carlo, N. M. Argolo-Neto, N. B. Nardi, P. H. Carvalho, P. Bonfa Lde, P. C. Chagastelles, H. N. Moreira, M. I. Viloria and B. S. Santos (2012). "Association of mesenchymal stem cells with platelet rich plasma on the repair of critical calvarial defects in mice." Acta Cir Bras **27**(3): 201-209.

Mook, O. R., A. Jonker, A. C. Strang, A. Veltien, G. Gambarota, W. M. Frederiks, A. Heerschap and C. J. Van Noorden (2008). "Noninvasive magnetic resonance imaging of the development of individual colon cancer tumors in rat liver." Biotechniques **44**(4): 529-535.

Moretta, A., C. Bottino, M. Vitale, D. Pende, C. Cantoni, M. C. Mingari, R. Biassoni and L. Moretta (2001). "Activating receptors and coreceptors involved in human natural killer cell-mediated cytolysis." Annu Rev Immunol **19**: 197-223.

Morgan, B. P. (2015). "The membrane attack complex as an inflammatory trigger." Immunobiology.

Moriyama, E. H., M. J. Niedre, M. T. Jarvi, J. D. Mocanu, Y. Moriyama, P. Subarsky, B. Li, L. D. Lilge and B. C. Wilson (2008). "The influence of hypoxia on bioluminescence in luciferase-transfected gliosarcoma tumor cells in vitro." Photochem Photobiol Sci **7**(6): 675-680.

Morrison, S. J. and D. T. Scadden (2014). "The bone marrow niche for haematopoietic stem cells." Nature **505**(7483): 327-334.

Mountziaris, P. M. and A. G. Mikos (2008). "Modulation of the inflammatory response for enhanced bone tissue regeneration." Tissue Eng Part B Rev **14**(2): 179-186.

Mountziaris, P. M., P. P. Spicer, F. K. Kasper and A. G. Mikos (2011). "Harnessing and modulating inflammation in strategies for bone regeneration." Tissue Eng Part B Rev **17**(6): 393-402.

Moustakas, A. and C. H. Heldin (2005). "Non-Smad TGF-beta signals." J Cell Sci **118**(Pt 16): 3573-3584.

Muller, I., S. Kordowich, C. Holzwarth, C. Spano, G. Isensee, A. Staiber, S. Viebahn, F. Gieseke, H. Langer, M. P. Gawaz, E. M. Horwitz, P. Conte, R. Handgretinger and M. Dominici (2006). "Animal serum-free culture conditions for isolation and expansion of multipotent mesenchymal stromal cells from human BM." Cytotherapy **8**(5): 437-444.

Mumaw, J., E. T. Jordan, C. Sonnet, R. M. Olabisi, E. A. Olmsted-Davis, A. R. Davis, J. F. Peroni, J. L. West, F. West, Y. Lu and S. L. Stice (2012). "Rapid Heterotrophic Ossification with Cryopreserved Poly(ethylene glycol-) Microencapsulated BMP2-Expressing MSCs." Int J Biomater **2012**: 861794.

Murphy, K. C., S. Y. Fang and J. K. Leach (2014). "Human mesenchymal stem cell spheroids in fibrin hydrogels exhibit improved cell survival and potential for bone healing." Cell Tissue Res **357**(1): 91-99.

Murphy, W. L., T. C. McDevitt and A. J. Engler (2014). "Materials as stem cell regulators." Nat Mater **13**(6): 547-557.

Muschler, G. F., C. Nakamoto and L. G. Griffith (2004). "Engineering principles of clinical cell-based tissue engineering." J Bone Joint Surg Am **86-A**(7): 1541-1558.

Nather, A., V. David, J. W. Teng, C. W. Lee and B. P. Pereira (2010). "Effect of autologous mesenchymal stem cells on biological healing of allografts in critical-sized tibial defects simulated in adult rabbits." Ann Acad Med Singapore **39**(8): 599-606.

Newcomb, J. D., C. T. Ajmo, Jr., C. D. Sanberg, P. R. Sanberg, K. R. Pennypacker and A. E. Willing (2006). "Timing of cord blood treatment after experimental stroke determines therapeutic efficacy." Cell Transplant **15**(3): 213-223.

Ng, F., S. Boucher, S. Koh, K. S. Sastry, L. Chase, U. Lakshmipathy, C. Choong, Z. Yang, M. C. Vemuri, M. S. Rao and V. Tanavde (2008). "PDGF, TGF-beta, and FGF signaling is important for differentiation and growth of mesenchymal stem cells (MSCs): transcriptional profiling can identify markers and signaling pathways important in differentiation of MSCs into adipogenic, chondrogenic, and osteogenic lineages." Blood **112**(2): 295-307.

Nishimura, R., K. Hata, F. Ikeda, T. Matsubara, K. Yamashita, F. Ichida and T. Yoneda (2003). "The role of Smads in BMP signaling." Front Biosci **8**: s275-284.

Novitskaya, E., P. Y. Chen, S. Lee, A. Castro-Cesena, G. Hirata, V. A. Lubarda and J. McKittrick (2011). "Anisotropy in the compressive mechanical properties of bovine cortical bone and the mineral and protein constituents." Acta Biomater **7**(8): 3170-3177.

Novosel, E. C., C. Kleinhans and P. J. Kluger (2011). "Vascularization is the key challenge in tissue engineering." Adv Drug Deliv Rev **63**(4-5): 300-311.

O'Neill, K., S. K. Lyons, W. M. Gallagher, K. M. Curran and A. T. Byrne (2010). "Bioluminescent imaging: a critical tool in pre-clinical oncology research." J Pathol **220**(3): 317-327.

Oest, M. E., K. M. Dupont, H. J. Kong, D. J. Mooney and R. E. Guldberg (2007). "Quantitative assessment of scaffold and growth factor-mediated repair of critically sized bone defects." J Orthop Res **25**(7): 941-950.

Oh, H. J., D. W. Hwang, H. Youn and D. S. Lee (2013). "In vivo bioluminescence reporter gene imaging for the activation of neuronal differentiation induced by the neuronal activator neurogenin 1 (Ngn1) in neuronal precursor cells." Eur J Nucl Med Mol Imaging.

Ohnishi, S., T. Yasuda, S. Kitamura and N. Nagaya (2007). "Effect of hypoxia on gene expression of bone marrow-derived mesenchymal stem cells and mononuclear cells." Stem Cells **25**(5): 1166-1177.

Olivo, C., J. Alblas, V. Verweij, A. J. Van Zonneveld, W. J. Dhert and A. C. Martens (2008). "In vivo bioluminescence imaging study to monitor ectopic bone formation by luciferase gene marked mesenchymal stem cells." J Orthop Res **26**(7): 901-909.

Ortiz, L. A., M. Dutreil, C. Fattman, A. C. Pandey, G. Torres, K. Go and D. G. Phinney (2007). "Interleukin 1 receptor antagonist mediates the antiinflammatory and antifibrotic effect of mesenchymal stem cells during lung injury." Proc Natl Acad Sci U S A **104**(26): 11002-11007.

Osugi, M., W. Katagiri, R. Yoshimi, T. Inukai, H. Hibi and M. Ueda (2012). "Conditioned media from mesenchymal stem cells enhanced bone regeneration in rat calvarial bone defects." Tissue Eng Part A **18**(13-14): 1479-1489.

Ottobrini, L., C. Martelli, D. L. Trabattoni, M. Clerici and G. Lucignani (2011). "In vivo imaging of immune cell trafficking in cancer." Eur J Nucl Med Mol Imaging **38**(5): 949-968.

Owen, M. and A. J. Friedenstein (1988). "Stromal stem cells: marrow-derived osteogenic precursors." Ciba Found Symp **136**: 42-60.

Parfitt, A. M. (1976). "The actions of parathyroid hormone on bone: relation to bone remodeling and turnover, calcium homeostasis, and metabolic bone disease. Part I of IV parts: mechanisms of calcium transfer between blood and bone and their cellular basis: morphological and kinetic approaches to bone turnover." Metabolism **25**(7): 809-844.

Parikh, S. N. (2002). "Bone graft substitutes in modern orthopedics." Orthopedics **25**(11): 1301-1309; quiz 1310-1301.

Peister, A., M. A. Woodruff, J. J. Prince, D. P. Gray, D. W. Hutmacher and R. E. Guldberg (2011). "Cell sourcing for bone tissue engineering: amniotic fluid stem cells have a delayed, robust differentiation compared to mesenchymal stem cells." Stem Cell Res **7**(1): 17-27.

Pelled, G. and D. Gazit (2004). "Imaging using osteocalcin-luciferase." J Musculoskelet Neuronal Interact **4**(4): 362-363.

Perri, B., M. Cooper, C. Lauryssen and N. Anand (2007). "Adverse swelling associated with use of rh-BMP-2 in anterior cervical discectomy and fusion: a case study." Spine J **7**(2): 235-239.

Perry, C. R. (1999). "Bone repair techniques, bone graft, and bone graft substitutes." Clin Orthop Relat Res(360): 71-86.

Pittenger, M. F., A. M. Mackay, S. C. Beck, R. K. Jaiswal, R. Douglas, J. D. Mosca, M. A. Moorman, D. W. Simonetti, S. Craig and D. R. Marshak (1999). "Multilineage potential of adult human mesenchymal stem cells." Science **284**(5411): 143-147.

Pluen, A., P. A. Netti, R. K. Jain and D. A. Berk (1999). "Diffusion of macromolecules in agarose gels: comparison of linear and globular configurations." Biophys J **77**(1): 542-552.

Poole, K. E., R. L. van Bezooijen, N. Loveridge, H. Hamersma, S. E. Papapoulos, C. W. Lowik and J. Reeve (2005). "Sclerostin is a delayed secreted product of osteocytes that inhibits bone formation." FASEB J **19**(13): 1842-1844.

Potapova, I. A., P. R. Brink, I. S. Cohen and S. V. Doronin (2008). "Culturing of human mesenchymal stem cells as three-dimensional aggregates induces functional expression

of CXCR4 that regulates adhesion to endothelial cells." J Biol Chem **283**(19): 13100-13107.

Poynton, A. R. and J. M. Lane (2002). "Safety profile for the clinical use of bone morphogenetic proteins in the spine." Spine (Phila Pa 1976) **27**(16 Suppl 1): S40-48.

Priddy, L. B., O. Chaudhuri, H. Y. Stevens, L. Krishnan, B. A. Uhrig, N. J. Willett and R. E. Guldberg (2014). "Oxidized alginate hydrogels for bone morphogenetic protein-2 delivery in long bone defects." Acta Biomater.

Prinz, F., T. Schlange and K. Asadullah (2011). "Believe it or not: how much can we rely on published data on potential drug targets?" Nat Rev Drug Discov **10**(9): 712.

Prockop, D. J. (1997). "Marrow stromal cells as stem cells for nonhematopoietic tissues." Science **276**(5309): 71-74.

Qian, H., K. Le Blanc and M. Sigvardsson (2012). "Primary Mesenchymal Stem and Progenitor Cells from Bone Marrow Lack Expression of CD44 Protein." J Biol Chem **287**(31): 25795-25807.

Quarto, R., M. Mastrogiacomo, R. Cancedda, S. M. Kutepov, V. Mukhachev, A. Lavroukov, E. Kon and M. Marcacci (2001). "Repair of large bone defects with the use of autologous bone marrow stromal cells." N Engl J Med **344**(5): 385-386.

Rai, B., M. E. Oest, K. M. Dupont, K. H. Ho, S. H. Teoh and R. E. Guldberg (2007). "Combination of platelet-rich plasma with polycaprolactone-tricalcium phosphate scaffolds for segmental bone defect repair." J Biomed Mater Res A **81**(4): 888-899.

Ratko, T. A., S. E. Belinson, D. J. Samson, C. Bonnell, K. M. Ziegler and N. Aronson (2010). Bone Morphogenetic Protein: The State of the Evidence of On-Label and Off-Label Use. Rockville (MD).

Rauch, C., E. Feifel, E. M. Amann, H. P. Spotl, H. Schennach, W. Pfaller and G. Gstraunthaler (2011). "Alternatives to the use of fetal bovine serum: human platelet lysates as a serum substitute in cell culture media." ALTEX **28**(4): 305-316.

Redler, L. H., S. A. Thompson, S. H. Hsu, C. S. Ahmad and W. N. Levine (2011). "Platelet-rich plasma therapy: a systematic literature review and evidence for clinical use." Phys Sportsmed **39**(1): 42-51.

Reed, G. L., M. L. Fitzgerald and J. Polgar (2000). "Molecular mechanisms of platelet exocytosis: insights into the "secrete" life of thrombocytes." Blood **96**(10): 3334-3342.

Reed, J. C., K. Doctor, A. Rojas, J. M. Zapata, C. Stehlik, L. Fiorentino, J. Damiano, W. Roth, S. Matsuzawa, R. Newman, S. Takayama, H. Marusawa, F. Xu, G. Salvesen, A. Godzik, R. G. Group and G. S. L. Members (2003). "Comparative analysis of apoptosis and inflammation genes of mice and humans." Genome Res **13**(6B): 1376-1388.

Reinisch, A., C. Bartmann, E. Rohde, K. Schallmoser, V. Bjelic-Radisic, G. Lanzer, W. Linkesch and D. Strunk (2007). "Humanized system to propagate cord blood-derived multipotent mesenchymal stromal cells for clinical application." Regen Med **2**(4): 371-382.

Ren, G., J. Su, L. Zhang, X. Zhao, W. Ling, A. L'Huillie, J. Zhang, Y. Lu, A. I. Roberts, W. Ji, H. Zhang, A. B. Rabson and Y. Shi (2009). "Species variation in the mechanisms of mesenchymal stem cell-mediated immunosuppression." Stem Cells **27**(8): 1954-1962.

Rendu, F. and B. Brohard-Bohn (2001). "The platelet release reaction: granules' constituents, secretion and functions." Platelets **12**(5): 261-273.

Renth, A. N. and M. S. Detamore (2012). "Leveraging "raw materials" as building blocks and bioactive signals in regenerative medicine." Tissue Eng Part B Rev **18**(5): 341-362.

Ripamonti, U., M. Heliotis and C. Ferretti (2007). "Bone morphogenetic proteins and the induction of bone formation: from laboratory to patients." Oral Maxillofac Surg Clin North Am **19**(4): 575-589, vii.

Roach, H. I. (1992). "Trans-differentiation of hypertrophic chondrocytes into cells capable of producing a mineralized bone matrix." Bone Miner **19**(1): 1-20.

Roberts, A. B. (1995). "Transforming growth factor-beta: activity and efficacy in animal models of wound healing." Wound Repair Regen **3**(4): 408-418.

Rolstad, B. (2001). "The athymic nude rat: an animal experimental model to reveal novel aspects of innate immune responses?" Immunol Rev **184**: 136-144.

Romanella, M., A. Aminian, W. R. Adam, M. J. Pearse and A. J. d'Apice (1997). "Involvement of both the classical and alternate pathways of complement in an ex vivo model of xenograft rejection." Transplantation **63**(7): 1021-1025.

Ross, R., E. W. Raines and D. F. Bowen-Pope (1986). "The biology of platelet-derived growth factor." Cell **46**(2): 155-169.

Rouwkema, J., N. C. Rivron and C. A. van Blitterswijk (2008). "Vascularization in tissue engineering." Trends Biotechnol **26**(8): 434-441.

Rubio-Azpeitia, E. and I. Andia (2014). "Partnership between platelet-rich plasma and mesenchymal stem cells: in vitro experience." Muscles Ligaments Tendons J **4**(1): 52-62.

Ruoslahti, E. (2003). "The RGD story: a personal account." Matrix Biol **22**(6): 459-465.

Rustad, K. C., V. W. Wong, M. Sorkin, J. P. Glotzbach, M. R. Major, J. Rajadas, M. T. Longaker and G. C. Gurtner (2012). "Enhancement of mesenchymal stem cell angiogenic capacity and stemness by a biomimetic hydrogel scaffold." Biomaterials **33**(1): 80-90.

Sacco, A., R. Doyonnas, P. Kraft, S. Vitorovic and H. M. Blau (2008). "Self-renewal and expansion of single transplanted muscle stem cells." Nature **456**(7221): 502-506.

Salama, A., B. Gottsche, V. Vaidya, S. Santoso and C. Mueller-Eckhardt (1988). "Complement-independent lysis of human red blood cells by cold hemagglutinins." Vox Sang **55**(1): 21-25.

Santo, V. E., A. R. Duarte, E. G. Popa, M. E. Gomes, J. F. Mano and R. L. Reis (2012). "Enhancement of osteogenic differentiation of human adipose derived stem cells by the controlled release of platelet lysates from hybrid scaffolds produced by supercritical fluid foaming." J Control Release **162**(1): 19-27.

Sart, S., T. Ma and Y. Li (2014). "Preconditioning stem cells for in vivo delivery." Biores Open Access **3**(4): 137-149.

Sarugaser, R., D. Lickorish, D. Baksh, M. M. Hosseini and J. E. Davies (2005). "Human umbilical cord perivascular (HUCPV) cells: a source of mesenchymal progenitors." Stem Cells **23**(2): 220-229.

Sawada, R., T. Ito and T. Tsuchiya (2006). "Changes in expression of genes related to cell proliferation in human mesenchymal stem cells during in vitro culture in comparison with cancer cells." J Artif Organs **9**(3): 179-184.

Schallmoser, K., C. Bartmann, E. Rohde, A. Reinisch, K. Kashofer, E. Stadelmeyer, C. Drexler, G. Lanzer, W. Linkesch and D. Strunk (2007). "Human platelet lysate can replace fetal bovine serum for clinical-scale expansion of functional mesenchymal stromal cells." Transfusion **47**(8): 1436-1446.

Schlosser, S., C. Dennler, R. Schweizer, D. Eberli, J. V. Stein, V. Enzmann, P. Giovanoli, D. Erni and J. A. Plock (2012). "Paracrine effects of mesenchymal stem cells enhance vascular regeneration in ischemic murine skin." Microvasc Res **83**(3): 267-275.

Schmidt-Bleek, K., H. Schell, N. Schulz, P. Hoff, C. Perka, F. Buttgereit, H. D. Volk, J. Lienau and G. N. Duda (2012). "Inflammatory phase of bone healing initiates the regenerative healing cascade." Cell Tissue Res **347**(3): 567-573.

Seeherman, H., J. Wozney and R. Li (2002). "Bone morphogenetic protein delivery systems." Spine (Phila Pa 1976) **27**(16 Suppl 1): S16-23.

Service, R. F. (2000). "Tissue engineers build new bone." Science **289**(5484): 1498-1500.

Sethe, S., A. Scutt and A. Stolzing (2006). "Aging of mesenchymal stem cells." Ageing Res Rev **5**(1): 91-116.

Shekaran, A., J. R. Garcia, A. Y. Clark, T. E. Kavanaugh, A. S. Lin, R. E. Guldberg and A. J. Garcia (2014). "Bone regeneration using an alpha 2 beta 1 integrin-specific hydrogel as a BMP-2 delivery vehicle." Biomaterials **35**(21): 5453-5461.

Sheyn, D., I. Kallai, W. Tawackoli, D. Cohn Yakubovich, A. Oh, S. Su, X. Da, A. Lavi, N. Kimelman-Bleich, Y. Zilberman, N. Li, H. Bae, Z. Gazit, G. Pelled and D. Gazit (2011). "Gene-modified adult stem cells regenerate vertebral bone defect in a rat model." Mol Pharm **8**(5): 1592-1601.

Sheyn, D., O. Mizrahi, S. Benjamin, Z. Gazit, G. Pelled and D. Gazit (2010). "Genetically modified cells in regenerative medicine and tissue engineering." Advanced Drug Delivery Reviews **62**(7-8): 683-698.

Shields, L. B., G. H. Raque, S. D. Glassman, M. Campbell, T. Vitaz, J. Harpring and C. B. Shields (2006). "Adverse effects associated with high-dose recombinant human bone morphogenetic protein-2 use in anterior cervical spine fusion." Spine (Phila Pa 1976) **31**(5): 542-547.

Silva, E. A. and D. J. Mooney (2007). "Spatiotemporal control of vascular endothelial growth factor delivery from injectable hydrogels enhances angiogenesis." J Thromb Haemost **5**(3): 590-598.

Simmons, P. J. and B. Torok-Storb (1991). "Identification of stromal cell precursors in human bone marrow by a novel monoclonal antibody, STRO-1." Blood **78**(1): 55-62.

Smucker, J. D., J. M. Rhee, K. Singh, S. T. Yoon and J. G. Heller (2006). "Increased swelling complications associated with off-label usage of rhBMP-2 in the anterior cervical spine." Spine (Phila Pa 1976) **31**(24): 2813-2819.

Spaggiari, G. M., A. Capobianco, H. Abdelrazik, F. Becchetti, M. C. Mingari and L. Moretta (2008). "Mesenchymal stem cells inhibit natural killer-cell proliferation, cytotoxicity, and cytokine production: role of indoleamine 2,3-dioxygenase and prostaglandin E2." Blood **111**(3): 1327-1333.

St John, T. A., A. R. Vaccaro, A. P. Sah, M. Schaefer, S. C. Berta, T. Albert and A. Hilibrand (2003). "Physical and monetary costs associated with autogenous bone graft harvesting." Am J Orthop (Belle Mead NJ) **32**(1): 18-23.

Suda, M., K. Tanaka, A. Yasoda, K. Natsui, Y. Sakuma, I. Tanaka, F. Ushikubi, S. Narumiya and K. Nakao (1998). "Prostaglandin E2 (PGE2) autoamplifies its production through EP1 subtype of PGE receptor in mouse osteoblastic MC3T3-E1 cells." Calcif Tissue Int **62**(4): 327-331.

Suda, T., I. Nakamura, E. Jimi and N. Takahashi (1997). "Regulation of osteoclast function." J Bone Miner Res **12**(6): 869-879.

Sun, N., A. Lee and J. C. Wu (2009). "Long term non-invasive imaging of embryonic stem cells using reporter genes." Nat Protoc **4**(8): 1192-1201.

Tamimi, F., P. Comeau, D. Le Nihouannen, Y. L. Zhang, D. C. Bassett, S. Khalili, U. Gbureck, S. D. Tran, S. Komarova and J. E. Barralet (2013). "Perfluorodecalin and bone regeneration." Eur Cell Mater **25**: 22-36.

Tanaka, H., M. Matsumura and I. A. Veliky (1984). "Diffusion characteristics of substrates in Ca-alginate gel beads." Biotechnol Bioeng **26**(1): 53-58.

Tasso, R., A. Augello, S. Boccardo, S. Salvi, M. Carida, F. Postiglione, F. Fais, M. Truini, R. Cancedda and G. Pennesi (2009). "Recruitment of a host's osteoprogenitor cells using exogenous mesenchymal stem cells seeded on porous ceramic." Tissue Eng Part A **15**(8): 2203-2212.

Taylor, A., K. M. Wilson, P. Murray, D. G. Fernig and R. Levy (2012). "Long-term tracking of cells using inorganic nanoparticles as contrast agents: are we there yet?" Chem Soc Rev **41**(7): 2707-2717.

Tejeda-Montes, E., K. H. Smith, M. Poch, M. J. Lopez-Bosque, L. Martin, M. Alonso, E. Engel and A. Mata (2012). "Engineering membrane scaffolds with both physical and biomolecular signaling." Acta Biomater **8**(3): 998-1009.

Termaat, M. F., F. C. Den Boer, F. C. Bakker, P. Patka and H. J. Haarman (2005). "Bone morphogenetic proteins. Development and clinical efficacy in the treatment of fractures and bone defects." J Bone Joint Surg Am **87**(6): 1367-1378.

Terrovitis, J., M. Stuber, A. Youssef, S. Preece, M. Leppo, E. Kizana, M. Schar, G. Gerstenblith, R. G. Weiss, E. Marban and M. R. Abraham (2008). "Magnetic resonance imaging overestimates ferumoxide-labeled stem cell survival after transplantation in the heart." Circulation **117**(12): 1555-1562.

Thomas, M. V. and D. A. Puleo (2011). "Infection, inflammation, and bone regeneration: a paradoxical relationship." J Dent Res **90**(9): 1052-1061.

Toma, C., M. F. Pittenger, K. S. Cahill, B. J. Byrne and P. D. Kessler (2002). "Human mesenchymal stem cells differentiate to a cardiomyocyte phenotype in the adult murine heart." Circulation **105**(1): 93-98.

Torisawa, Y. S., A. Takagi, Y. Nashimoto, T. Yasukawa, H. Shiku and T. Matsue (2007). "A multicellular spheroid array to realize spheroid formation, culture, and viability assay on a chip." Biomaterials **28**(3): 559-566.

Torricelli, P., M. Fini, G. Giavaresi, V. Borsari, A. Carpi, A. Nicolini and R. Giardino (2003). "Comparative interspecies investigation on osteoblast cultures: data on cell viability and synthetic activity." Biomed Pharmacother **57**(1): 57-62.

Toyoda, T., S. Mae, H. Tanaka, Y. Kondo, M. Funato, Y. Hosokawa, T. Sudo, Y. Kawaguchi and K. Osafune (2015). "Cell aggregation optimizes the differentiation of human ESCs and iPSCs into pancreatic bud-like progenitor cells." Stem Cell Res **14**(2): 185-197.

Tzioupis, C. and P. V. Giannoudis (2007). "Prevalence of long-bone non-unions." Injury **38 Suppl 2**: S3-9.

Ulbrich, C., M. Wehland, J. Pietsch, G. Aleshcheva, P. Wise, J. van Loon, N. Magnusson, M. Infanger, J. Grosse, C. Eilles, A. Sundaresan and D. Grimm (2014). "The impact of simulated and real microgravity on bone cells and mesenchymal stem cells." Biomed Res Int **2014**: 928507.

Ungrin, M. D., C. Joshi, A. Nica, C. Bauwens and P. W. Zandstra (2008). "Reproducible, ultra high-throughput formation of multicellular organization from single cell suspension-derived human embryonic stem cell aggregates." PLoS One **3**(2): e1565.

Uzarski, J. S., B. M. Bijonowski, B. Wang, H. H. Ward, A. Wandinger-Ness, W. M. Miller and J. A. Wertheim (2015). "Dual-purpose bioreactors to monitor non-invasive physical and biochemical markers of kidney and liver scaffold recellularization." Tissue Eng Part C Methods.

Vaananen, H. K., H. Zhao, M. Mulari and J. M. Halleen (2000). "The cell biology of osteoclast function." J Cell Sci **113 (Pt 3)**: 377-381.

van den Dolder, J., R. Mooren, A. P. Vloon, P. J. Stoelinga and J. A. Jansen (2006). "Platelet-rich plasma: quantification of growth factor levels and the effect on growth and differentiation of rat bone marrow cells." Tissue Eng **12**(11): 3067-3073.

Vos, J. G., J. G. Kreeftenberg, B. C. Kruijt, W. Kruizinga and P. Steerenberg (1980). "The athymic nude rat. II. Immunological characteristics." Clin Immunol Immunopathol **15**(2): 229-237.

Vreys, R., S. J. Soenen, M. De Cuyper and A. Van der Linden (2011). "Background migration of USPIO/MLs is a major drawback for in situ labeling of endogenous neural progenitor cells." Contrast Media Mol Imaging **6**(1): 1-6.

Waese, E. Y., R. A. Kandel and W. L. Stanford (2008). "Application of stem cells in bone repair." Skeletal Radiol **37**(7): 601-608.

Wagner, W., P. Horn, M. Castoldi, A. Diehlmann, S. Bork, R. Saffrich, V. Benes, J. Blake, S. Pfister, V. Eckstein and A. D. Ho (2008). "Replicative senescence of mesenchymal stem cells: a continuous and organized process." PLoS One **3**(5): e2213.

Wakitani, S., T. Saito and A. I. Caplan (1995). "Myogenic cells derived from rat bone marrow mesenchymal stem cells exposed to 5-azacytidine." Muscle Nerve **18**(12): 1417-1426.

Walczak, P., D. A. Kedziorek, A. A. Gilad, B. P. Barnett and J. W. Bulte (2007). "Applicability and limitations of MR tracking of neural stem cells with asymmetric cell division and rapid turnover: the case of the shiverer dysmyelinated mouse brain." Magn Reson Med **58**(2): 261-269.

Walenda, G., H. Hemeda, R. K. Schneider, R. Merkel, B. Hoffmann and W. Wagner (2012). "Human Platelet Lysate Gel Provides a Novel Three Dimensional-Matrix for

Enhanced Culture Expansion of Mesenchymal Stromal Cells." Tissue Eng Part C Methods.

Wang, C. C., C. H. Chen, S. M. Hwang, W. W. Lin, C. H. Huang, W. Y. Lee, Y. Chang and H. W. Sung (2009). "Spherically symmetric mesenchymal stromal cell bodies inherent with endogenous extracellular matrices for cellular cardiomyoplasty." Stem Cells **27**(3): 724-732.

Wang, E. A., V. Rosen, P. Cordes, R. M. Hewick, M. J. Kriz, D. P. Luxenberg, B. S. Sibley and J. M. Wozney (1988). "Purification and characterization of other distinct bone-inducing factors." Proc Natl Acad Sci U S A **85**(24): 9484-9488.

Wang, H., F. Cao, A. De, Y. Cao, C. Contag, S. S. Gambhir, J. C. Wu and X. Chen (2009). "Trafficking mesenchymal stem cell engraftment and differentiation in tumor-bearing mice by bioluminescence imaging." Stem Cells **27**(7): 1548-1558.

Wang, J. C., L. E. Kanim, S. Yoo, P. A. Campbell, A. J. Berk and J. R. Lieberman (2003). "Effect of regional gene therapy with bone morphogenetic protein-2-producing bone marrow cells on spinal fusion in rats." J Bone Joint Surg Am **85-A**(5): 905-911.

Wang, W., K. Itaka, S. Ohba, N. Nishiyama, U. I. Chung, Y. Yamasaki and K. Kataoka (2009). "3D spheroid culture system on micropatterned substrates for improved differentiation efficiency of multipotent mesenchymal stem cells." Biomaterials **30**(14): 2705-2715.

Wartenberg, M., F. Donmez, F. C. Ling, H. Acker, J. Hescheler and H. Sauer (2001). "Tumor-induced angiogenesis studied in confrontation cultures of multicellular tumor spheroids and embryoid bodies grown from pluripotent embryonic stem cells." FASEB J **15**(6): 995-1005.

White, J. C., W. L. Stoppel, S. C. Roberts and S. R. Bhatia (2013). "Addition of perfluorocarbons to alginate hydrogels significantly impacts molecular transport and fracture stress." J Biomed Mater Res A **101**(2): 438-446.

Wiemann, M., H. M. Rumpf, D. Bingmann and H. P. Jennissen (2001). "The binding of rhBMP-2 to the receptors of viable MC3T3-E1 cells and the question of cooperativity." Materialwissenschaft Und Werkstofftechnik **32**(12): 931-936.

Wimalawansa, S. J. (2010). "Nitric oxide and bone." Ann N Y Acad Sci **1192**: 391-403.

Wolfram, U., H. J. Wilke and P. K. Zysset (2010). "Rehydration of vertebral trabecular bone: influences on its anisotropy, its stiffness and the indentation work with a view to age, gender and vertebral level." Bone **46**(2): 348-354.

Woodbury, D., E. J. Schwarz, D. J. Prockop and I. B. Black (2000). "Adult rat and human bone marrow stromal cells differentiate into neurons." J Neurosci Res **61**(4): 364-370.

Wozney, J. M., V. Rosen, A. J. Celeste, L. M. Mitsock, M. J. Whitters, R. W. Kriz, R. M. Hewick and E. A. Wang (1988). "Novel regulators of bone formation: molecular clones and activities." Science **242**(4885): 1528-1534.

Yamaguchi, Y., J. Ohno, A. Sato, H. Kido and T. Fukushima (2014). "Mesenchymal stem cell spheroids exhibit enhanced in-vitro and in-vivo osteoregenerative potential." BMC Biotechnol **14**(1): 105.

Yang, X., B. F. Ricciardi, A. Hernandez-Soria, Y. Shi, N. Pleshko Camacho and M. P. Bostrom (2007). "Callus mineralization and maturation are delayed during fracture healing in interleukin-6 knockout mice." Bone **41**(6): 928-936.

Yang, Z., H. Yuan, W. Tong, P. Zou, W. Chen and X. Zhang (1996). "Osteogenesis in extraskeletally implanted porous calcium phosphate ceramics: variability among different kinds of animals." Biomaterials **17**(22): 2131-2137.

Yates, A. J., G. E. Gutierrez, P. Smolens, P. S. Travis, M. S. Katz, T. B. Aufdemorte, B. F. Boyce, T. K. Hymer, J. W. Poser and G. R. Mundy (1988). "Effects of a synthetic peptide of a parathyroid hormone-related protein on calcium homeostasis, renal tubular calcium reabsorption, and bone metabolism in vivo and in vitro in rodents." J Clin Invest **81**(3): 932-938.

Yew, T. L., T. F. Huang, H. L. Ma, Y. T. Hsu, C. C. Tsai, C. C. Chiang, W. M. Chen and S. C. Hung (2012). "Scale-up of MSC under hypoxic conditions for allogeneic transplantation and enhancing bony regeneration in a rabbit calvarial defect model." J Orthop Res **30**(8): 1213-1220.

Yokota, K., M. Kusaka, T. Ohshima, S. Yamamoto, N. Kurihara, T. Yoshino and M. Kumegawa (1986). "Stimulation of prostaglandin E2 synthesis in cloned osteoblastic cells of mouse (MC3T3-E1) by epidermal growth factor." J Biol Chem **261**(33): 15410-15415.

You, L., S. Temiyasathit, P. Lee, C. H. Kim, P. Tummala, W. Yao, W. Kingery, A. M. Malone, R. Y. Kwon and C. R. Jacobs (2008). "Osteocytes as mechanosensors in the inhibition of bone resorption due to mechanical loading." Bone **42**(1): 172-179.

Younger, E. M. and M. W. Chapman (1989). "Morbidity at bone graft donor sites." J Orthop Trauma **3**(3): 192-195.

Yu, Y., T. Leng, D. Yun, N. Liu, J. Yao, Y. Dai, P. Yang and X. Chen (2010). "Global analysis of the rat and human platelet proteome - the molecular blueprint for illustrating multi-functional platelets and cross-species function evolution." Proteomics **10**(13): 2444-2457.

Zand, M. S., T. Vo, J. Huggins, R. Felgar, J. Liesveld, T. Pellegrin, A. Bozorgzadeh, I. Sanz and B. J. Briggs (2005). "Polyclonal rabbit antithymocyte globulin triggers B-cell and plasma cell apoptosis by multiple pathways." Transplantation **79**(11): 1507-1515.

Zara, J. N., R. K. Siu, X. Zhang, J. Shen, R. Ngo, M. Lee, W. Li, M. Chiang, J. Chung, J. Kwak, B. M. Wu, K. Ting and C. Soo (2011). "High doses of bone morphogenetic protein 2 induce structurally abnormal bone and inflammation in vivo." Tissue Eng Part A **17**(9-10): 1389-1399.

Zhang, C., K. Cho, Y. Huang, J. P. Lyons, X. Zhou, K. Sinha, P. D. McCrea and B. de Crombrugghe (2008). "Inhibition of Wnt signaling by the osteoblast-specific transcription factor Osterix." Proc Natl Acad Sci U S A **105**(19): 6936-6941.

Zhang, D. and K. A. Kilian (2013). "The effect of mesenchymal stem cell shape on the maintenance of multipotency." Biomaterials **34**(16): 3962-3969.

Zhang, S. J. and J. C. Wu (2007). "Comparison of imaging techniques for tracking cardiac stem cell therapy." J Nucl Med **48**(12): 1916-1919.

Zhang, Z. Y., A. W. Huang, J. J. Fan, K. Wei, D. Jin, B. Chen, D. Li, L. Bi, J. Wang and G. Pei (2013). "The potential use of allogeneic platelet-rich plasma for large bone defect treatment: immunogenicity and defect healing efficacy." Cell Transplant **22**(1): 175-187.

Zhang, Z. Y., S. H. Teoh, J. H. Hui, N. M. Fisk, M. Choolani and J. K. Chan (2012). "The potential of human fetal mesenchymal stem cells for off-the-shelf bone tissue engineering application." Biomaterials **33**(9): 2656-2672.

Zhao, F. and T. Ma (2005). "Perfusion bioreactor system for human mesenchymal stem cell tissue engineering: dynamic cell seeding and construct development." Biotechnol Bioeng **91**(4): 482-493.

Zhong, W., Y. Sumita, S. Ohba, T. Kawasaki, K. Nagai, G. Ma and I. Asahina (2012). "In Vivo Comparison of the Bone Regeneration Capability of Human Bone Marrow Concentrates vs. Platelet-Rich Plasma." PLoS One **7**(7): e40833.

Zhou, Q., J. Y. Zhou, Z. Zheng, H. Zhang and S. S. Hu (2010). "A novel vascularized patch enhances cell survival and modifies ventricular remodeling in a rat myocardial infarction model." J Thorac Cardiovasc Surg **140**(6): 1388-1396 e1381-1383.

Zhu, J. (2010). "Bioactive modification of poly(ethylene glycol) hydrogels for tissue engineering." Biomaterials **31**(17): 4639-4656.

Zimmermann, J. A. and T. C. McDevitt (2014). "Pre-conditioning mesenchymal stromal cell spheroids for immunomodulatory paracrine factor secretion." Cytotherapy **16**(3): 331-345.